Resilient Power and Propulsion System Design for eVTOL Aircraft

PhD Thesis

Shadan Altouq

Rolls Royce University Technology Centre
Department of Electronic and Electrical Engineering
University of Strathclyde, Glasgow

This thesis is the result of the author's original research. It has been composed by the author and has not been previously submitted for examination which has led to the award of a degree.

Abstract

The continuous increase in population in megacities has led to a more pronounced issue of road congestion. Electrical vertical take-off and landing (eVTOL) aircraft have been proposed as a solution to alleviate road congestion by enabling greener and quieter aviation, providing a more time-efficient commuting option compared to helicopters. However, the realization of innovative eVTOL aircraft heavily relies on advancements in high-power and energy-dense power system technologies for lightweight electrical power systems (EPS). The limited maturity of lightweight EPS technologies and their safe integration into the aircraft pose challenges in terms of payload capacity and achievable range for eVTOL aircraft. This significantly impacts the performance of fully electric eVTOL aircraft for Urban Air Mobility (UAM) missions. Therefore, it is crucial to explore innovative approaches and new technologies for optimized EPS architecture and aerodynamic design at an early stage of the design process to achieve economical flight for UAM. These unique attributes of eVTOL aircraft differ significantly from conventional aircraft technologies and systems, emphasizing the need for a comprehensive understanding of aerodynamic-electrical failure interdependencies and EPS protection methodology to ensure a reliable EPS

Therefore, the main research contributions of this thesis include the development of a novel design methodology to capture a certification-compliant EPS architecture for an eVTOL at the preliminary design phase. This methodology integrates mission requirements, aircraft aerodynamics, projected future availability of EPS technologies, and safety requirements. The development of the EPS architecture is carried out in parallel to the design of non-electrical systems to ensure future compliance with certification requirements. The methodology enables the identification of key design trades

that minimise EPS system weight while ensuring that baseline safety criteria are met and future compliance with certification requirements. The results show that incorporating safety measures at a later stage will have a snowball effect on the aircraft design to meet certification requirements or stay within design constraints, such as weight. Furthermore, a novel abstract design methodology was developed to enable critical assessment of different aircraft aerodynamic configurations and explore new design spaces and novel architecture options. This methodology summarizes the relationship between aircraft aerodynamics and EPS requirements in a readily usable format. By combining the preliminary design methodology for a certification-compliant EPS architecture with the abstract design methodology, the complete assessment of various aircraft configurations and reliable EPS architecture designs and their weight for economic UAM missions can be achieved.

Other main contributions of this thesis include the development of a preliminary certification compliance assessment for the use of non-resettable protection devices, specifically the Pyrofuse protection device, in eVTOL concept designs. The non-resettable nature of the device poses a challenge in the certification process for its integration into eVTOL electrical system protection. The assessment results demonstrate that the Pyrofuse protection device can achieve airworthiness in various roles as the primary protection for eVTOL EPS. However, the airworthiness is heavily influenced by the physical design of the aircraft, the proposed location of non-resettable protection devices, and their ability to withstand common mode and common cause failures to maintain minor failures. Model-based analysis plays a critical role in supporting this evaluation. Consequently, a comprehensive design methodology has been developed to transiently model Pyrofuse operation, which is publicly available. The results indicate that the Pyrofuse offers a significant level of resilience against transient events, minimising nuisance-tripping, while swiftly clearing short circuit faults. This model enables further assessment of Pyrofuse performance and susceptibility to different failure modes, including common mode failures.

Contents

List of Figures

List of Figures

List of Tables

List of Tables

Acknowledgements

This endeavour would not have been possible without the indispensable support and encouragement of my family, mentors, and friends, in which I would like to express my sincerest gratefulness for. First, my academic supervisors Dr. Patrick Norman and Dr. Kenny Fong, thank you for your for giving me the freedom to follow my interests, for believing in me and pushing me forward and beyond, for the unwavering support, and for every single discussion that grew my research and technical skills. Secondly, Dr. Catherine Jones for your valuable time and support to push in the last few months of my PhD to complete it on time.

I would like to acknowledge the financial support from University of Strathclyde and Rolls-Royce UTC. I would like to thank Prof. Graeme Burt, and Prof. Min Zhang for giving me the opportunity to undertake this exciting PhD research. I would also like to extend my gratitude to the State of Kuwait for sponsoring my bachelor and masters education in the UK. To the colleagues and friends in the Advanced Aero-team, to the friends I made during my stay in Glasgow and UK, to the friends and cousins back home, thank you all for the good times and laughs that made this PhD journey during Covid era less stressful and more memorable.

Words cannot ever describe how grateful I am to my parents, brothers, and baby sister. You are my rock! Thank you truly for all the support and joy you have given me throughout this journey. Thank you for believing in me to pursue my interests. I did it! and cannot wait for the upcoming endeavours. This thesis is dedicated to myself, my mother Khaledah Al-Tammar, and father Atef Al-Touq.

Abbreviations

ATI Aerospace Technology Institute

APCUK UK Advanced Propulsion Centre

ARP Aerospace Recommended Practice

CCA Common Cause Analysis

DEP Distributed Electric Propulsion

DOE US Department of Energy

EASA European Union Aviation Safety Agency

EV Electric Vehicles

EIS Entry to Service

eVTOL Electrical Vertical and Take-off

EMI Electromagnetic Interference

EPS Electrical Power System

FAA Federal Aviation Administration

FTA Fault Tree Analysis

FHA Functional Hazard Analysis

FMECA Failure Modes and Effects Criticality Analysis

List of Tables

FMEA Failure modes and effects analysis

GaN Gallium Nitride

L/D Lift to Drag

Li-S Lithium-Sulfur

MCCB Electro-mechanical Molded Case Circuit Breaker

MTOW Maximum take-off weight

NASA National Aeronautics and Space Administration

NRPD Non-resettable Protection Device

PMSM Permanent Magnet Synchronous Motor

PSSA Preliminary System Safety Assessment

RPM Revolution per minutes

SSPC Solid State Power Controller

SSCB Solid State Circuit Breaker

SiC Silicon Carbide

TRL Technology Readiness Level

TCC Time Current Curve

UAM Urban Air Mobility

UAV Unmanned Aerial Vehicle

Chapter 1

Introduction

The continuous increase of population in megacities has led to road congestion becoming more pronounced. It was reported in 2018 that 55% of global population are currently residing in urban areas, and is projected to increase to 68% by 2050 [4]. With the growth of urbanisation trends, public transportation will face substantial pressure, and the proliferation of vehicles will exacerbate congestion problems in ground transportation. This consequently leads to travel delays, longer journeys inconvenience, and economic losses. This highlights the need for solutions in the existing transportation and infrastructure systems to increase the allowed capacity to tackle the traffic congestion, especially in peak hours.

The introduction of Urban Air Mobility (UAM) offers an alternative transportation system by using uncluttered lower airspace over urban areas to reduce both road congestion and gas emissions of cars stuck in traffic. The UAM also aims to provide on-demand aerial transportation for people to commute faster utilising a novel hybrid or Electrical Vertical and Take-off (eVTOL) aircraft. This new transportation system allows a faster commute from San Francisco to San Jose during peak hours in 15 minutes compared to a 1.5 hour commute using a private vehicle [5]. For these aircraft to operate in urban areas they need to be atleast as safe as general aviation, the noise level of these vehicle to be below the noise level limits for urban areas, and the design of the aircraft to be technological viable and economical for feasible UAM missions [5].

Currently, helicopters are being used for to perform UAM missions. However, heli-

copters are noisy hence cannot operate in mass in urban areas. As such, the enabling technology of eVTOL aircraft is the Distributed Electric Propulsion (DEP), this technology allows new design freedom in terms of the number and location of the propulsors around the aircraft, which adds safety and reduces the noise footprint of eVTOL aircraft compared to traditional helicopters. The DEP also replaces the mechanical complexity and the need of onboard fuel consumption compared to traditional helicopters in the UAM operations. For example, noise measurements published by aircraft manufacturers states that noise of their aircraft at a cruise altitude of 2,000 feet is measured around 45 dBA [6], and another manufacturers' vehicle noise level is measured around 45 dBA at altitude of 1640 ft [7], this value is assumed to be 1,000 times quieter than helicopters' [6–8]. Hence, using eVTOL for UAM transportation not only lower the road congestion and commute time, but also costs and noise footprint for operation in urban areas when compared to helicopters [9, 10].

However, there are still key factors limiting the commercialisation of eVTOL aircraft. The support infrastructure for the charging, maintenance, and take-off/landing all require significant investment to adopt large scale capacity of eVTOL aircraft [11,12]. Current existing helicopter pads can be used for eVTOLs in the short-term only as it would be insufficient for large scale of eVTOL aircraft. However, this necessitates universal standard for a charging solution is required to be followed by all eVTOL manufacturers prior to development of charging sites is yet to be developed [13]. This is required to ensure the charging infrastructure can be used by all eVTOL aircraft operating in UAM. The regulatory bodies are working on developing infrastructure for vertiports specific for eVTOL aircraft and operation certification [14]. Certification bodies are working with aircraft developers to find the best path that defines their aircraft type and to certify their eVTOL aircraft with safety as the primary goal [15, 16]. Standardised certification requirements for the design, production, airworthiness, and operation of eVTOL aircraft are yet to be developed, this is to prevent restricting design novelty of this emerging market [17].

There are various aerodynamic designs of VTOL aircraft where the number of propulsion units varies from 6 to up to 30 motors. For fully eVTOL aircraft, the

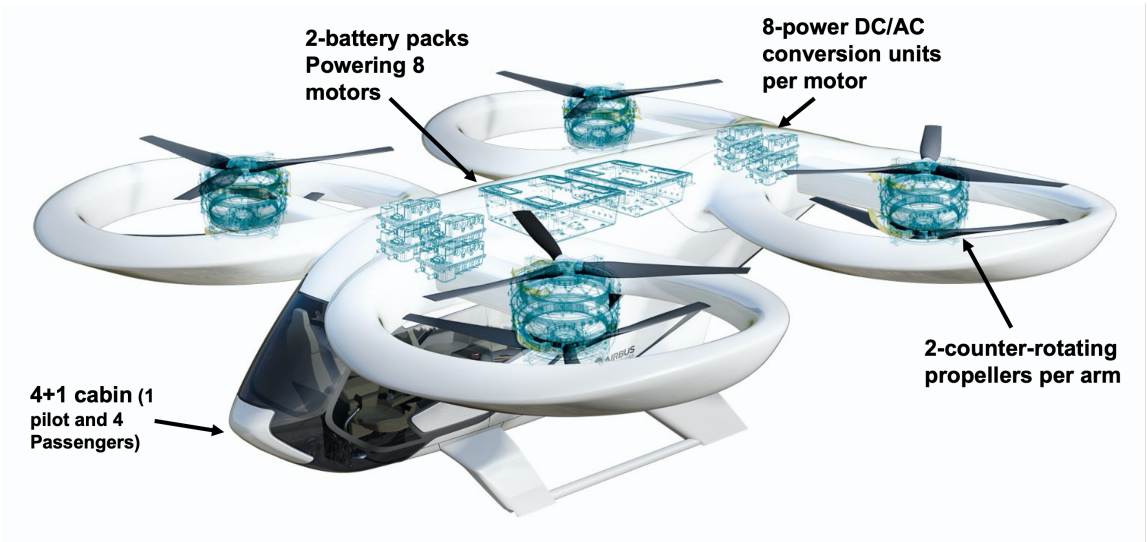

Figure 1.1: Overview of CityAirbus demonstrator eVTOL powertrain [18]

propulsion unit are usually AC electric motors powered purely by batteries. Therefore, DC/AC power conversion units are used to enable the use of AC electric motors. To ensure that a single failure in the system does not affect healthy systems and result in a complete loss of the aircraft, protection devices are typically placed at the battery terminals, motor terminals, and in between (especially for long cables) hence preventing fault propagation. An example of a fully eVTOL is shown in Figure 1.1, where two battery packs supply power to 8 electric motors, and each motor has its own power conversion unit. Whereas, for hybrid electric eVTOL, the motors are supplied power from a generator that is driven by a split between a battery and an engine. The number of batteries and EPS distribution architecture should be designed and sized to withstand a single or multiple failures, depending on the design objective. Electrically driven propulsion systems for aircraft represent a significant step change from the use of electrical power for secondary on-board systems for state of the art more-electric aircraft. Electrical systems for more electric aircraft utilises 230/400 VAC and 270 Vdc [19]. While electrical systems for eVTOL aircraft is around 800 VDC with high power requirements to lift the aircraft vertically [42]. With this high voltage and power requirements, novel lightweight high voltage EPS technologies are required for an economic aircraft design. Furthermore, the design of an integrated EPS to meet perfor-

mance (e.g. weight), functionality, and certification regulations, combined with much greater levels of coupling with non-electrical systems, such as aerodynamics, presents a significant challenge for electrification of these aircraft propulsion systems. Hereby this novel electrical-aerodynamic dependent systems raises new failure modes and causes of catastrophic failure that requires developers to demonstrate reliable and failsafe aircraft design.

The highly interconnected aerodynamic-electrical system design in eVTOL aircraft has further highlighted the need for more stringent safety measures to maintain the power level and aerodynamic control. While the methodologies available in the current literature do not incorporate the investigation of the safety measures into the EPS sizing to estimate the weight of the aircraft or mission range for technological viable economic design. Therefore, to ensure the safe and energy-efficient aircraft design system, this change in aircraft design compared to traditional aircraft necessitates the use of new EPS architectures in parallel with the aerodynamic design to ensure certification-compliant aircraft within design constraints. Key to this realisation is the availability of lightweight EPS technologies. This constitutes one of the key motivations in this thesis where thesis objectives are derived and presented in section 1.3.

1.1 UAM operations and eVTOL Aircraft

The UAM market for commercial operations are distinguished for intra-city and inter-city missions. The mission distance in intra-city operations are around 30-100 km suitable for commuting around metropolitan areas, airport shuttle, or air ambulance. Distances longer than 100 km is considered as an inter-city. However, the energy storage technology remains a bottleneck limiting the range and number of passengers, especially for battery-powered eVTOL aircraft [20–22]. The current available energy density of batteries might allow the aircraft to perform intra-city missions, but for inter-city and multi-mission intra-city a battery with an energy density of 500 wh/kg is required, which is expected to be available by 2030 [23]. Therefore, based on the mission and application, the aircraft configuration is developed for the intended UAM market.

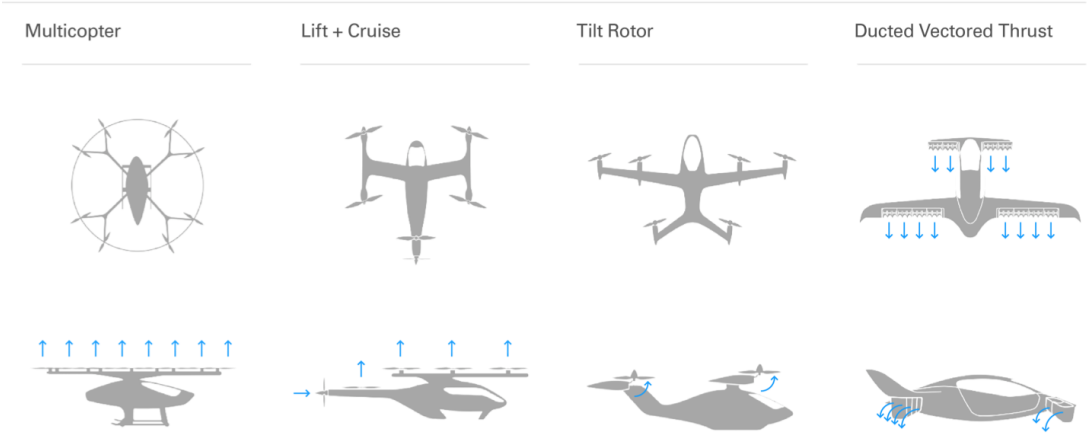

Figure 1.2: Different types of VTOL concepts [picture taken from reference [24]]

From Figure, there are different eVTOL configurations these are, wingless "multi-rotor", and winged "vectored thrust" and "lift+thrust" designs. Wingless multirotor eVTOL operates similar to a helicopter featuring high hovering efficiency, offers design simplicity compared to other configurations in manufacturing, certification, small foot-print, and flight manoeuvring/control [15]. However, multirotor concepts are limited to short-haul intra-city transportation less than 100 km with current technologies. The second configuration is vectored thrust eVTOL, this concept combine the high cruise efficiency of conventional aircraft with the vertical lift capability of multirotor eVTOL concepts. There are different subtypes of vectored thrust eVTOLs such as tilt-rotor and tilt-wing. This configuration uses all of its propulsion to tilt and provide thrust for all the flight phases. The third configuration is the lift+cruise eVTOL where it uses fixed propulsion for hovering and tilt propulsion for all flight phases. Both vectored thrust and lift+cruise can offer long UAM missions of up to 241 km using the current battery technology as shown in Table 1.1. Although winged eVTOLs offer longer range, their rotating design introduces complexity in control and subsequently complexity in certification regulation. Additionally, the vectored thrust and lift+cruise configurations requires larger parking spaces in the charging infrastructure in contrast to multirotor eVTOLs due to the length of the wingspan. Table 1.1 also presents the certification

status and the intended target for commercial operations of eVTOL aircraft currently in development.

Table 1.1: Specifications and Certification Status of eVTOL Aircraft Under Development.

Company	Vehicle Name	Concept Configuration	PAX	No. of Motors	Cruise Speed (km/h)	Range (mi)	Certification EIS
Volocopter [25, 26]	VoloCity	Multirotor	2	8	90	22	mid-2024
Volocopter [27]	VoloConnect	Fixed-wing	3-4	6 motors +2 fans*	110	60	2026
e-Hang [28, 29]	e-Hang 216	Multirotor	2	16	100	∼21	obtained CAAC type certificate in Oct. 2023
Airbus [30, 31]	NextGen	Lift+cruise	3+1	8	120	80	2025
Airbus [32]	CityAirbus	Multirotor	4	8	120	60	Demonstrator
Bell [33, 34]	4EX	Wingless Tilt-rotor	4+1	6	241	60	2025-2030
Lilium [35, 36]	Lilium Jet	Tilt-jet	6+1	36	280	155+	2025
Joby [37]	S4	Tilt-rotor	4+1	6	322	150	2024-2025
Vertical Aerospace [38]	VX4	Tilt-rotor	4+1	6	241	100	2026
Hyundai [39, 40]	S-A2	Tilt-rotor	4+1	8	193.12	40	2028
Archer [41]	Maker	Tilt-rotor	2	12	241	60	Demonstrator
Archer [42]	Midnight	Lift+Cruise	4+1	12	241	60	2024-2025
Overair [43]	Butterfly	Tilt-rotor	4+1	4	322	>100	2025-2026
ASX [44]	MOBI-One V3	tilt-wing	4+1	9	240	>65	2026
Dufour Aerospace [45, 46]	aEro 3	Tilt-wing	5-7	4	350	75	2025-2026

*Propulsion fans

1.2 Differences in Traditional Certification Methods

The novel configuration of eVTOL aircraft represent significant difference from the conventional aircraft and more electric aircraft in terms of design and operation. This difference in design varies from the aerodynamic design of the aircraft, EPS and the propulsive system to mode of operation, and flight controls [15, 47]. In particular, the 1) configuration design which relates to the integration of the distributed electric propulsion into the aircraft which enables various novel aerodynamic designs, and the 2) flight mechanism which relates to the ability to land and take-off vertically and the

transitions between flight phases. These differences necessitates the regulatory bodies to present certification path for the manufacturers to adhere to in order to facilitate the operation of eVTOLs in an airspace above metropolitan areas.

To address the need for a new established requirements to certify eVTOL aircraft for air taxi missions, the FAA have adjusted the currently used certification rules alongside additional performance-based regulations suitable for eVTOL aircraft [48,49], while the European Union Aviation Safety Agency (EASA) have developed new certification and amendments documentation tailored for eVTOL and air taxi missions specifically [50]. Therefore, the change in certification affirms the need for different design approach for the EPS architecture to address the safety requirement of the regulatory bodies than what is currently followed for helicopter or conventional aircraft.

However, there is a lack of a system level approach to design the EPS in the literature for eVTOL aircraft, which captures the potential electrical failures, safety requirements from regulatory bodies and associated the safety protection measures. This change in approach to the EPS design can affect the feasibility of the aircraft intended mission if not considered at an earlier stage of the development of the aircraft.

On the other hand, the power-to-weight ratio of key EPS technologies is one particular area where further technology development is required. Example of key EPS technologies are batteries, power machines, power conversion units, and protection. The current available EPS technologies suitable for use in eVTOL aircraft are at low maturity. This low maturity of power and energy dense technologies can considerably contribute to the overall weight of the aircraft. In which additional challenges arise to design a safe and low weight EPS architecture capable of transporting passengers to long distances or multiple short missions.

With advances in the power and energy density of electrical propulsion and energy storage in the automotive and aerospace industry, the purely-electric solution is expected to become more competitive in the future. Therefore, further study on technologies availability, roadmapping, and suitability for the design, in order to exploit the full potential of eVTOL aircraft. This can be achieved through effective integrated solution from technology selection to system level design, with the aim of meeting the

design objectives and certification requirements.

1.3 Research Objectives

During the process of identifying the novelty of research at the start phase of the PhD, the pathway is paved towards near-term research outcomes from the assessment and viability of key electric technologies in short and long term for eVTOL economic mission to developing a methodology for a lightweight and resilient EPS and propulsion systems for eVTOL aircraft. Therefore, the research questions derived from the discussions in sections 1.1 and section 1.2 highlights the need for comprehensive understanding of the safe integration of EPS technologies and the aerodynamic-electrical failure dependencies to derive a design methodology for economic eVTOL design in the public domain.

> ***"Research Question (1)***
> ***What are the essential factors to consider when designing an economically efficient and lightweight eVTOL aircraft"***

> ***"Research Question (2)***
> ***What is the process for designing a certifiable power system architecture that incorporates non-resettable protection devices for primary protection"***

Accordingly, in order to answer the above-mentioned research questions, the research conducted in this thesis addresses them in three main objectives:

1. Explore the UAM market and understand the difference in the design of eVTOL aircraft configuration and mission profiles.

2. Define relationships and design drivers for the EPS and aerodynamics design trade-offs, and sizing effects against available and projected technologies on the mission profile.

3. Investigate regulatory rules to implement resilient protection strategies suitable for different eVTOL architectures.

   (a) Establish a system level safety assessment of Pyrofuse compliance with certification regulations in aerospace applications.

   (b) Establish a methodology to develop a certifiable EPS architecture within the design weight budget.

   (c) Evaluate the certifiability of non-resettable protection devices (NRPD) for use in eVTOL aircraft.

1.4 Research Contributions

The novelty of the presented PhD research and contributions to knowledge are provided as follows:

- A first-of-its-kind design methodology to capture a certification-compliant EPS architecture at the preliminary design phase of an eVTOL aircraft. The methodology provides a systematic process to integrate the aircraft concept design including mission requirements and aircraft aerodynamics, projected future availability of EPS technologies, and safety requirements to identify a certification-compliant EPS architecture. Furthermore, it enables the quantification of the impact of the available technologies and the certification-compliant EPS on the aircraft concept design and mission profile.

- A first of its kind preliminary certification compliance assessment for the use of NRPDs, such as Pyrofuses, in eVTOL concept designs is established. The design approach categorise the resultant system behaviour for different eVTOL configurations, and more specifically, the impact on available thrust arising from a single or series of failure events, and the implications of implementing NRPDs in the EPS architecture.

- The first complete design methodology to transiently model a Pyrofuse device in the public domain is developed. This initiative aims to assist in the exploration

and accelerating low-weight protection technologies for use in eVTOL aircraft.

- A novel abstract design methodology summarising the relationship between aircraft aerodynamics and EPS requirements in a readily usable format for EPS assessment studies is developed. The design methodology allows the user to identify design boundaries based on mission requirements, enabling multidisciplinary design analysis at the initial stage of aircraft design. Additionally, to explore the viability of different aircraft configurations based on the design of the EPS architecture, certification requirements, and available technology.

- The first comprehensive overview of the power and energy density of EPS technologies for eVTOL aircraft in 10-year roadmaps is developed. The developed technology roadmaps can support aircraft developers to build effective system-level design solutions; using up-to-date EPS technologies available in a certain timeline inline with the intended entry to service target.

1.5 Publication

- **S. Altouq**, K. Fong, P. Norman, G. Burt, "Pyrofuse Modeling for eVTOL Aircraft DC Protection", SAE Technical Paper, 2021. doi:10.4271/2021-01-0041.

- **S. Altouq**, K. Fong, P. Norman, G. Burt, "Preliminary Certification Compliance Assessment for Non-Resettable Protection Devices in eVTOL Applications". (*Submitted to IET Electrical Systems in Transportation on 25th of November 2023*).

- **S. Altouq**, K. Fong, C. Jones, P. Norman, G. Burt, "Integrated Safety Design Methodology for a Certifiable Power System for eVTOL Aircraft". (*Submitted to IEEE Transactions in Transportation Electrification on 12th of December 2023*).

- **S. Altouq**, K. Fong, C. Jones, P. Norman, G. Burt, "Abstraction of Aerodynamic-Electrical Relationships for Accelerated eVTOL Conceptual Design Process", 2022. (*Expected submission date to IEEE Transactions in Transportation Electrification is June 2024*).

1.6 Thesis Outline

The structure of this thesis is divided into three main categories based on the research outputs from the identified objectives and the summarised contributions in 1.3 and 1.4. This thesis structure is illustrated as Figure 1.3. The main contributions of research work in this thesis are presented in each of the following chapters.

Chapter 2 presents an overview of the eVTOL aircraft design requirements for EPS technologies. From this, 10-year roadmaps were developed for key eVTOL EPS technologies based upon a multiplicity of public-domain information sources to consolidate the possible progression and key milestones of the technology space. The technologies covered in the proposed 10 year roadmaps include batteries, power electronics, power machines, and protection devices. This Chapter also discusses the challenges and attributes of these technologies for eVTOL applications.

Chapter 3 highlights the lack of published literature of the Pyrofuse device implementation in aerospace applications. In particular, the non-resettable nature of the Pyrofuse device whose exclusive use for electrical protection present potential operational hazards and certification challenges. Model-based analysis is critical in supporting this evaluation. The chapter is thus dedicated to provide more understanding of the device structure, operation, and performance. From this, the first design methodology to transiently model Pyrofuse operation, drawing characteristics from commercially available datasheets. Lastly, case studies were used to analyse the associated device and system level operational capabilities and limitations in a candidate eVTOL electrical system architecture.

Consequently, **Chapter 4** lists the latest version of amendments and regulatory advice available at the time of writing. This includes a thorough overview of existing certification standards related to the use of NRPDs in critical roles of eVTOL EPS, in order to highlight corresponding compliance requirements for Pyrofuse deployment. The chapter also highlights potential hazards which could lead to common mode failures. To address constraints, first of its kind preliminary certification compliance assessment which provides guidance for compliant integration of NRPDs such as Pyro-

fuses in eVTOL concept designs. The approach combines regulatory rules, the existing Functional Hazard Analysis (FHA) method and the identification of key eVTOL safety design drivers for a more cohesive airworthy design.

Building upon certification requirements related to the EPS for eVTOL aircraft, **Chapter 5** presents an overview of the industry standards safety assessment guidelines and design methodologies in literature. The literature review in this chapter highlights that the detailed design of the EPS to meet regulatory safety requirements is often oversimplified at an early stage. The chapter presents and describes the proposed first-of-its kind design methodology to capture a certification-compliant EPS architecture at the preliminary design phase of an eVTOL aircraft. Finally, the chapter illustrate the impact of technology advancement, using the database of key EPS technologies from the 10-year roadmaps in Chapter 2, and the impact of a certification-compliant EPS architecture design on the weight and mission profile when considered at a later stage of the design process.

Given the detailed aerodynamic design of the methodologies in the literature, **Chapter 6** presents a novel abstraction design methodology summarising the relationship between aircraft aerodynamics and EPS requirements in a readily usable format for EPS assessment studies. The case studies demonstrates the developed abstraction design methodology offers high correlation for a wide range of aircraft sizes and configurations.

Finally, **Chapter 7** concludes the research in this thesis highlighting the main results, key limitations and associated recommendations for future work.

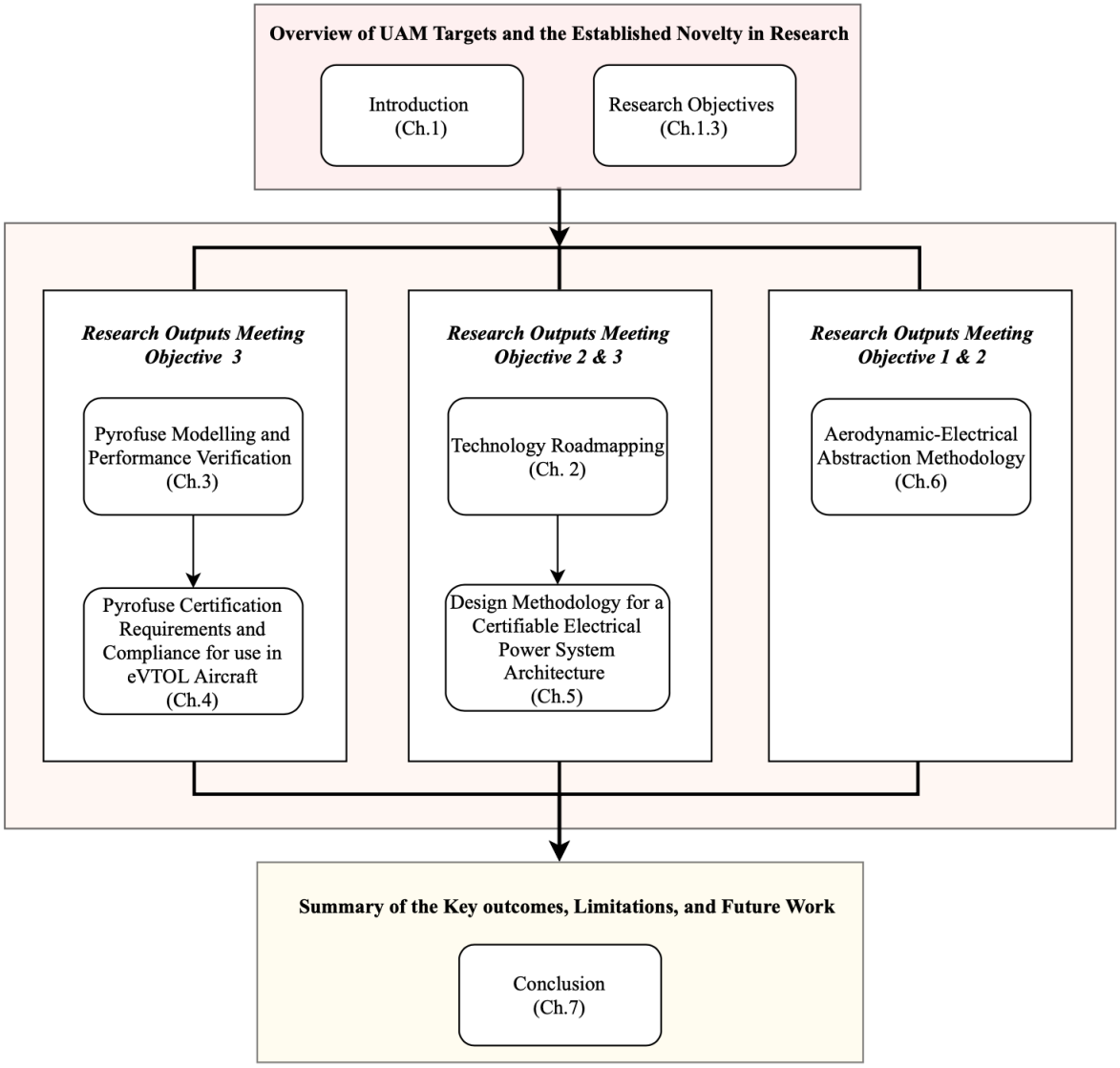

res

Figure 1.3: Flowchart of the Thesis Outline

Chapter 2

Technology Maturity Roadmaps for Power System Components

The viability of aerial taxi missions is highly dependent on the mass and reliability of the EPS to supply uninterrupted power to the propulsion [51–53]. Yet, the electrical power system is limited by the low maturity, in terms of power and energy density, of the current available critical technologies. Therefore, the integration of the technologies into a single power and propulsion system requires significant attention to provide a viable solution capable of supporting the mission requirements.

Following from this, there is a clear need for a consolidated capture and project of relevant electrical technology capability and availability in order to develop effective solutions. This Chapter presents a summary and discussion of 10-year roadmaps for key electrical technologies required for eVTOL design as seen in Figure 1.1. This first step is critical into understanding the impact of technologies on the design of the power system and on the overall aircraft performance. As discussed in Chapter 1, the key electrical technologies covered in this chapter are energy storage (i.e. battery technologies), power electronics, power machines, and protection devices. Power-to-weight and energy-to-weight ratios have been obtained from public domain sources on existing technologies and market or research-based projections in order to establish technological progression trendlines. These can subsequently be used to influence electrical power and propulsion system design choices and strategies for future platforms.

A total of 5 roadmaps have been developed and presented in this chapter. One roadmap was developed for energy storage, two roadmaps were developed for power electronics: one for AC/DC and DC/AC, and one for DC/DC. This distinction is due to the different configurations of DC/DC compared to AC/DC and DC/AC units. DC/DC units can include switching regulators, transformers, and capacitors to achieve the desired voltage conversion, while AC/DC or DC/AC systems mostly consist of diodes, switches, and filters.

Additionally, two roadmaps were created for electrical machines: one for high-torque motors and one for high speed motors. This distinction is due to the high-speed motors are lighter and has higher power density than high-torque motors, and are currently used in the automotive industry. It is important to note that the technology roadmaps do not include protection devices due to insufficient data on power-to-weight ratios and technology progression available in the public domain.

The roadmaps of the key technologies presented in this Chapter provide means to estimate the weight of the of the EPS in the literature for higher fidelity evaluation of the mission range with the required payload weight. Also for aircraft at conceptual level, technological roadmapping provides an indication on when a certain mission range is achievable and the allowable passengers payload.

2.1 Energy Storage - Battery Technologies

Higher specific energy density battery technology can provide longer mission range and/or increased mission rates between recharging. Power dense batteries are required for eVTOLs to allow high discharge rates for the high power requirement during the hovering and landing phases, and allow faster charging, extending battery longevity and safety margins. Batteries with high power discharging are especially essential for eVTOL aircraft designs with high disc loading which compromises the energy density of the battery [54, 55]. This shows an evident trade-off between high energy and power dense batteries to support the flight mechanism and mission economics of eVTOL aircraft. From this, depending on the aircraft design, appropriate selection of batteries can be attained through a tailored combination of battery cell chemistry to achieve

energy dense batteries with high power capabilities to satisfy the mission requirements all while focusing on maintaining low weight and volume.

Lithium-ion batteries are the main energy dense, market-available option for eVTOL applications, whilst the emerging Lithium air (Li-air)/Lithium-Sulfur (Li-S) [56–58] and Lithium metal polymer/Solid State battery technologies [59, 60], are being pursued for further increased energy density. In terms of energy density levels of battery technology, the UAM community has published various projections. At a cell level, Roland Berger indicated that in 2019, the maximum Lithium-ion battery cell level energy density was around 300 Wh/kg [61], but by 2025 Lithium metal polymer/solid state batteries should achieve energy densities of greater than 400 Wh/kg, and by 2030 an energy density of greater than 500 Wh/kg may be achieved using lithium air technologies. In conjunction, NASA has published projected cell level projections of 400 Wh/kg by 2025 and with a higher projection of 600 Wh/kg by 2030 [62]. The UK ATI also provides a 500 Wh/kg cell level projection for 2030, similar to Roland Berger [19].

Combining the various energy density data projected by the UAM community above with other publicly available information for cell level energy density from manufacturers [63]- [88]. Figure 2.1 presents a combined roadmap of battery technology from 2016 to 2030 (including the 10 year projection from 2020 to 2030). The data points for cell energy density are labelled as "prior" for technology available from 2017 to the start of 2022 and projected densities from later 2022 to 2032 are labelled as "projected" densities. In this, a linear trendline was chosen to link all past and projected energy densities data in Figure 2.1 to determine the technology progression over the following years. In contrast to the UAM specific data presented in the roadmap, there is evidence that automotive and UAV sectors have already reached or exceeded the 400 Wh/kg threshold in 2018-2019 [65, 66].

An outlier to the Lithium-ion battery projections is discussed above, in 2019 Innolith announced intentions to develop a novel electrolyte variant aimed for cell level energy density of 1000 Wh/kg battery by 2024 with lifespan greater than 800 cycles [87]. To this date, the company has not posted any follow up of the technology in development. As such, due to lack of any updates the energy density projection of this technology

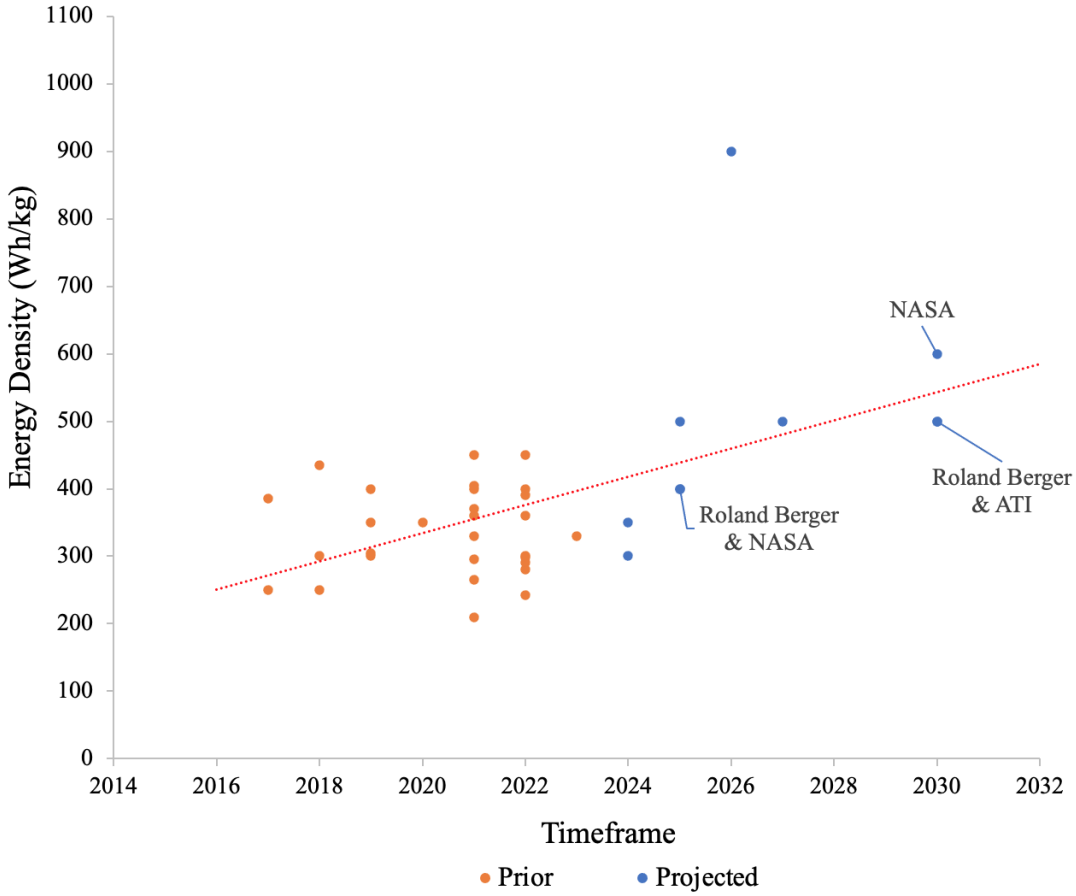

Figure 2.1: Batteries Roadmap Highlighting Technology Energy Density Prior to 2022 and Projected.

have not been included in the roadmap presented in Figure 2.1. Additionally, Lyten is currently developing a graphene based Li-S battery with potential to achieve 900 Wh/kg with cycles greater than 1,400 for electric vehicles [88]. Recent news in 2023 have shown that Lyten have secured funding to automate pilot line to produce Li-S batteries three times greater than a lithium-ion battery [89]. Thus Lyten's energy density projection has been considered in the roadmap presented in Figure 2.1. However, due to the large amount of data points around 200-500 Wh/kg, the trendline was not much affected by the single 900 Wh/kg data point.

From the linear trendline in Figure 2.1, (2.1) is extracted and can be used to estimate the energy density progression of batteries in the following years.

$$Battery = 20.938 \cdot Y - 41961 \quad (Wh/kg) \tag{2.1}$$

Where Y in (2.1) corresponds to a given year. In addition to the cell level energy density road mapping, the battery energy density is reduced by roughly by a further 25% when taking into account the battery overhead packaging and the operating range of the battery's state of charge [71,72], thus reducing the usefulness of the full energy density. The lifespan of some of the novel cell technologies are currently limited to a low cycle which increases the operational and maintenance costs of the aircraft. Furthermore, a range of technologies are in the process for production in the upcoming year/s [77, 78], others are in continued development requiring additional years for certification, production, and ready for commercialisation [69, 73, 87, 88].

2.2 Electric Motors for Propulsion

Electric motors convert the power from the electrical system to the mechanical propulsion system to provide the thrust required to maintain flight. The main design drivers for electric motors in the UAM market and eVTOL applications are high power and torque density, and efficiency for a light-weight design [16, 92, 93]. The design and the nature of flight phases of the eVTOL aircraft demands a motor with high torque capability and limited speed range. DEP enable significant reduction of the noise level to operation requirement in UAM setting compared to helicopters [6–8]. While the current available and technology progression of motors in the automotive industry is focused on the production of high speed motors for EV applications [93], high-torque electric motors are currently available at low power density and thus suffer from increased weight in comparison to high speed motors.

With regards to motor types, permanent magnet motors (e.g., Permanent Synchronous Motor (PMSM) appear to be the most appropriate choice for eVTOL aircraft propulsion. This is as a result of its high torque density, compact sizing, high efficiency and fast transient response [94, 95]. The capability of PMSMs to maintain full torque is well suited for the requirements of eVTOLs', in particular the higher consumption

take-off and landing flight phases. Having said that, PMSMs are costly and require complex control system when compared to other motor technologies [94, 95].

In terms of current technology levels, the automotive industry has been the main application driver for developing light-weight high speed motors for EV applications. Recent published advancements in the automotive industry have achieved power densities up to 13 kW/kg with plans to excel beyond 15 kW/kg [96, 97]. These technologies are high speed motors with a potential use for aerospace applications but require mechanical reduction gearbox to control the speed range of the motors. Whereas motors operating at low speed range with high-torque capability offer a direct drive system which enables low noise emission without the need of a gearboxes and reduces the reliability and power loss of the mechanical system [16].

In terms of technology projections, the ATI have published the achieved power density by 2020 is at around 3 kW/kg for small aircraft/urban air transport applications, with subsequent projections of 7.5 kW/kg by 2026 [19] for sub-regional aircraft, and 12 kW/kg by 2030 for mid-size commercial aircraft. While NASA 10 years research goals are targeting a power density of 13 kW/kg by 2025, and 15-years goals of 16 kW/kg by 2030 with improved efficiency [98].

However, the high power densities achievable might still not be all suitable for eVTOL applications due to their aforementioned low speed high torque requirements coupled with noise requirements. Two roadmaps for electrical machines, that might be suitable for eVTOL aircraft are presented. The first one is for machines configured for rated speeds between 1000 RPM and 2500 RPM consistent with ranges of known eVTOL designs with ten or less rotors Figure 2. The second one, shown in Figure 2.3, is to cover the progression of higher speed motors, which may be more suited to small-diameter eVTOL applications with over ten rotors, which the machines can operate at higher RPM while maintaining low noise levels [99, 100]. This could be achievable as Lilium claims their aircraft is well under the regulation requirements to operate in urban areas while having an aircraft design with 36 small diameter motors rotating in a high RPM [24].

To reiterate the fact that the selection of electric motors is highly dependent on the

aircraft design, weight budget, and the product availability. The recent development of technologies has presented different options for electrical motors suitable for eVTOL applications, such as direct driven high torque motors, high speed motors with a reduction gearing system, or compact motor design with integrated power electronics. The current aerospace and automotive market show an increase of development in integrated high speed electric motor design which includes power electronics and reduction gears, if needed, in a single compact packaging. This integrated design offers increased power density for power electronics and machines altogether up to and greater than 11 kW/kg (e.g., [101–106]). For high power dense products introduced by the automotive industry, re-design or re-packaging is required to comply with the aerospace standards, these necessary changes might reduce the published power density of the product. Besides that, the detrimental factor of the selection is based on the noise emitted from the propeller tip speed and propulsion system, which in turn is heavily dependent on the aircraft design and motor arrangement.

Combining the power density data projected by ATI and NASA discussed with other publicly available power density references for existing 1000 RPM to 2500 RPM range motors from manufacturers in [107]- [116], Figure 2.2 presents the combined data for motor technology suitable for eVTOL designs with less than 10 rotors. The data points are labelled as "prior" for technology available from 2016 to the start of 2022 and projected densities from later 2022 to 2032 are labelled as "projected" densities. In this, a linear trendline was chosen to link all past and projected energy densities data in Figure 2.2 to determine the technology progression over the following years. . From the linear trendline in Figure 2.2, (2.2) is extracted and can be used to estimate the energy density progression of electric motors with a speed of 1000 RPM to 2500 RPM in the following years.

$$Low\ Speed\ Motor\ = 0.5769 \cdot Y - 1160.3 \quad (kW/kg) \tag{2.2}$$

Due to the lack of data between 2022 and 2026, the trendline in Figure 2.2 is highly affected by the 10 and 12 kW/kg power density projections presented by ATI.

Similar to Figure 2.2, Figure 2.3 presents a combined roadmap of motor technology

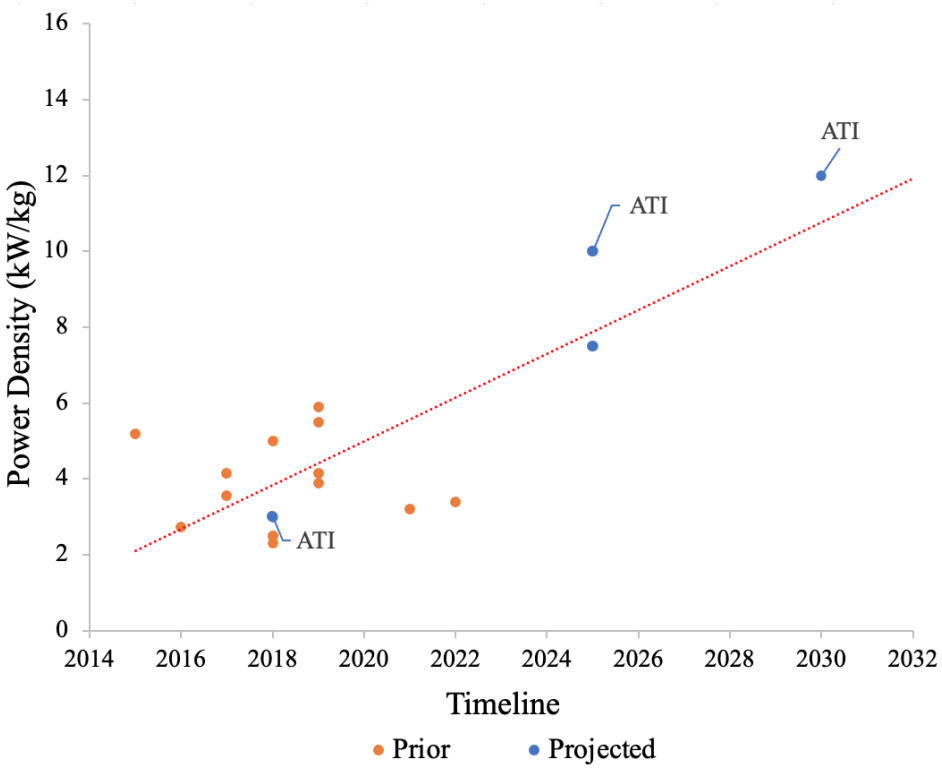

Figure 2.2: High Torque Electric Propulsion Motor Roadmap Highlighting Technology Power Density Prior to 2022 and Projected. Suitable for eVTOL of and less than 10 Direct Drive Rotors.

eVTOL designs with 10 rotors and higher with RPM range of and over 2500 from manufacturers in [117]- [127]. The projections of power density for high speed motors (2500+ RPM) are higher than low speed motors (1000-2500 RPM). This is mainly due to the automotive efforts to develop high speed motors for EV applications [93]. All the data presented for the projections are based on what is available in the public domain. In this, a linear trendline was chosen to link all past and projected energy densities data in Figure 2.3 to determine the technology progression over the following years.

In Figure 2.3 a high power density motor is projected, in 2022 Denso has developed a motor weighing approximately 4 kg and having an output of 100 kW forr Lilium aircraft high-speed motor requirement [125]. This power density projection data point is included in the roadmap presented in Figure 2.3. However, due to the large amount of data points around 5-12 kw/kg, the trendline was not much affected by the single 25 kW/kg data point.

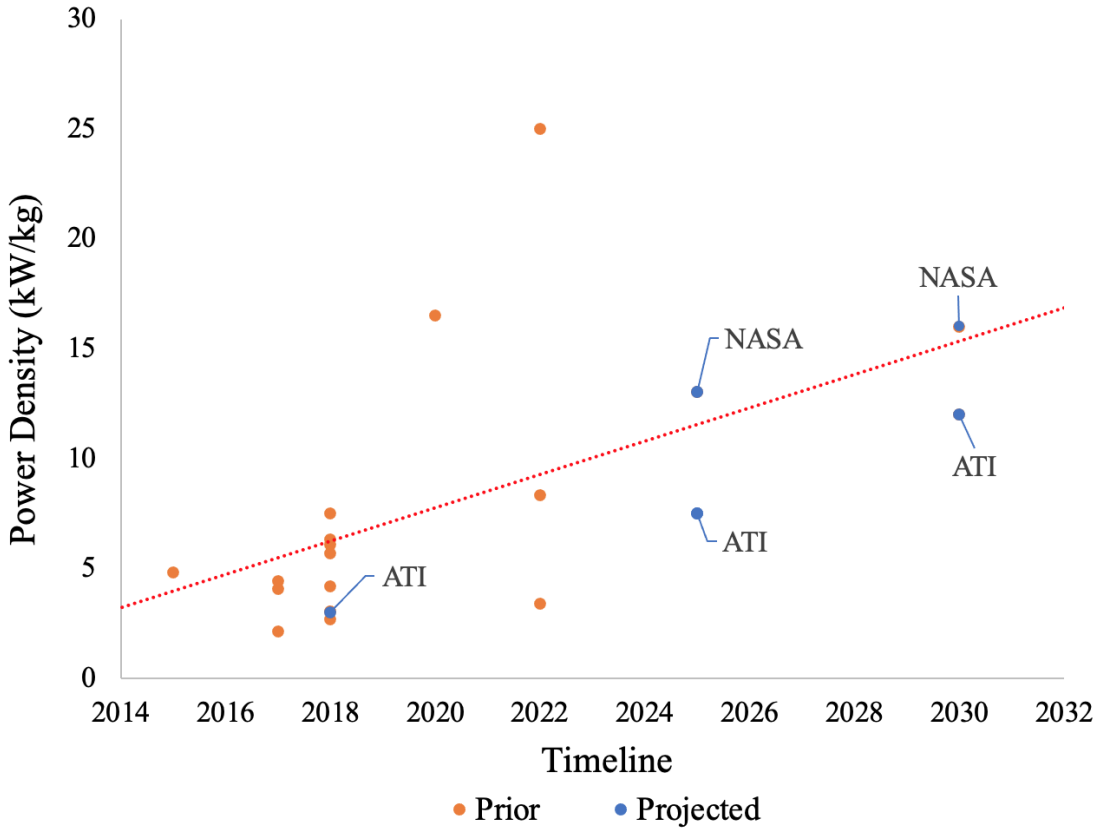

Figure 2.3: High Speed Electric Propulsion Motor Roadmap Highlighting Technology Power Density Prior to 2021 and Projected Suitable for eVTOL with More Than 10 Geared Rotors.

From the linear trendline in Figure 2.3, (2.3) is extracted and can be used to estimate the energy density progression of electric motors with a speed of 2500+ RPM in the following years.

$$High\ Speed\ Motor\ = 0.7582 \cdot Y - 1523.9 \quad (kW/kg) \tag{2.3}$$

In addition to the presented roadmaps, thermal cooling systems are an important factor to consider as the choice of the cooling method highly affects the weight and motor arrangement. According to [128], the thermal cooling system can contribute up to 30% of the motor dry weight. However, the weight of the thermal cooling system is often not incorporated as a part of the published power density of the motor, it is considered separate which reduces the published power density. There are many types of

cooling system, yet for eVTOL aircraft and high torque density applications air-cooling is widely used due to the airflow surrounding the motors [16]. Air-cooling motors are thus lighter in weight due to the use of the surrounding air and less complex in design than liquid cooled motors [16]. However, they have less effective heat rejection than liquid cooled motors. As such, cooling systems are chosen depending on the propulsion design, location, and access to abundant airflow around the motors.

2.3 Power Electronics

Power electronics are used to regulate the power from the energy storage in order to drive the electric motors. The main requirements of power electronics devices is to regulate and control the power flow with high efficiency and reduced volume and weight.

Recent development in wide-band gap materials i.e. Gallium Nitride (GaN) and Silicon Carbide (SiC) offer lighter switches and fewer losses than Silicon modules. SiC modules are expensive and are currently utilised in aerospace niche markets thereby widely available in high voltages [136]. With the current demands for the electrification of the automotive industry, mass production will drive the costs associated with power electronics modules down [129]- [132]. The progress of these technologies is mainly for the automotive industry and thus would require further adaptation for aerospace airworthiness certification to be used in eVTOL aircraft.

In terms of power density targets for power conversion devices, advisory bodies have divided the projections for AC/DC and DC/AC different than projections to DC/DC devices. This is mainly AC/DC and DC/AC having the same components and configuration in comparison to DC/DCs. For AC/DC and DC/AC inverters, the US Department of Energy (DOE) has funded research projects in widegap semiconductors and inverters in the automotive industry for a power density target of more than 14.1 kW/kg by 2020 [133]. The UK Advanced Propulsion Centre (APCUK) has set different targets for the power density by 2025 for inverters to be 22 kW/kg [134], while Horizon 2020 European project aims to achieve a target of 15 kW/kg with an efficiency of 99%, a reported TRL was 5 in 2018 [135]. The ATI aims to achieve a target of 10 kW/kg by

2025 [19].

The power density targets for DC/DC converter are as follows, the DOE funded research projections for 2-port (bidirectional buck-boost) to be 15 kW/kg and 6 kW/kg by 2025 [134]. NASA has set a power density goal of 19 kW/kg sponsoring research with General Electric to produce SiC/Silicon DC/DC converter but has not set a specific date. The 2-port DC/DC converter is a bidirectional buck-boost with 2 non-isolated ports [134]. Although SiC and GaN based power conversion devices are the trend in automotive and aerospace industries, there are limited data on the weight and power density of power conversion devices available in the public domain.

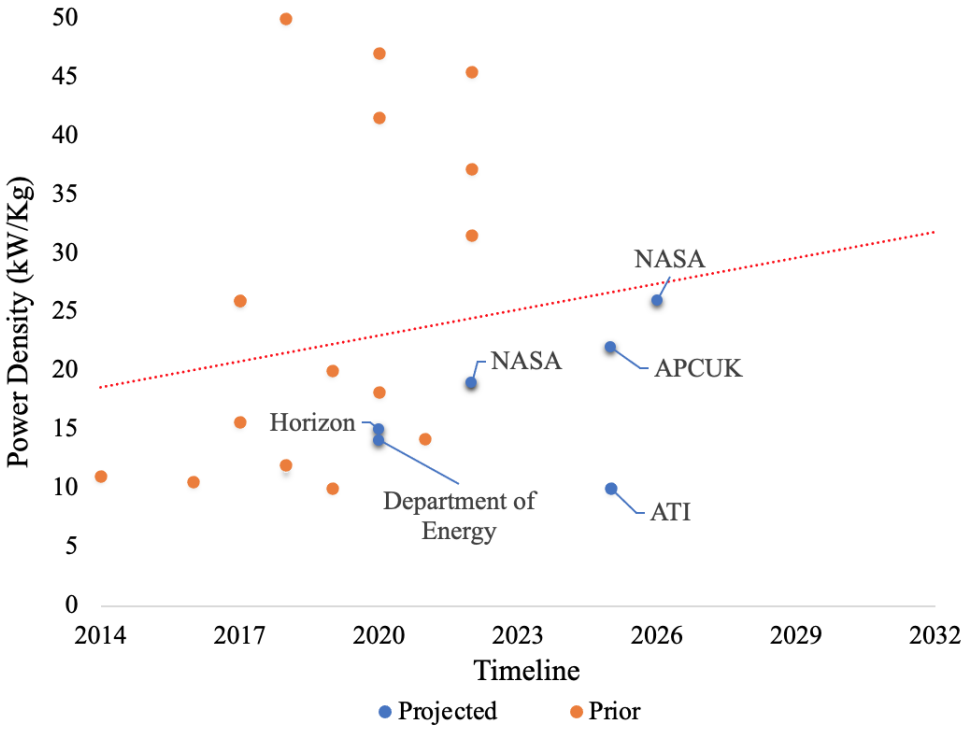

Figure 2.4: AC/DC-DC/AC Power Conversion Roadmap Highlighting Technology Power Density Prior to 2022 and Projected.

Combining the power density data projected by DOE and ATI discussed with other publicly available power density references for AC/DC and DC/AC devices. Figure 2.4 presents a combined roadmap of AC/DC and DC/AC power conversion devices using the following referenced data points [130]- [146]. From this, a linear trendline was

chosen to link all past and projected energy densities data in Figure 2.4 to determine the technology progression over the following years. In the Figure, the data points for the power density advertised from manufacturers and from research prototypes are labelled as "Prior" and are available from 2014 to the start of 2022. Projected densities from later 2022 to 2032 are labelled as "projected" densities.

Nonetheless, as eVTOLs powered by batteries have a DC distribution system, DC/AC power conversion devices are used. As the internal components and design of AC/DC is similar to DC/AC power conversion units, advisory bodies have used the same projections for the units. Hence, the trendline presented in Figure 2.4 can be used for DC/AC projections.

From the trendline in Figure 2.4, (2.4) is extracted and can be used to estimate the energy density progression of inverters (e.g., AC/DC and DC/AC) in the following years.

$$DC/AC\ or AC/DC = 0.7331 \cdot Y - 1457.8 \quad (kW/kg) \tag{2.4}$$

While Figure 2.5 presents a combined power density data projected by DOE, ATI, NASA, etc, discussed with other publicly available power density references for DCDC devices. The reference of these data points are [135, 147]- [154]. In this Figure, the data points for the power density advertised from manufacturers and from research prototypes are labelled as "Prior" and are available from 2014 to the start of 2022. Projected densities from later 2022 to 2032 are labelled as "projected" densities. In this, a linear trendline was chosen to link all past and projected energy densities data in Figure 2.5 to determine the technology progression over the following years. From the linear trendline in Figure 2.5, (2.5) is extracted and can be used to estimate the energy density progression of converter (DC/DC) in the following years. Where Y in (2.5) corresponds to a given year.

$$DC/DC\ = 0.5094 \cdot Y - 1012.3 \quad (kW/kg) \tag{2.5}$$

The presented data points of the power electronics devices has limited information

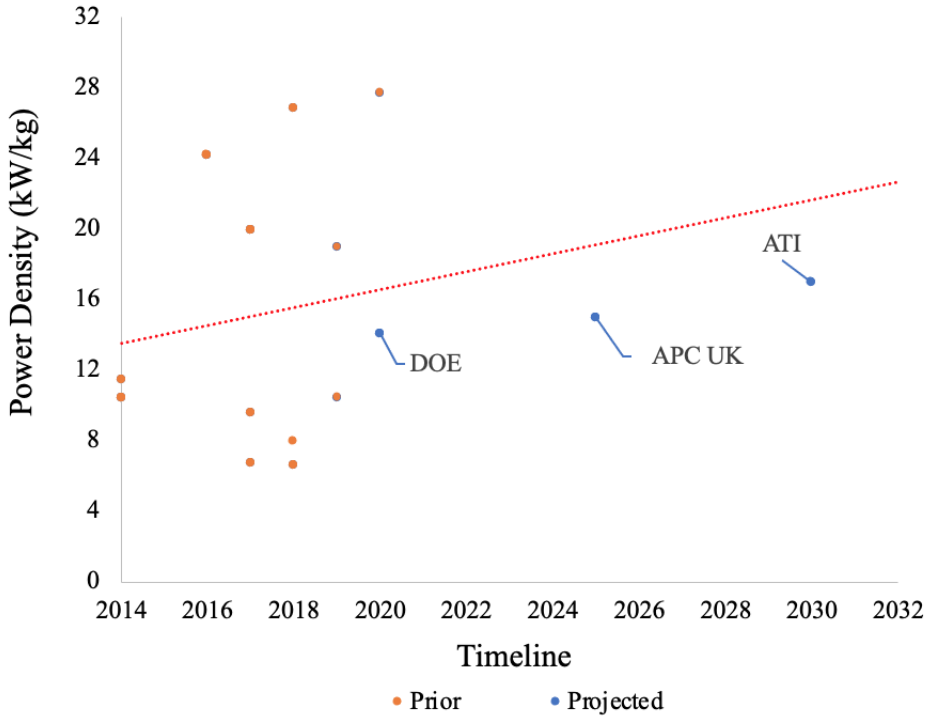

Figure 2.5: DC/DC Power Conversion Devices Roadmap Highlighting Technology Power Density Prior to 2021 and Projected

regarding what is included in the advertised power density, an example being the filtering components. The weight and size of the Electromagnetic Interference (EMI) filter has a significant impact on the overall weight of the power electronics devices contributing to between 25% to 40% of the total device weight [155, 156].

2.4 Power Protection

Protection devices are essential to isolate any potential faults that might occur during a journey, and ensure the aircraft can maintain flight after experiencing a fault. The main requirement of protection devices for eVTOL aircraft is the ability to isolate the fault rapidly for high voltages and fault current.

Conventional resettable protection devices are Electro-mechanical molded case circuit breaker (MCCB), circuit breakers and DC contactors. MCCBs are available in high DC voltages for the Photovoltaic industry [157, 158], yet they have relatively slow

response time for DC systems and are also susceptible to arcing damage causing low lifetime [166]. The DC contactors and conventional circuit breakers have their limitations for high voltage and high power demands for EV or electric aircraft applications [159].

Fuses are available in a wide range of high voltages, are cheap, and small in size. With the recent development in the automotive industry, hybrid Pyrofuse protection device was developed as a solution to similar issues faced in the state of the art electric vehicles [159, 160]. Pyrofuse is unlike conventional fuses as it has characteristics such as: excellent at clearing low fault currents, better cycling performance, lower conduction losses, and the time-current curve can be tuned to fit the system [159, 160]. In terms of current development, Panasonic [161] have presented a new type of Pyrofuse to provide fault protection and isolation for high power density battery applications. Bosch [162] and Texas Instruments [163] are developing current sensing circuits for externally triggered Pyrofuses. Mersen have developed a hybrid Pyrofuse protection solution for fast DC overcurrent limitation suitable for high voltage requirements for aerospace applications [159, 164]. The authors in [159] have presented the testing of Mersen's self-triggered Xp-series Pyrofuse with a fault level of 11 kA at 500 VDC.

With regards to the implementation of Pyrofuses in an aerospace environment, Mersen [164] in 2016 had also stated its intention to test the Xp-series Pyrofuse in an Airbus concept aircraft, although no publicly available update on this test has been provided to date. Safran and Pyroalliance are also developing protection solutions using Pyrofuses for high voltage electric aircraft applications [165]. However, Pyrofuse devices are non-resettable, which introduces further constraints on the integration into the electrical power system for airworthy operation. Further discussion on the performance of the device is presented in Chapter 3.

The recent development in resettable semiconductor devices succeeded in the limitation of conventional protection devices, offering a fast tripping speed against short-circuit faults [166]. As a consequence, solid-state circuit breaker (SSCB) and solid-state power controller (SSPC) have recently received extensive attention in research [167]. The SSCBs offer fault current interruption; it trips when the current exceeds the threshold. Similarly, SSPC can detect abnormal excess of fault energy (I^2) which trips ac-

cording to a threshold current. In addition to that, the SSPC also has the capability to detect arc faults, fast fault clearance, and power-load management with the control of a digital processor [168, 169].

SSCBs are available commercially in high voltages for non-aerospace applications (e.g. 1kV and up to 5 kA [170]). Similarly, SSPCs are available but at low voltages, as shown in Table 2.1. The on-state losses of a SSCB is significantly greater than in typical circuit breakers [171]. Therefore when scaling up, the increased on-state and energy losses of both SSPCs and SSCBs leads to increased requirements for cooling which contributes to a significant portion of the devices' weight [171, 172]. Active and liquid cooling systems offers reduced size and weight of the overall system compared with passive cooling methods [171]. Further development is required to reduce the volume and weight of the cooling and packaging of these devices which in turn will reduce the weight of the power system in eVTOL aircraft. It is important to highlight that the presented weight of the SSPC modules in Table 2.1 obtained from the manufacturer datasheet do not include heatsinks or external cooling.

Table 2.1: List of Current Available SSPCs [173]- [177]

Reference no.	**Voltage (V)**	**Current (A)**	**Power (kW)**	**Weight (g)**	**Power Density (kW/kg)**
SPDP50D375	375	50	1.5	650	28.8
SPDP50D28-1	55	50	2.75	40	68.75
SSP-21116	270	15	4.05	115	35.2
MDSPC270M-50xL	270	500	135	350	385.7
P800	28	150	4.2	500	8.4
P600	28	80	2.24	500	4.48

As there is limited information available on protection devices in the public domain thus with insufficient data points a 10-year technology roadmap is not feasible. The following projections can provide a timeline for SSPCs maturity. From the roadmap in [178], SSPC fault current interruption devices with 100 kW and 750 VDC is highly probable to be available at market in N+1 timeframe (according to [179], initial opera-

tional capability in 2015-2025), and power up to 1MW and 750 VDC in N+2 timeframe (According to [179], translates to 2025-2030). While SSCBs devices maturity will have a TRL of 4-6 by 2025 [178].

2.5 Summary

From the presented literature review in this chapter there is a notable increase in the development of battery and power electronics technologies suitable for the use in eVTOL aircraft. While the requirement for the development of power machines for the automotive industry is different than the requirement for eVTOL and aerospace applications; this show slower pace improvement in the power density. Additionally, there is a lack of information published from manufacturers regarding development targets and power density of the power protection devices in the public domain. Whilst solid-state switch improvements in power electronics can potentially be transferred to the development of power protection components, nothing is published unfortunately regarding that as well. However, it is most likely that aircraft developers might be developing novel in-house technologies or collaborating with a supplier to custom design a technology that suits their aircraft needs accelerate. As discussed, collaboration between denso and Lilium to develop a motor that suits their aircraft performance, similarly is likely to be done for power protection and power electronics. As these technologies are considered novel, additional years are required to obtain for product type certification, production, and ready for commercialisation. The earlier the collaboration commence the higher chance the eVTOL developer to hit their targeted EIS timeline.

Using the trendlines from the Figures presented in this Chapter, Table 2.2 provides a summary of the power and energy density of current existing technologies from 2017 and future projections in 2025 and 2030. The technologies covered are critical to the power system design and include batteries for the energy storage, power electronics, and power machines. With regards to protection devices, due to insufficient data points, a 10-year technology roadmap was not feasible.

Most importantly to note is that these technologies are still low in maturity for the

Table 2.2: Current Existing and Future Projections of Technological Parameters Abstracted from the Roadmaps

Technologies		**Energy/Power Density**		
		2017	**2025**	**2030**
Batteries (Wh/kg)	Cell level	270.9	438.5	543.1
	Pack level	203.2	328.8	407.35
Electric Machines	High torque motors	3.3	7.9	10.8
(kW/kg)	High speed motors	5.4	11.5	15.2
Power Electronics	Converter (DC/DC)	15.2	19.2	21.78
(kW/kg)	Inverter (AC/DC or DC/AC)	20.9	26.7	30.39

use in eVTOL aircraft which can hinder the exploration of novel designs, and increases the challenges of designing light weight aircraft with high reliability and redundancy viably satisfy a range of missions. This highlights the need to understand a holistic integration for viable EPS and aircraft aerodynamic design to achieve the mission targets without compromising the safety of the aircraft. This has been further explored in chapter 6 where presents a methodology to design a certification compliant EPS architecture in the preliminary design phase of the eVTOL aircraft is presented.

The recently introduced Pyrofuse device in the literature show a potential for use in aerospace applications. This device can offer low-weight solutions as a protection device in the power system architecture. However, it is non-resettable which requires further work to investigate the performance and robustness of the Pyrofuse device to assist the acceleration in this emerging market. Therefore, the first step into assessing the use of the Pyrofuse is by modelling the device in an aerospace environment enabling the capability for further investigations, this is further studied in Chapter 3.

Chapter 3

Transient model of Pyrofuse DC Protection Device for eVTOL Aircraft

Chapter 2 highlights the need for high DC voltage protection devices available in light-weight suitable for eVTOL aircraft. There is continuous development of solid-state protection devices in literature for non-aerospace applications due to their fast fault interruption times and arc-less performance [167–169]. However, the potentially short term EIS targets for proposed eVTOL platforms mean that suitably rated devices available in light-weight and volume for aerospace applications may not be ready in time for use [178, 179].

The relatively recent emergence of Pyrofuse devices offers an opportunity for use in eVTOL aircraft with light-weight benefits, high power density, fast fault isolation. Crucially, despite their other attractive qualities, Pyrofuses are non-resettable devices and with the lack of precedence of their operation in aerospace, better understanding of the Pyrofuses within eVTOL applications is required. Therefore, this chapter presents the first modelling methodology for a self triggered Pyrofuse circuit model available in the public domain to allow the exploration of the Pyrofuse device. Using the model, a performance analysis of the protection device was conducted in a generic eVTOL architecture under different simulated fault conditions that are likely to occur

in aerospace environments to highlight the advantages and limitations of its use. The modelling methodology utilises parameters extracted from manufacturers' datasheets to allow for a more accurate representation of tripping profiles. The proposed method exhibits some limitations and assumptions which are also discussed in this Chapter.

The work in this chapter aims to assist in the exploration and assessment of low-weight overcurrent protection technologies for high voltage aerospace applications such as in eVTOL aircraft applications.

3.1 Pyrofuse Fundamentals

A Pyrofuse is unlike conventional fuses as it has characteristics such as: excellent at clearing low fault currents, better cycling performance, lower conduc- tion losses, and the time-current curve can be tuned to fit the system [159, 160]. This is because of the hybrid configuration of the Pyrofuse; where a pyroswitch (also named as pyrotechnic switch), and a fuse are connected in parallel. This parallel configuration allows the designer to can choose the best components of each type which enables tunability. This type of a Pyrofuse requires an external electronic signal to isolate a fault from the system. Figure 3.1 shows the parallel configuration of an external triggered Pyrofuse, where the pyroswitch is grey, and the fuse is white [164].

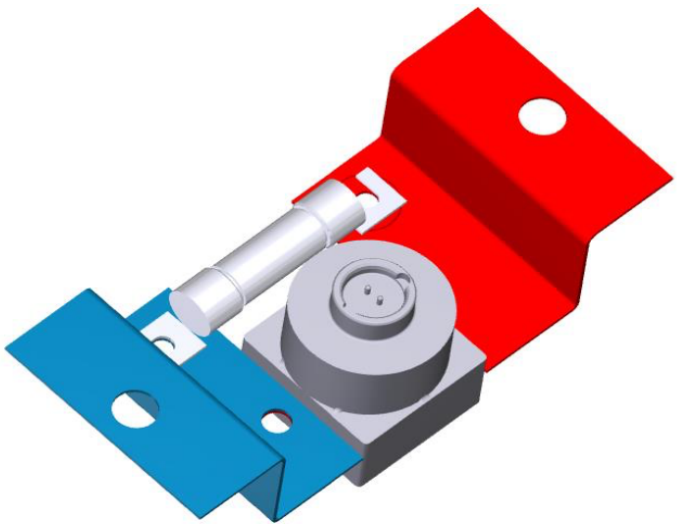

Figure 3.1: Parallel configuration of the external triggered Pyrofuse device [164]

To use an external triggered Pyrofuse, a current sensor, electronic circuit board to configure the triggering signal, and a power supply to power the electronic circuit board. Figure 3.2 presents the schematic of external triggered Pyrofuse device. During normal operation, the pyroswitch and fuse is closed and is connected to the rest of the system allowing nominal current to flow. During failure event, the sensor detects the abnormal current which is above the configured rated current and sends a signal to the pyroswitch to trigger [159, 164].

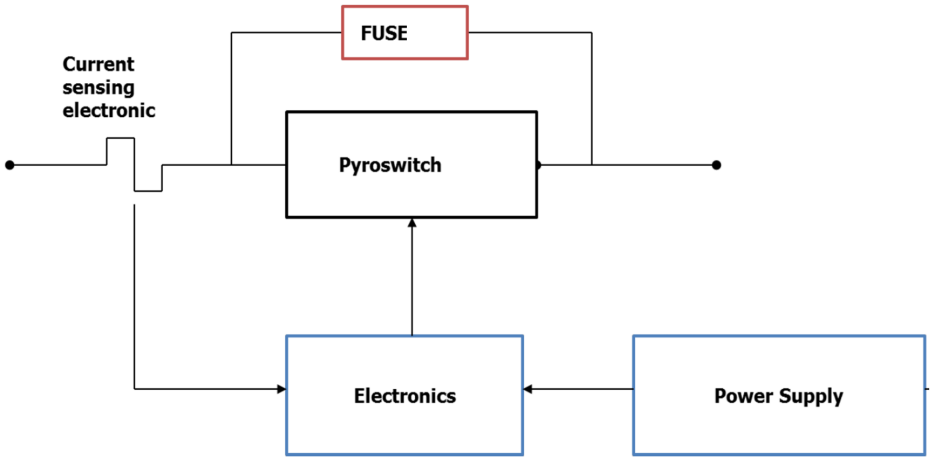

Figure 3.2: Schematic of an electronic-triggered Pyrofuse device [164]

The second type of a Pyrofuse is self-triggered which consists of two fuses and a pyroswitch, one fuse is used as a sensor and the other fuse is in parallel to the pyroswitch as in the external triggered Pyrofuse. The self-triggering method offers cost savings and less complexity than an electronic controlled Pyrofuse, as it eliminates the need for current sensor in the system, electronic circuit board to configure the triggering signal, and a power supply. Furthermore, electronic signal devices are prone to EMI failures which can result in triggering the Pyrofuse in normal operations. However, self- triggered devices provide less functionality for tuning tripping characteristics [159]. And, the current sensor fuse is a normal DC fuse which is dependent on the magnitude of current.

In this Chapter, the self-triggering version of the Pyrofuse is modelled as this is the

more complex version of two Pyrofuse options. The Pyrofuse design published in [159] was used as a reference for the model development. Figure 3.3 presents a schematic of a self-triggered Pyrofuse device consists of a pyroswitch (PS) shown in an yellow-coloured box, two fuses (F1, F2) and a resistor ($R_{ignition}$). Similarly, the electronically triggered Pyrofuse can be easily derived from this model by replacing the sensor fuse (F1) with an alternative trigger signal in the model.

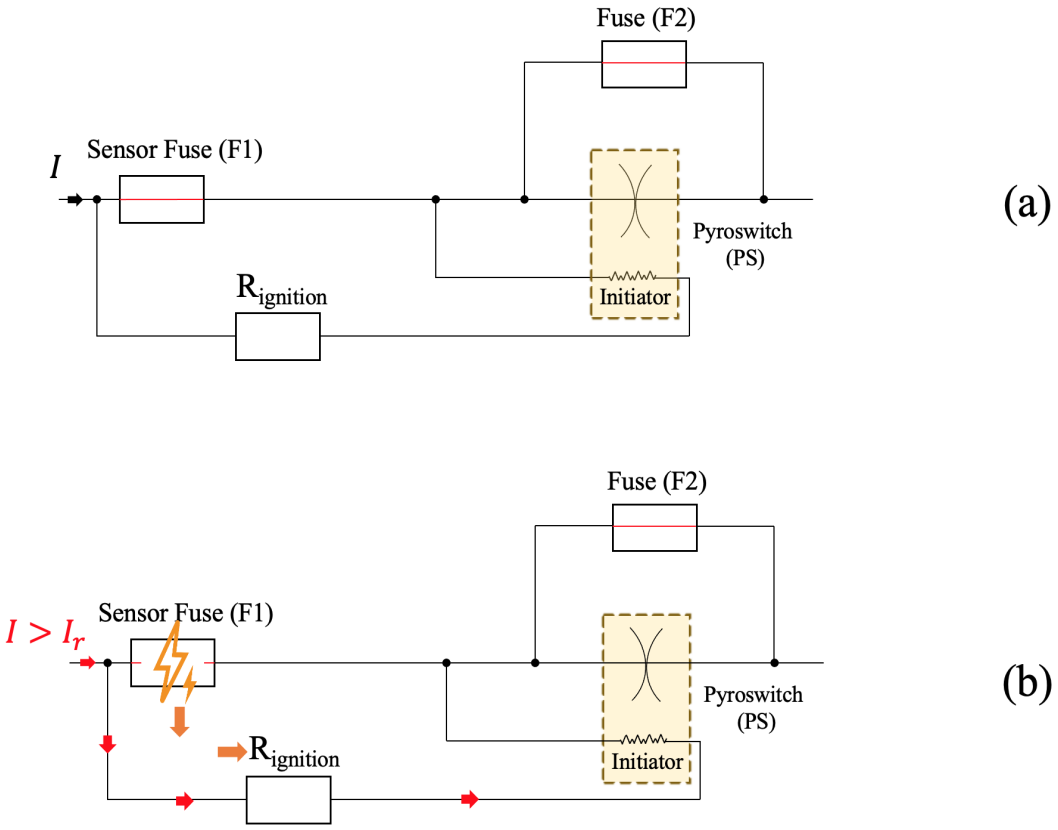

Figure 3.3: The operating conditions of self-triggered Pyrofuse device. (a) shows normal operating conditions, and (b) shows abnormal operating conditions

In hardware, the PS is placed on top of a copper conductor and utilises a pyrotechnic trigger and miniature guillotine to achieve the force through the conductor and hence disconnecting the circuit [164]. The trip sequence starts with the F1 which is sized for the nominal circuit current flow and is underrated for voltage. F1 is in series with the conductor of the PS and allows nominal current flow. F1 operates when the initial accumulated fault current exceeds the trip threshold, which in turn causes the current to

divert through the $R_{ignition}$. An electrical arc is present between F1 terminals and will sustain as F1 is underrated for voltage, as shown in orange Figure 3.3. This arc is used as a voltage source by the initiator. While the speed of the PS ignition is depicted by the diverted current through the $R_{ignition}$ which in turn separates the conductor. From this, the parallel fuse (F2) to the conductor is rated at nominal voltage, subsequently opens, extinguishing the inductive arcing that occurs as the conductor separates and of F1.

The sub model for F1 and F2 have the same model structure and operating sequence. This is further discussed in the section 3, including the sub model for the PS.

3.2 Model Formation

3.2.1 Fuse Sub-Model

The fuse design published in [180, 181] is used as a reference for fuse elements F1 and F2 in the Pyrofuse circuit model. The flowchart in Figure 3.4 summarises the working sequence and control of the fuse model under short transient and permanent fault conditions. The component layout of the fuse model is illustrated in Figure 3.5. The fuse's switch state is 1 when it is closed ($F_s = 1$), and 0 when it is opened ($F_s = 0$).

Under normal conditions, the fuse switch is closed and the circuit current conducts through the fuse. If the current (I) rises above the rated current threshold (I_r) of the fuse, indicating the potential occurrence of a fault in the power system, the model will start to calculate the accumulated melting energy of the fuse (E_{melt}). This calculation is performed over the period (S_{tmelt}) from the fault occurrence (t_1) to (t_2), where (t_2) is either the instance at which (E_{melt}) is high enough to melt the fuse or the point at which (I) becomes less than (I_r) again, resetting the melting energy calculation to zero. This accumulated melting energy E_{melt} is calculated using (3.1).

$$E_{melt} = \int_{t1}^{t2} I^2 \cdot t \, dt \quad (A^2 s) \tag{3.1}$$

The catalog energy (E_c) is the peak value of the melting energy of the fuse. If the calculated (E_{melt}) is larger than the threshold (E_c), the fuse will melt. The parameters

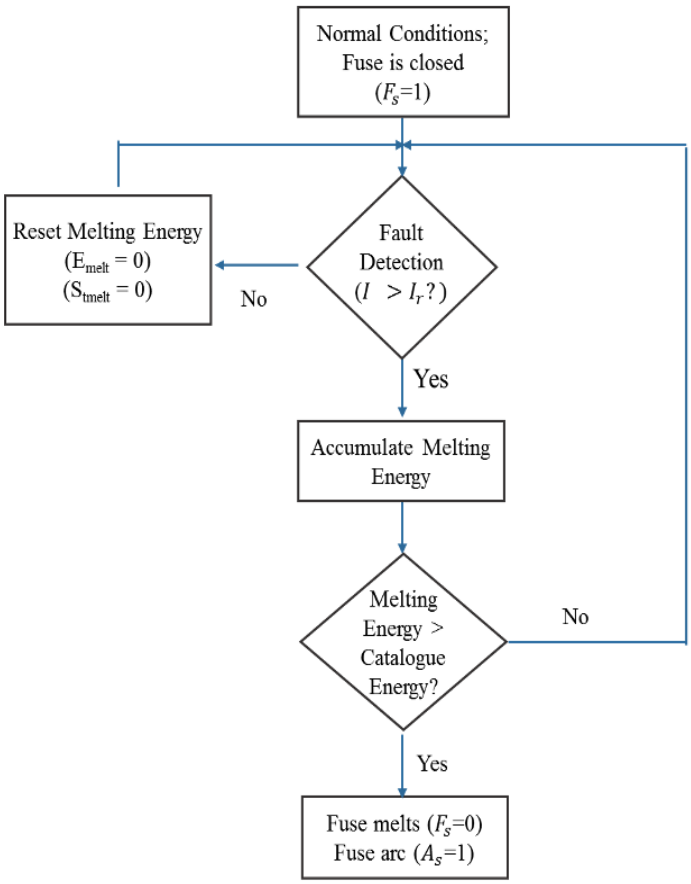

Figure 3.4: Flowchart of the Fuse Model Working Principle

to calculate (E_c) are obtained from manufacturer's datasheet Time Current Curve (TCC). The authors in [181] have identified that polynomial model was the best choice for fuse TCC data fitting amongst other models such as exponential, and Two-Terms Gaussian. Therefore, polynomial regression function is selected for curve fitting in this study. The data from the E_c can be curve fitted using a polynomial regression function like that shown in (3.2) within the sub model to dynamically calculate (E_c) within the simulation model.

$$E_c = a + b_0(x)^1 + b_1(x)^2 + b_2(x)^3 .... + b_k(x)^{k-1} \tag{3.2}$$

Where variable x in (3.2) is the melting time from the TCC, a $b_1 ....b_k$ are polynomial coefficients, and k is degree of a polynomial.

When the fuse melts, the transition to arcing is modelled through the simultaneous opening of switch (F_s) and closing of the arcing path switch (A_s) as shown in Figure 3.5. To emulate the arcing behaviour of the fuse, an RC equivalent circuit is utilised. This is highlighted in Figure 3.5. There is limited information in the literature on specifying fuse arcing time, with most of the published papers acquiring the arcing time from either the clearing time in the manufacturer datasheet, experimental data or by utilising the IEEE 1584 arcing time assumption [180–182]. The presented Pyrofuse model employs the IEEE assumption for the arcing time, and a method outlined in [181] whereby RC values are empirically tuned to provide a desired arcing time (t_{arc}) and peak current (I_0).

Once the circuit current reaches zero, the arc is considered to be extinguished and the switch (AS) is opened again.

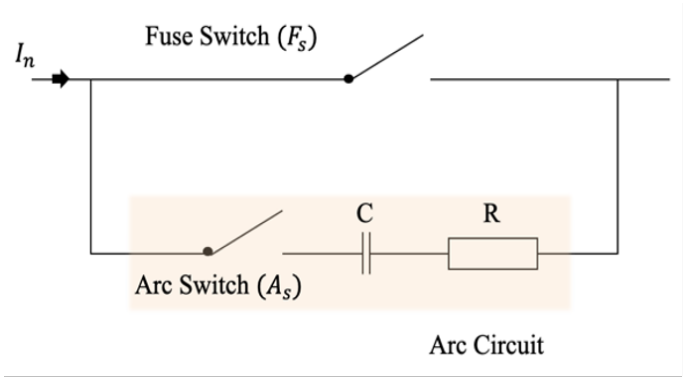

Figure 3.5: Equivalent Circuit of the Fuse when blown

3.2.2 Pyroswitch Sub-Model

The PS element within the Pyrofuse is an interrupter device that cuts into the conductor to isolate the fault. This disconnection is achieved by a small pyrotechnic charge actuating a miniature guillotine which cuts through the conductor [164]. An example of PS operation from [164] is illustrated in Figure 3.6. From this, The flowchart in Figure 3.7 summarises the control sequence of the PS model used to represent this disconnection under normal and fault conditions.

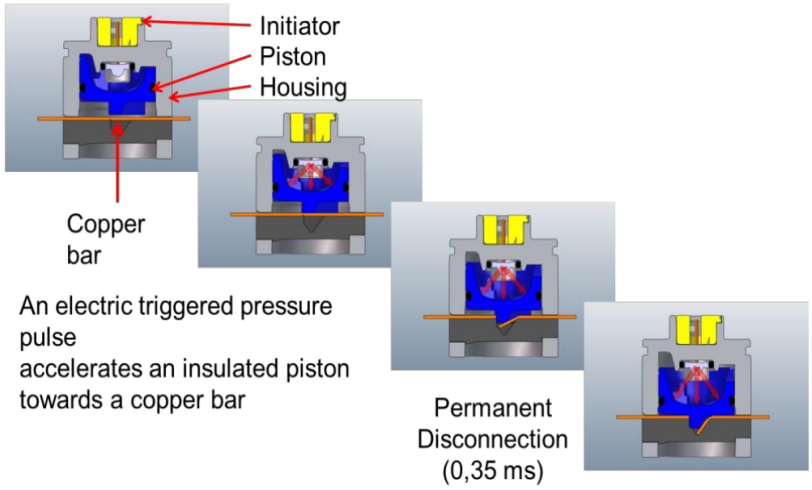

Figure 3.6: Illustration of the pyroswitch operation [164]

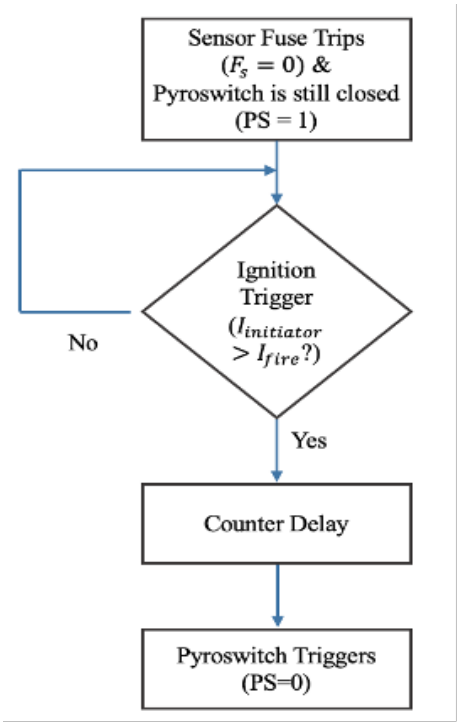

Figure 3.7: Flowchart of the Operating Conditions of Pyroswitch Device

As shown previously in Figure 1, when the F1 operates, the current is forced to flow through the $R_{ignition}$ into the PS component. When the current in the resistive path ($I_{initiator}$) exceeds the firing current threshold (I_{fire}), the guillotine operation

is activated. This action is emulated in the model by opening the associated switch element after a prescribed delay, representing the operating time of the guillotine (as specified on the product data sheets).

Under normal conditions F2 is in the closed state, but conducting minimal current (the PS element is considered to have a much lower impedance than F2). When the PS opens, current is diverted through F2, extinguishing any arc across the opened conductor of the PS.

3.3 Fuse Sub-Model Parameterisation and Testing

This section describes the parameterisation of the presented fuse sub- model using manufacturer's datasheet extracts, and validates the operating time of the modelled device against datasheet specifications. A 1000 V, 800 A FWJ fuse was chosen for this validation exercise [183].

The catalogue energy for the FWJ-800 A fuse was extracted from the manufacturer's TCC [183], based on melting time and corresponding current. In the presented case, this was facilitated by utilising a customised fit type function of a polynomial regression (3.2) to derive a mathematical representation of the TCC as a function of time. This equation represents the TCC curve for FWJ-800A from 5 kA to 30 kA. Figure 3.8 shows the comparison of the data obtained from the TCC with customised curve fitting Equation. The resultant customised function is shown in (3.3). In this work, the 9^{th} order for the polynomial regression equation was found as the most optimal order that best fits the data in the logarithmic scale.

$$\begin{aligned} E_c = {} & 8.431e4 + 2.963e7 \cdot (x) - 6.706e7 \cdot (x^2) + 1.879e8 \cdot (x^3) - 3.182e8 \cdot (x^4) \\ & + 2.779e8(x^5) - 8.538e7 \cdot (x^6) - 2.509e7 \cdot (x^7) + 1.528e7 \cdot (x^8) \end{aligned} \tag{3.3}$$

To validate the modelled melting time, a range of different steady state fault current values were injected into the model and the resulting melting times were compared with associated values in the datasheet. Table 3.1 shows this comparison for fault currents ranging from 8000 A to 25,000 A. It can be seen that the simulation results are typically

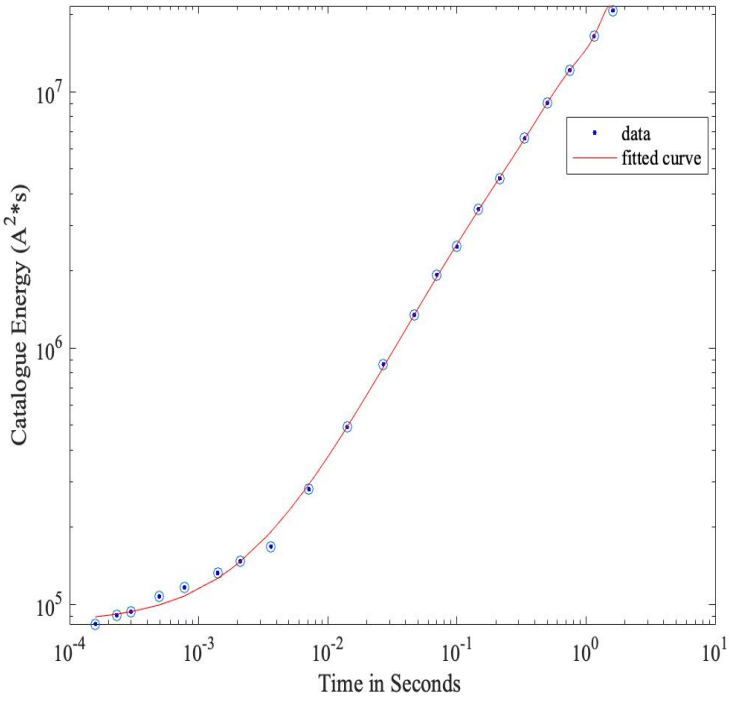

Figure 3.8: Curve-fitting the Catalogue Energy data and the Melting Time extracted from Manufacturer's datasheet using (3.3), where catalogue energy and time values are plotted using a base 10 logarithmic scale on the x-axis and y-axis [184].

within a ±10% tolerance of the data acquired from the TCC in the manufacturer's datasheet.

Table 3.1: Fuse Melting Time Difference between Simulation and Manufacturer's TCC

Fault Current (A)	**Datasheet Melting Time (s)**	**Simulation Melting Time (s)**	**Error (%)**
8000	0.00238	0.00249	5.04201681
8500	0.001982	0.001985	-0.1009082
9000	0.0017	0.00164	-2.3529412
9500	0.00142	0.001396	-2.1126761
10000	0.00133	0.0012	-9.7744361
15000	0.00036	0.00034	8.33333333
20000	0.00024	0.00023	-4.1666667
25000	0.000148	0.000144	-4.0540541

The arcing time can be deduced from the manufacturer's datasheet if the total clearing time is provided, as the arcing time is the difference between the the total clearing time and the melting time. However, that is not the case for FWJ-800 A fuse datasheet, so assumptions were required to represent the arcing time in the model. IEEE-1584 specifies that the fuse's arcing time can be set to 10% of melting time plus an additional 0.004 s [17]. If the melting time for a specific fault is less than 0.01 s, then 0.01 s is to be used for the arcing time [182].

Therefore, as the modelled fuse melting time was consistently less than 0.01 s, the modelled RC values were set for an arcing time of 0.01 s. For example, in case of a steady state fault of 20 kA occurring at 0.01 s, the fuse melts after a subsequent 0.00023 s, and since the 10% of 0.00023 s is less than 0.01 s, the modelled arcing time is thus set to 0.01 s. The resulting total clearing time of the fault is 0.01023 s. The arcing profile shown in Figure 3.9.

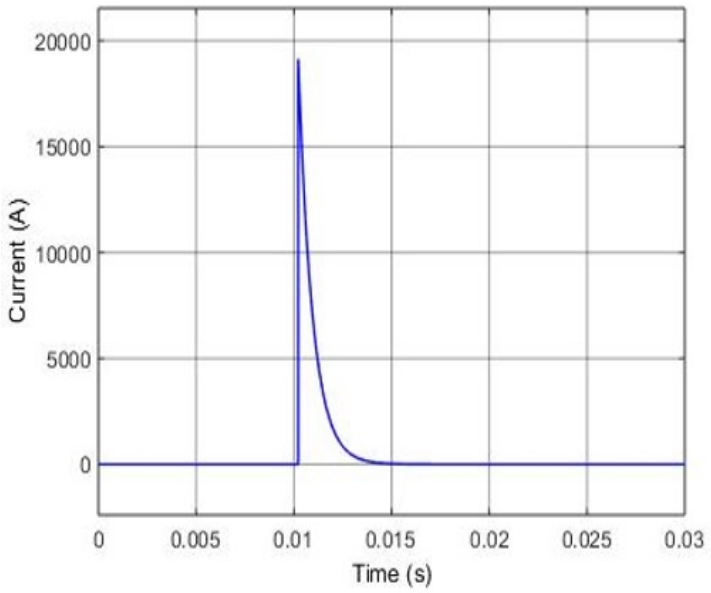

Figure 3.9: Arcing Current Profile through Arcing Path based on IEEE-1854 Assumption, using R= 1.77e-3 Ω, C=20e-3 F

Although the IEEE-1584 specifications are sufficient for second-based time frame applications, future DC eVTOL and electric aircraft applications are likely to feature fault transients based on a millisecond time frame. As such, further study is required

to derive a more accurate arcing time representation.

3.3.1 Model Limitations

Although the presented modelling method is comprehensive for performing an evaluation of Pyrofuse operation within an aircraft electrical system model, limitations of the model methodology exist and are presented below.

1. In case of intermittent faults, the fuse model does not account for the effect of the fuse's thermal cycling degradation after one fault peak.

2. When there is limited information in the manufacturer datasheet regarding the arcing time, assumptions or alternative calculations have to be made.

3. The model currently does not consider the ambient temperature of the fuse surroundings [16], nor the altitude impact on the Pyrofuse operating characteristics.

3.4 Pyrofuse Simulation

Using the presented modeling methodology, a representation of the Pyrofuse, as described in Figure 3.3, was modelled in Simulink, as shown in Figure 3.10. The following sections first show the model tested separately under different scenarios to illustrate the performance of the Pyrofuse model. Then a system level evaluation of multiple Pyrofuse models is performed using a simplified eVTOL power system architecture. The system level simulation demonstrates the tuning of multiple Pyrofuses to achieve protection coordination.

Table 3.2 shows the key parameters used for the power system model with an operating voltage of 600 VDC and a nominal current flow of ≈300 A. The datasheet used for obtaining the required parameters to model the fuses is given in [183].

3.4.1 Pyrofuse Permanent and Transient faults Tests

This section demonstrates the performance of the fuses and pyroswitch as a complete Pyrofuse model as shown in Figure 3.10. The current rating for the fuses in Figure

Table 3.2: Key Parameter Values used in Simulation

Key Parameters	**Value**
Circuit Voltage (Battery)	600 V
Circuit Current	$\approx$ 300 A
Cable Resistance (R)	0.1 m Ω
Cable Inductance (L)	0.01 μ H
DC Source Internal Resistance	0.053 Ω
DC Source Internal Capacitance	250 nF

3.10 is 350 A for F1, and 70 A for the parallel F2. For simplicity, the rating of the sensor fuse in this exercise is chosen to the nearest value of 120% of the nominal current and no de-rating values were applied. The model is tested by applying two transient self-cleared faults followed by a permanent fault as illustrated in Figure 3.11.

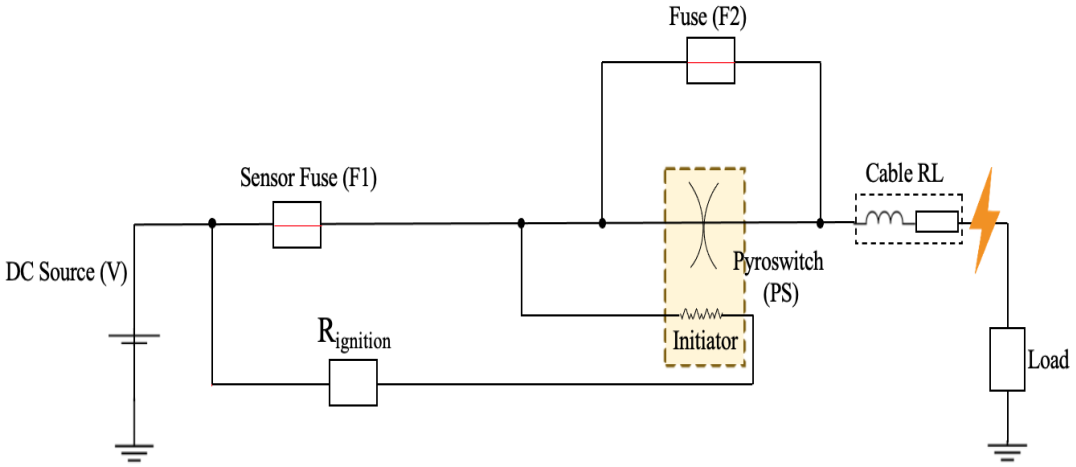

Figure 3.10: Complete Pyrofuse Model in Simulink

The short-circuit faults are applied across the emulated motor load terminals as indicated in Figure 3.10. To test the sensitivity of the Pyrofuse model it was tested with different fault impedances. The fault is emulated using a snubberless ideal switch of 0.028 Ω and 0.24 Ω, creating a transient current peak of 21.8 kA and 2.7 kA accordingly.

The first transient fault occurs at 0.01 s with a duration of 0.011 ms, and the second

at 0.015 s with a duration of 0.27 ms. It can be seen in Figure 3.11 that the first two transient faults do not cause the melting energy in F1 to reach the catalogue energy threshold. Figure 3.12 shows an a zoomed in capture of the melting energy versus the catalogue energy of F1 during the second transient fault. The melting energy was very close to reach the catalogue energy and trip the fuse. However, 0.27ms of fault transient was not enough to trip the fuse. Thereby a reset signal was issued when the two transient faults were self-cleared, as indicated in Figure 3.11, resetting the melting time accumulation to zero. Since the catalogue energy is also a function of time, the melting time accumulation feeds into the catalogue energy for the calculation; hence resetting the catalogue energy. This restrains F1 from tripping the circuit. In practice, there may still be some thermal energy transiently retained in the fuse element, shortening the subsequent melting time.

When the permanent fault occurs at 0.02 s, the melting time starts accumulating. As the catalogue energy and melting energy are a function of time, the energy calculation starts with the melting time accumulator as seen at 0.02 s in Figure 3.11. The extended fault duration causes the melting energy to exceed the catalogue energy and thus F1 trips at 0.02019 s (0.19 ms after fault occurrence). The current starts to flow into the resistive path. After passing a threshold specific to the PS, it is triggered and hence the circuit is cut at 0.0207 s (0.7 ms after fault occurrence). Immediately after the circuit is cut, the low rated current of F2 trips 0.1 ms after the PS has tripped, at 0.0208 s, extinguishing the arcing from F1 and F2. The tripping sequencing of F1, PS and F2 is shown in Figure 3.13. Thus the total clearing time of the PS model is 1.6 ms for a 21.8 kA low impedance fault.

The Pyrofuse model was also tested for a higher impedance fault, where a current of 2.7 kA was injected in the model at 0.02 s. With this fault type, F1 tripped at 0.4048 s after the fault occurrence, the PS then cut the circuit at 0.4063 s (1.5 ms after F1 tripping), and F2 tripped at 0.4064 s. Following the extinction of the circuit arcing, the total fault clearing time was 0.432 s.

Moreover, Figures 3.11 and 3.13 show that the tripping sequence of the individual component models in the Pyrofuse model is working as required, and show the stability

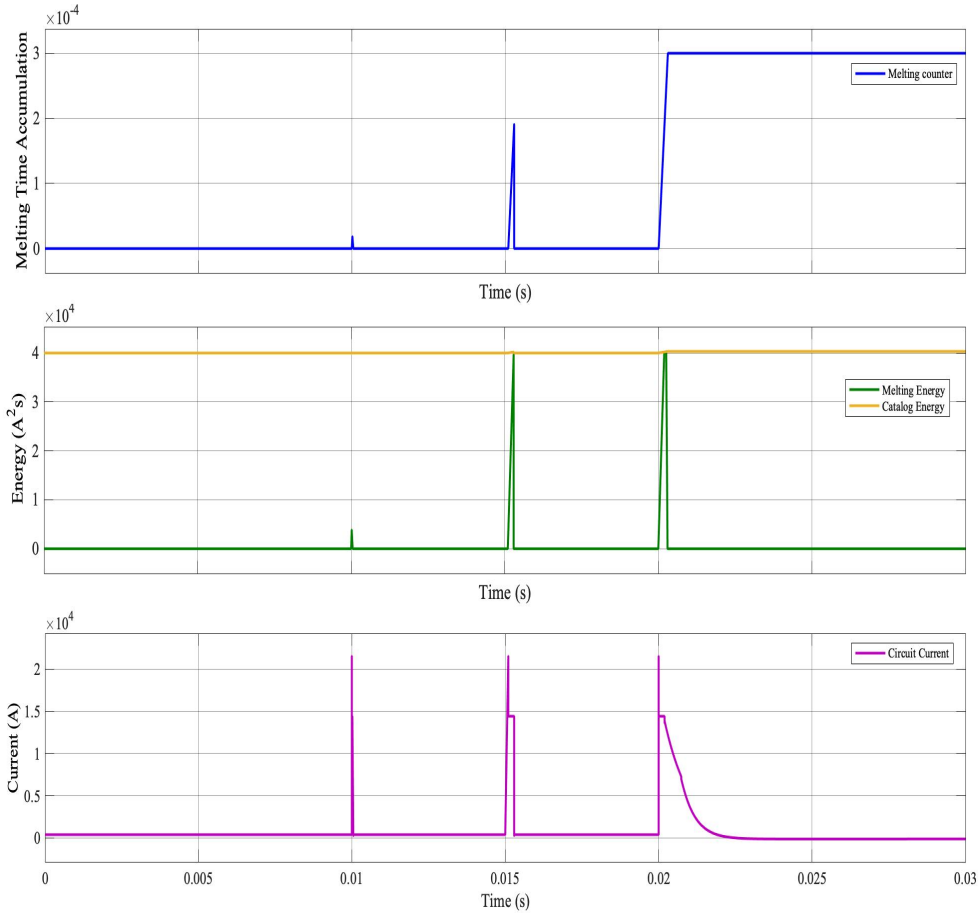

Figure 3.11: Performance Results of Sensor Fuse in the Pyrofuse Model under Short-duration and Permanent fault at 21.8.kA

of the Pyrofuse under transient fault conditions. The coordination of multiple devices in a circuit is explored further in the following case study.

3.4.2 Pyrofuse Coordination Validation

A simplified circuit to represent a single branch in a generic eVTOL aircraft power system architecture was modelled in Simulink, as shown in Figure 3.14. The generic model is utilised to illustrate the protection grading and coordination of multiple Pyrofuse models for effective full-system protection. In this manner, only the Pyrofuse devices in the nearest upstream location of the fault should operate in order to preserve the security of supply to the loads where possible. The key parameters used in the circuit are given in Table 3.2 (shown earlier), while the ratings of the fuses used

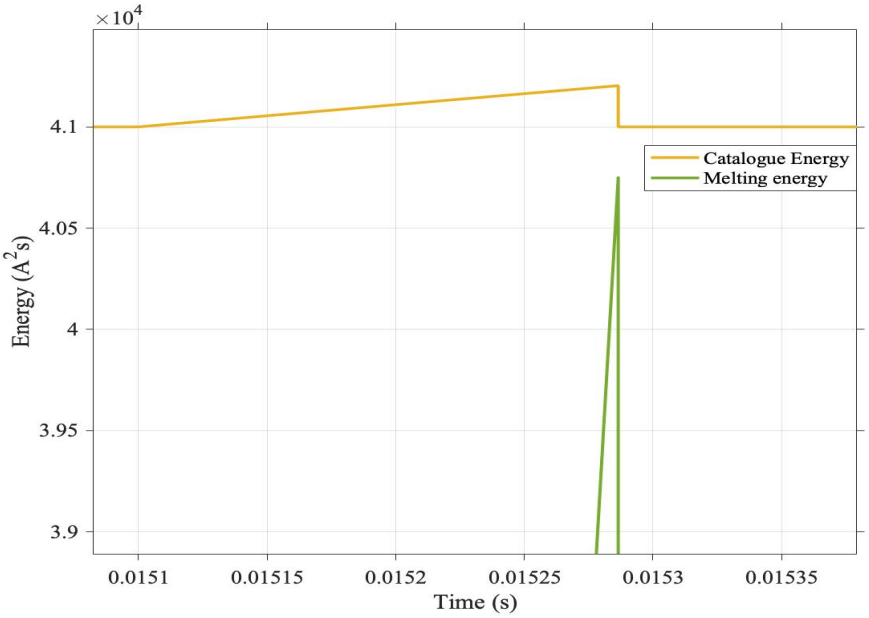

Figure 3.12: F1 Melting Energy versus Catalogue Energy during the second transient fault at 0.015s

in the different Pyrofuse models are given in Table 3.3; these are the sensor fuse (F1), and the parallel fuse (F2).

Permanent short-circuit faults were applied at different locations in the power system architecture. These faults were initiated at 0.02 s of simulation time and were realised using a snubberless ideal switch of 0.028 Ω, causing a theoretical transient peak in the circuit of 7.5 kA. The location of the injected faults is illustrated in Figure 3.14:

1. Across the emulated motor load terminals.

Table 3.3: Fuses rating selection for the Pyrofuses model in Figure 3.14

Device Model	**Sensor Fuse (F1)**	**Fuse (F2)**
Pyrofuse-350 A	FWJ-350 A	FWP-70 A
Pyrofuse-600 A	FWJ-600 A	FWP-100 A
Pyrofuse-800 A	FWJ-800 A	FWP-150 A

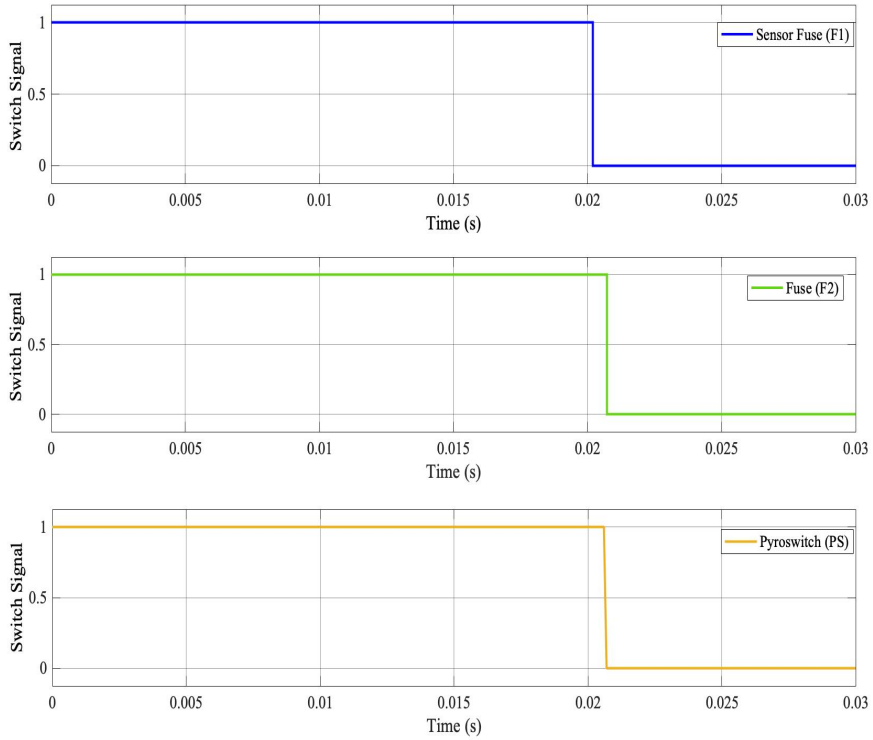

Figure 3.13: The Sequence of the Fuses and Pyroswitch tripping in the Pyrofuse Model for a fault of 21.8 kA

2. Between Pyrofuse 600 A and the DC Bus.

3. Between Pyrofuse 600 A and Pyrofuse 800 A.

Table 3.4 shows the operating times of various elements of the modelled Pyrofuse devices in different fault locations (Figure 3.14). For each of the fault locations, it can be seen that only the Pyrofuses nearest to the fault operate, enabling a continued supply of power to the healthy load. For instance, a fault in location 1 (see Figure 3.14) has only tripped the Pyrofuse nearest to the fault location hence isolating Load-1, while the upstream Pyrofuses (Pyrofuse 600 and Pyrofuse 800) and the downstream Pyrofuse-350 of Load-2 are still connected providing uninterrupted power to Load-2. [However, it is important to note that in reality, the uninterrupted current flow and continuous system operation are dependent on the motor's capability to withstand a dip in voltage caused by a fault for a certain period of time. This is one of the protection requirements that determines the selection of the Pyrofuse. The Pyrofuse should be chosen based on

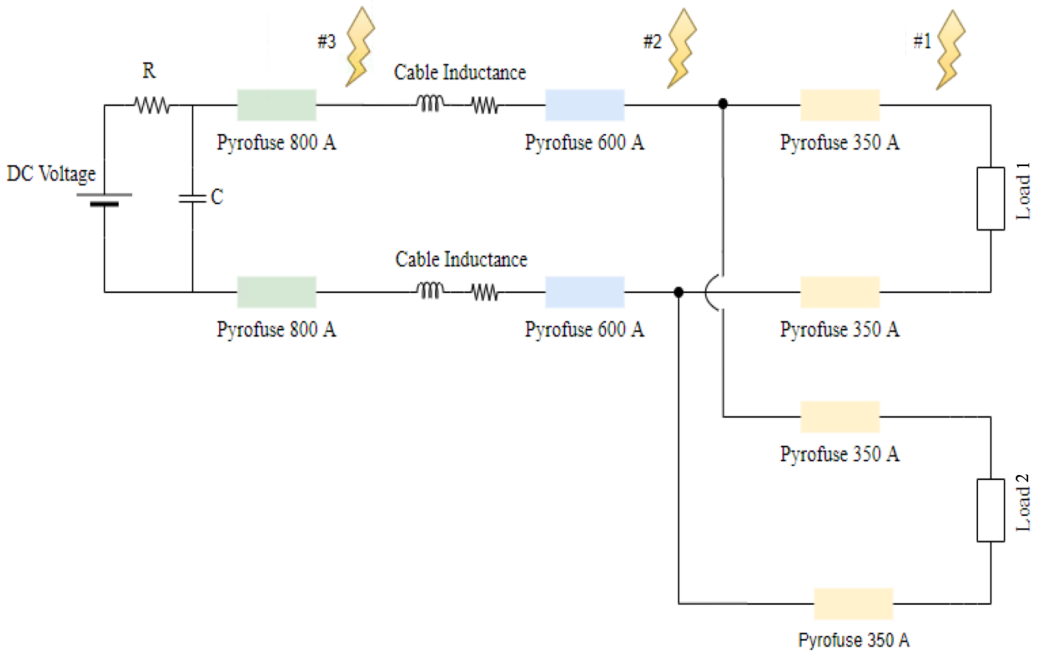

Figure 3.14: Simplified Model of a Single branch of eVTOL Power System Architecture

its ability to clear the fault and recover the voltage of the system within the motor's capability to withstand the dip in voltage, while maintaining graded protection in the system.

Table 3.4: Operating times of Pyrofuse elements for fault locations 1-3

Fault location	**Pyrofuse 350**	**Pyrofuse 600**	**Pyrofuse 800**
Fault #1	F1 = 0.0214 PS = 0.0222 F2 = 0.0223	None	None
Fault #2	None	F1 = 0.0238 PS = 0.0247 F2 = 0.0248	None
Fault #3	None	None	F1 = 0.0247 PS = 0.0256 F2 = 0.0259

The results demonstrate that sensitivity and coordination of multiple Pyrofuses in a circuit is achievable; where in this study, only the Pyrofuse nearest to the fault location operated and isolated the fault. Additionally, the results shows that the tripping sequence of the components in each of the Pyrofuse models are as expected.

3.5 Summary

In response to the high demand for advancements in light-weight, high voltage protection devices available for near term applications, this chapter presents the first published methodology for a complete circuit model of a Pyrofuse. The presented model in this chapter is the first step into answering the second research question of this thesis by enabling the exploration of the design characteristics and operation of Pyrofuses within a DC system.

The Pyrofuse model has been shown to successfully remain stable during short-duration transient faults whilst clearing permanent low impedance faults in millisecond timescales, and shows sensitivity to high impedance faults. In addition, the tunability of the Pyrofuse device for use in a graded protection system has been demonstrated. This functionality, along with the potential for use of externally tripped devices, suggests that good protection coverage against a range of faults and failure modes can be realised with a purely Pyrofuse based protection system.

Following the identification of the Pyrofuse as a possible option for overcurrent protection, yet Pyrofuses are non-resettable which presents challenges for use as a primary protection for the EPS. Where the EPS is subject to overvoltage transients due to various scenarios such as lightning strikes, switching impulses, thus can lead to nuisance tripping of all Pyrofuses in the system. Further analysis to investigate the Pyrofuse behaviour under overvoltage events, and address a mitigation plan to prevent mass tripping of the devices and damages to sensitive components in the EPS. As such, Chapter 4 presents further exploration work is required to assess the potential compliance of a Pyrofuse-based protection system with regulatory rules for potential use in eVTOL or other aerospace applications.

Chapter 4

Pyrofuse Certification Requirements and Compliance in eVTOL Applications

The presented modelling methodology of a self-triggered Pyrofuse in Chapter 3 have demonstrated the capability of using Pyrofuse for graded protection across the EPS architecture. Although the results showed that the Pyrofuse can successfully clear different impedance faults within milliseconds and whilst achieving good stability during other short-duration transients. However, it is important to consider that the Pyrofuse is a non-resettable device, whose use may be potentially challenging to certify in eVTOL aircraft. This aspect has not yet been explored sufficiently in the research literature. NASA has published FHA and failure modes and effects analysis (FMEA) studies focused on different eVTOL aircraft configurations in order to abstract safety and reliability requirements [185]. However, these studies do not consider safety requirements specific to the use of NRPDs for primary protection nor do they address the challenges of demonstrating airworthiness at the system/aircraft level.

To address this potential issue, this chapter presents a first of its kind preliminary certification compliance assessment for the use of NRPDs, such as Pyrofuses, in eVTOL concept designs. To underpin the development of the methodology, the chapter first provides an overview of U.S FAA and EASA approaches to eVTOL certification. This

is then followed by a summary of key FAA and EASA certification rules which are specific to the implementation of electrical protection devices in aircraft. Additional requirements and constraints around the use of NRPDs are then derived from FHAs, each one specific to a particular configuration of eVTOL aircraft. These categorise the resultant system behaviour, and more specifically, the impact on available thrust arising from a single or series of failure events, with the implications of implementing NRPDs defined. In addition, potential hazards which could lead to common failures are highlighted, with proposals made for the mitigation of these. Building on the outcome of the FHA, potential power system location-specific roles of NRPDs are then considered, highlighting a natural opportunity for use in the protection of power sources and propulsion motors. This chapter concludes with summative discussions on the future of NRPDs in eVTOL applications and on further research required for more wide- spread implementation.

4.1 Certification Guidelines

This section presents certification requirements from the EASA and FAA regulatory bodies that are applicable to the deployment of NRPDs in eVTOL applications. It should be noted at this point that the formulation of regulations is still ongoing with the certification process also still under development/amendment. As such, this chapter lists the latest version of amendments and regulatory advice available at the time of writing.

4.1.1 Approaches to eVTOL Certification

One of the main approaches to certification for the past 5 years was through the utilisation of the FAA revised Part 23 (airworthiness standards for small aircraft) in accordance with Part 21.17(a) for winged eVTOL, and wingless eVTOLs which are considered as a special class powered lift aircraft under Part 21.17(b) [48, 49] The accepted means of compliance (MOC) within Part 23 is ASTM 23-64, where the F44 committee has recently updated the MOC for the certification of small electric aircraft [186, 187].

Building on this, the European regulatory board, EASA, has proposed the new special conditions with associated MOC for VTOL certification, which are extensively based on CS-23 and elements of CS-27 [50, 188]. The UK Civil Aviation Authority (CAA) has adopted EASA's special conditions certification standards for eVTOL aircraft [189]. The FAA and EASA requirements for type certification are performance-based instead of being prescriptive design rules; this is in order to accommodate the continuous development in technologies and novel aircraft designs.

More recently, the FAA has modified its approach to certifying eVTOL aircraft through FAA part 21.17(b) as special class powered lift aircraft for all eVTOL types [49, 190, 191]. This certification approach is tailored for aircraft with novel technologies or designs that the current regulations do not cover, which includes applications such as electric propulsion, tilt-rotor, tilt-wing, advanced flight control, etc. [190]. This regulation combines all the policies of Parts 23, 24, 27, 29, 33, and 35 together, providing appropriate standards for the innovative aspects of eVTOL aircraft. As such, the FAA encouraging early-stage engagement with aircraft developers in order to identify these potential gaps in regulations [190, 191].

4.1.2 Requirements for Non-Resettable Protection Devices

More specific to electrical protection devices, Part 23 and EASA's special condition provide the following circuit breaker and fuse circuit protection requirements for certification:

1. "If the ability to reset a circuit breaker or replace a fuse is essential to safety in flight, that circuit breaker or fuse must be so located and identified that it can be readily reset or replaced in flight." According to 23.1357(d) [192] and CS 23.1357 [193]. The definition of "essential to safety" according to CS 23.1357(b) amendment 3 is that, "Essential to flight safety is related to those whose failure are classified as "major," "hazardous," or "catastrophic".

2. "When the failure condition of the loss of the function is determined to be "major," "hazardous," or "catastrophic" [according to § 23.1309 and AC 23.1309-1E

safety assessment, which also considers operational and airworthiness requirements], it has a significant impact on safety in flight and is considered "essential to safety in flight" [192, 197].

3. According to 23.1357(b) "Protective devices, such as fuses or circuit breakers, must be installed in all electrical circuits other than – (b) a protective device for a circuit essential to flight safety may not be used to protect any other circuit" [192, 193].

4. "Each resettable circuit protective device ("trip free" device in which the tripping mechanism cannot be over-ridden by the operating control) must be designed so that (2) if an overload or circuit fault exists, the device will open regardless of the position of the operating control". 23.1357(c)(2) [192, 193].

4.1.3 Challenges in the Certification-Compliant Use of Non-Resettable Protection Devices

Considering all of these requirements further, it is clear that it is necessary to first determine the impact of a failure in the systems/subsystems protected by non-resettable devices. Where the aircraft/EPS design is such that the impact of a failure is considered to be less severe than 'major', there appears to be a degree of freedom in the use of non-resettable devices. However, if the impact of any associated failures is considered to be 'major' or worse, then significant restrictions will apply.

In this manner, point 1) effectively impedes the use of non-resettable devices as primary protection devices in most applications with a 'major' or worse failure severity unless it can be shown that the need to reset such devices is not essential to safety in flight or that device replacement is possible. As it is likely to be difficult to replace Pyrofuses manually and in a timely manner in flight, it is therefore necessary to demonstrate that the likelihood of potential causes for the need to reset devices in flight, e.g. spurious maloperation due to failure effects such as EMI, lightning strike or thermal ageing, is sufficiently low.

The requirements laid out in point 2) place restrictions on the design of the non-

resettable devices and the surrounding EPS, requiring that the impact of a single failure does not cause a 'major' or worse impact to flight safety. Assuming that the loss of the protected system will result in this condition, it is therefore necessary to either demonstrate that the protection device design is single fault tolerant or to revisit the EPS design so that the loss of the protection device no longer results in this condition.

In point 3), the requirement to use separate protection devices for essential-to-safety loads to prevent a protection response to failures in non-essential loads causing a subsequent loss an essential function can be readily demonstrated. Additionally, according to point 4), each resettable device must be designed to isolate a persisting fault regardless of the location and not be resettable by operating control [194]. This is readily also the case for naturally non-resettable devices, yet assurance is required to show that the device will not trip under nominal operating conditions and severe load transients.

4.2 Propulsion-Focused Functional Hazard Assessment of Different eVTOL Configurations

As the impact and severity of propulsion failures on an aircraft are influenced by its aerodynamic configuration and propulsion design, the acceptability of the use of non-resettable primary protection devices will be in part, shaped by the design of the aircraft configuration, and electrical and propulsion systems. Methods like FHA [195, 196] are necessary to derive the architecture-specific severity of failures of subsystems which are considered essential to flight safety, helping shape the acceptability of the use of NRPDs in these applications. The FHA is initiated at the beginning of the aircraft development cycle. The FHA starts with identifying failure of each function in the system. Then, identify the effect of the loss of this function on aircraft and passengers. The definitions and classification of failure conditions (i.e., minor, major, hazardous, and catastrophic) according to the severity of a fault and impact on aircraft and passengers as based upon AC 23.1309-1E [197] are shown in Table 4.1. The failure condition severity determines the quantitative safety objective or the functional development assurance level (i.e.

probability of occurrence of a single failure condition: 10^{-3} per flight hour for major, 10^{-5} per flight hour for hazardous, etc.) as given in Table 4.1. As the aircraft development progresses, new functions or failure conditions might arise which in turn requires the FHA to be updated. As such, the FHA is a continuous and iterative process to best represent the final aircraft and system design. The process of system design and safety assessment to demonstrate compliance to certification bodies is further discussed in Chapter 5.

Table 4.1: The Definition of Failure Conditions According to the Severity of a Fault and its Impact on the Aircraft and Passengers.

Failure conditions	**Failure Impact on Aircraft**	**Quantitative Safety objectives**
Negligible	No effect on safety margins, aircraft functional capabilities, or passenger comfort.	-
Minor	Slight reduction in safety margins or functional capabilities of the aircraft, resulting in physical discomfort to passengers.	$\leq$ 1x10^{-}3
Major	Significant reduction in safety margins or functional capabilities of the aircraft, resulting in physical distress to passengers. Aircraft can continue safe flight but at reduced efficacy	$\leq$ 1x10^{-}5
Hazardous	Large reduction in safety margins or functional capabilities of the aircraft, resulting in serious injury to passengers. Aircraft descent possible but with limited control.	$\leq$ 1x10^{-}7
Catastrophic	Loss of the aircraft and the inability to continue flight or land safely resulting in passenger injuries or fatalities.	$\leq$ 1x10^{-}8

This section presents FHA studies for three conceptual eVTOL design configura-

tions. These are 1) multirotor, 2) vectored thrust, and 3) lift+cruise. A brief description of these configurations is presented to support each FHA and underpin later understanding of the unique resultant failure behaviour.

4.2.1 Multirotor Configuration

Multirotor configurations are wingless aircraft with fixed axis distributed electric motors, utilised for powered lift during the hovering and cruise phases. The large combined total rotor surface area provides an improved hover capability but with reduced cruise speed and efficiency compared with other eVTOL configurations. These attributes make this eVTOL type best suited for short distance transportation [15]. As this concept consume high amount of energy during cruise and with the low TRL of batteries with high energy density viable for multiple missions profile, companies adopting this concept design has declined considerably due its unviable economical and technological design. The power and energy consumption of this concept is further investigated in Chapter 5.

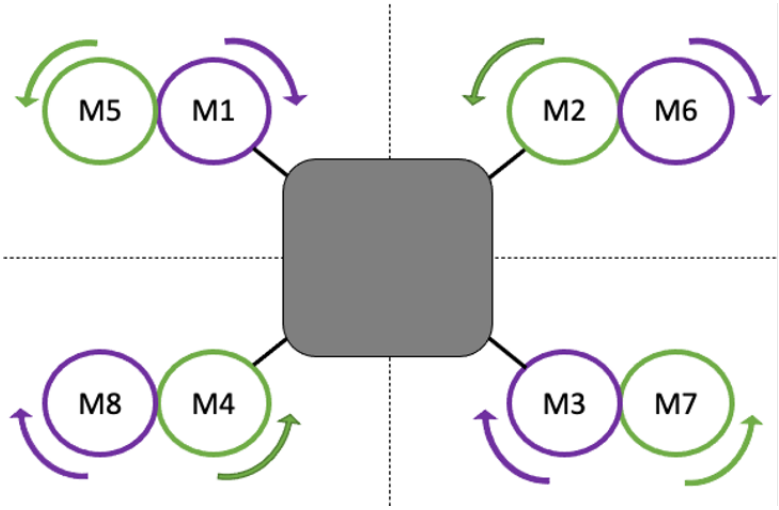

Figure 4.1: Example of a Multirotor Configuration (based on City Airbus demonstrator [32])

Figure 4.1 shows an illustration of a multirotor eVTOL configuration. This particular example is a quadrotor configuration with stacked motors and fans adopted from the concept of City Airbus demonstrator [32]. The motors are coloured differently to

illustrate the clockwise and anticlockwise rotation of the rotors.

The example in Figure 4.1 shows a multirotor with 8 motors, where each 2 motors are stacked. The loss of one motor in a stacked 8-motors configuration would create an offset from nominal hovering states requiring the opposite motor to reduce power in order to balance the resultant asymmetric thrust, effectively reducing the number of thrust-producing motors to 6. The loss of any further motor will result in the ability of the aircraft to provide control and maintain altitude. In conclusion, for a multirotor configuration with less than 10 motors, any loss of the available motors is likely to be a classified as a major failure or worse, unless a significant degree of oversizing is employed in the propulsion motors and associated drives.

However, for a multirotor configuration with 10 motors or more, the loss of one motor would leave a minimum of 8 effective motors remaining (allowing for symmetric thrust balancing). As such, even the loss of a further motor should at worst lead to there being 6 remaining useful motors, from which, continued flight at a reduced efficacy would be assumed to be possible. Accordingly, the loss of a single motor would likely be classified as a minor failure, assuming that appropriate motor oversizing and off-nominal flight control is implemented.

Based on this analysis, the use of NRPDs for system protection functions cannot be used in multirotor configurations of less than 10 motors where the loss of the protection device can lead to a major failure at best. In multirotor configurations featuring 10 or more propulsion motors, NRPDs could potentially be utilised as long as the loss of a single protection device does not lead to more than 1 propulsion motor being lost, or if it does, that the worst case loss of propulsion motors does not constitute as a major or worse failure.

4.2.2 Vectored Thrust Configuration

Vectored thrust configurations utilise DEP along with a wing to generate additional lift during the cruise phase. Thrust vectoring or the tilting of propulsion fans is employed for cruise thrust. This type of configuration possesses attractive advantages over multirotor designs in that it combines a vertical take-off capability with higher

cruise efficiency [15]. However, the tilting mechanisms of the vectored thrust configurations present additional reliability considerations during the transition phase, where the tilting actuators represent an additional failure point in the system [198, 199].

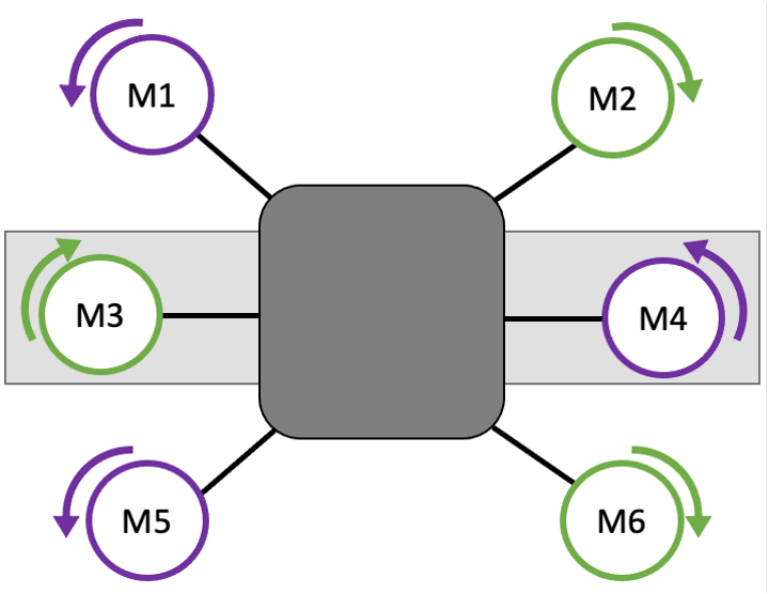

Figure 4.2: Example of Vectored Thrust Configuration (based on Joby aviation's concept [7])

Figure 4.2 shows an example of a vectored thrust configuration with 6 rotors, where M3 and M4 are the wing tip motors. The motors are coloured differently to represent the clockwise and anticlockwise rotation of rotors, where each motor is rotating in the opposite direction to the adjacent motors to produce balanced torque. The shaded grey rectangular box represents the aircraft wing.

Similar to the multirotor configuration, the number of installed motors on the UAM platform has a large impact on the nature of the failure conditions and their associated severity classification. As before, the loss of a single motor is likely to require a reduction of thrust from an additional motor in order to symmetrically balance thrust. As such, it can be assumed again that for vectored thrust configurations with less than 10 motors, the loss of a single motor considerably impacts the safety margins of the aircraft, resulting in a major failure classification unless significant oversizing is employed. Whilst the aircraft can be designed to land safely with only wingtip motors operating in

conventional flight mode (hence potentially accommodating the failure of several other motors), this ability is clearly dependent on the availability of the wingtip motors and hence does not reduce the failure severity of non-wingtip motor loss. Similar to the multirotor configuration, the loss of one motor in a vectored thrust aircraft with more than 10 motors would likely result in a minor failure condition.

On this basis, the use of NRPDs for system protection functions could only be considered in vectored thrust configurations with less than 10 motors where the loss of the protection device can be shown never to directly lead to the equivalent loss of one or more propulsion motors. While the conditions for the use of NRPDS in vectored thrust configurations for 10 motors and more are the same as multirotor configuration with 10 motors and more. However, the increased criticality of the wingtip motors is such that the use of NRPD's for the protection of these subsystems is unlikely to be possible without the incorporation of additional redundancy measures.

4.2.3 Lift + Cruise Configuration

The lift+cruise configuration is similar to the vectored thrust design but with a mixture of fixed and tilting propellers rather than all rotors being fully tilting or vectoring [200]. An example of this architecture is shown as Figure 4.3. The fixed propulsion rotors are mounted for the hovering phase with a reduced blade count to reduce drag. In hovering mode, all the propulsion rotors are used to lift the aircraft, while for cruise phase only the tilting propulsion rotors are used for generating longitudinal thrust with the lift support from the wing. The fixed propulsion rotors can provide additional lift thrust and redundancy for VTOL operations. The tilting components have increased criticality as they provide control during all phases and facilitate manoeuvring necessary for safe landing.

An example of a lift + cruise configuration with 4 tilting rotors and 4 fixed VTOL rotors is shown in Figure 4.3. The shaded grey rectangular box represents the aircraft wing with 6 mounted motors. The motors are coloured differently to represent the clockwise and anticlockwise rotation of thrust, and the colour filling represents the tilting rotors that provide thrust generation during both lift and cruise. Each motor

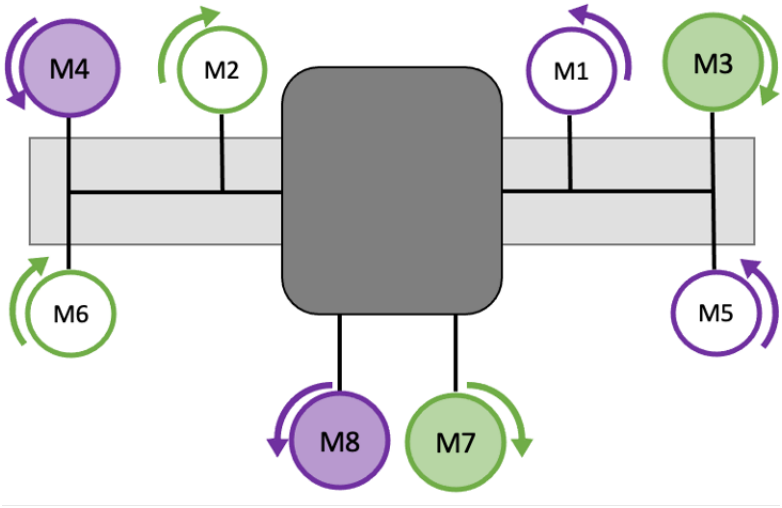

Figure 4.3: Example of Lift+Cruise Configuration (based on Hyundai S-A1 concept [39])

is rotating in the opposite direction to the adjacent motors in the opposite axis to generate balanced torque.

The loss of any single motor in a lift + cruise configuration with fewer than 10 motors is likely to result in a hazardous failure condition, restricting the use of NRPDs in the manner described for previously considered configurations. In addition, the increased criticality of the tilting motors may also prevent the application of NRPDs for their protection without the implementation of additional subsystem or system-level safety features.

4.3 Causes of Common Failures Modes and Impact on the Use of Non-resettable Devices

Once the system-level classification of thrust-loss failure conditions has been established, it is then necessary to consider the potential root causes of common mode failure conditions that might impact on the requirements and use of NRPDs. In doing so, any need for additional protection, redundancy and fail-safe mechanisms can be identified.

Table 4.2 shows a range of potential electrical common failure modes which could

lead to the loss of a propulsion motor and which are ultimately relevant to the considered use of NRPDs. These include short circuit line-line and line-ground faults, lightning strikes and EMI. For each of these failure conditions, the potential effects on the EPS and propulsion system, and associated protection system requirements are described. Further discussions around these failure modes are provided in the following subsections.

Table 4.2: Causes of Key Electrical Common Failure Modes and the Impact on the EPS with Associated Protection Devices.

Root cause	**Effect on the system**	**Protection Requirements**
Short circuit fault (line to line and/or to ground)	Large current and voltage transients (unless fault is to IT ground or high-resistance ground). High energy at point of fault. Electrical equipment in fault path may also be damaged.	Fast isolation of fault, minimisation of the extent of isolation of healthy equipment, and timely restoration of power supply to remaining loads.
Lightning strike	Transient high voltage/current waveforms. May induce multiple or common-mode failures.	Inclusion of overvoltage protection. Diversion of high transient energy away from sensitive electrical systems to avoid/minimise damage and other disruption to operation.
Electromagnetic Interference (EMI)	Disturbance to, and potential maloperation. of aircraft systems and electronic devices.	Shielding, filtering, and proper bounding to suppress EMI propagation.

4.3.1 Short Circuit Faults

Following the occurrence of a short circuit fault on an EPS and propulsion system, the electrical protection systems should isolate the faulted components from the remainder of the EPS network in as short as time as possible [178]. In addition, protection devices whose operation is not required to isolate the faulty equipment should not trip, as doing so may lead to a more widespread loss of thrust. Hence, the use of NRPDs requires the early identification of potential short circuit cases which may cause the (mal)operation of multiple protection devices. In particular, previous studies have identified the risk of fault-induced capacitor discharge events in DC power systems leading to the tripping of multiple overcurrent protection devices [201] which would require careful attention

if non-resettable devices were to be utilised.

4.3.2 Lightning Strike

Lightning strike-induced current and voltage surges can be damaging to the carbon fibre material used in the aircraft surface as well as its internal structure and joints [202]. In addition, the electrical surges can cause damage to the propeller structure or cause misalignment of the motor bearings which could potentially lead to motor failure [203]. This necessitates adequate surface protection to shield the lightning surges from damaging the carbon fibre material and entering the EPS [204]. Methods used to minimise/prevent damage include the design of passive surface protection according to lightning zoning on the aircraft, which identifies the probability/severity of the lightning current magnitude at different locations on the aircraft [204, 205]. The embedded metallic mesh and diver tips used in this create a conductive path for the large current to flow, diverting the current away from sensitive components to a suitable exit point without causing hazardous damage [204].

Yet, a lightning strike could still potentially enter the electrical system indirectly through the cables and cause damage to its insulation and sensitive devices. This could potentially result in a catastrophic condition where multiple protection devices trip due to the induced voltage and current surges. This failure scenario is particularly concerning for non-resettable devices, where the mal-triggering of protection could lead to a significant reduction in available thrust, with no option to subsequently restore service. Hence, it will be necessary to assure the effectiveness of a dedicated EPS overvoltage protection strategy for indirect lightning effects against mal-tripping of non-resettable circuit protection devices before their use could be considered.

4.3.3 Electromagnetic Interference (EMI)

The key concern around the impact of EMI on the utilization of NRPDs in aircraft applications relates to the use of external triggering of these devices, where EMI may potentially cause maloperation of any digital and electronic systems on the aircraft. This will cause the external triggering device to erratically trip all the Pyrofuses on

the aircraft. Consequently, the software used for the triggering control of the Pyrofuses must demonstrate the highest level of design assurance level (DAL) of 1x10-9 per flight hour. This will necessitate redundant controls with immunity to EMI effects. The recent published patent in [206] has proposed a method for redundant control of externally triggered Pyrofuse consisting of digital signal and analog-to-digital signal to that addresses common mode failures, yet demonstration of immunity to EMI effects is required.

Currently used methods of EMI suppression/containment include cable shielding and filters [208, 209]. In particular to Pyrofuses, the use of a self-triggered Pyrofuse device can provide an additional layer of mitigation.

4.4 Impact of Protection Device Location

The final stage of analysis required for potential use of NRPDs is the consideration of their location within the EPS. In this manner, the impact of the loss of the device or failure to reset can be established. For consistency, the author recommended quantifying the extent of the impact in terms of number of motors lost (drawing on the FHA, and associated linkage to requirements, conducted previously). In this manner, it will be possible to evaluate whether the anticipated EPS configuration may alleviate or compound the severity of a failure associated with loss of a particularly protection device.

The following sub-sections consider the application of non-resettable devices at broad locations within an eVTOL EPS; protecting the feeders to motor drives, protecting the power distribution system busbars and interconnecting cables, and providing energy source isolation/protection.

4.4.1 Source and Source Feeder Protection

Protection devices at the terminals of electrical energy sources (e.g. batteries) or their designated interfaces typically provide two functions. The first is to disconnect the energy source if an electrical fault occurs within the supplied element of the EPS that

cannot otherwise be removed by another dedicated protection device (or if that dedicated device has failed to operate). The second function is to isolate the source from the EPS if the source itself fails (e.g. as a result of an internal short circuit event). This second function may require an external trip capability within the device as self-tripping due to overcurrent transients may not be possible. For non-resettable devices, this external trip requirement may impact on the resilience to EMI-related spurious trip issues.

The impact of a energy source loss (as a result of the loss of an associated non-resettable protection device) on the number of available thrust motors is ultimately determined by the number of energy sources utilised in the eVTOL EPS, the level of interconnectivity between sources and propulsion motors, and the extent of power and energy capacity overrating in the energy sources. In this manner, if an eVTOL aircraft utilised only 2 energy sources, the loss of a single battery would likely result in hazardous failure condition, even if appropriate EPS interconnectivity and source overrating were implemented, as the further loss of a energy source would be catastrophic. However, in aircraft with 3 or more energy sources, the loss of one battery could potentially result in major failure condition and the aircraft could still tolerate a further failure without catastrophic consequences. In this scenario, non-resettable devices could potentially be used for this protection function, even if the aircraft itself, features fewer than 10 motors otherwise additional considerations required for motor feeder protection, as long as the risks of common-mode failure-driven multiple protection device losses are acceptably low. On this aspect, if the risks of EMI-related spurious trips for externally triggered non-resettable devices cannot be sufficiently mitigated, the use of a separate resettable contactor might offer a useful alternative.

4.4.2 DC Busbar and Interconnecting Cable Protection

The DC busbars and interconnecting cabling are the main power transmission links in the EPS, ensuring flexible and redundant power flow from the energy sources to the propulsion motors. Protection devices for these systems must be fast acting against faults on the protected equipment, whilst being restrained to responding faults else-

where in the EPS.

Similar to a source loss, the impact of a loss of a busbar or interconnecting cable (as a result of the loss of an associated non-resettable protection device) on the number of available thrust motors is ultimately determined by the level of interconnectivity between sources and propulsion motors, and the extent of power and energy capacity overrating in the energy sources. In addition, the impact of combinatorial faults must be considered, whereby the loss of a busbar or cable may result in a more severe consequence of a subsequent source loss. In this sense, in highly interconnected networks, the loss of a busbar or interconnecting cable actually may be more severe (i.e. resulting in a greater number of propulsion motors lost) than the loss of a source or motor feeder. Consequentially, unless a large number of low-connectivity busbars are implemented, it is unlikely that the use of non-resettable devices for their protection will be possible. Split or ring-bus arrangements may offer a route to lessening the severity of a bus protection device loss (i.e. leading to only a partial bus loss), although if busbar sectioning is realised with non-resettable devices, the risk of common-mode faults (for example due to DC fault transients) must be shown to be sufficiently low.

4.4.3 Propulsion Motor and Feeder Protection

Protection devices for propulsion motors, drives and feeders is primarily required to act quickly in response to a fault on the protected cable and equipment in order to minimise the disruption to the remainder of the EPS, and prevent the operation of backup protection at the busbars or energy sources.

The impact of a protection device loss on the number of motors lost here is easiest to quantify due to the direct connection between devices, with the aircraft-level FHA undertaken earlier providing clear guidance between the number of installed propulsion motors and their position on the airframe or role on the applicability of the use of non-resettable devices for their protection. The use of dual-redundant drives (mechanically or electrically coupled) may serve to lessen the impact of a single protection device failure (and hence may be attractive for use in wingtip or vectored thrust motor applications). Particular susceptibility to lightning strike-induced common-mode failures

may also need additional consideration.

4.5 Discussions

From the analysis and literature, the most suitable use of Pyrofuses is for energy source protection. This is mainly for its rapid operation time preventing hazardous current and fire in the battery, and readily available at a high TRL. The use of Pyrofuses is suitable as long as there is redundancy in energy sources redundancy and/or interconnectivity in the EPS design for a continued safe flight after a single failure. This is to satisfy the regulations' safety requirement that the loss of a single critical device should not cause a "major" impact on aircraft safety. Although the redundant control method published by [206] may provide resilience against common mode EMI effects, there is no redundancy against common mode power-event failure such as fault current transients or lightning strike. Therefore, the challenge to demonstrate that the loss of a single Pyrofuse protecting a battery is less than major remains.

Whilst for motor protection, the feasibility of NRPDs is directly linked to the number of motors and aircraft design. For example, the use of NRPDs is feasible for multirotor configurations with more than 10 non-stacked motors, or a minimum of 8 propulsion arms for stacked-motors are required for minor classification. For vectored thrust and lift+cruise configurations with less than 10 motors, dual redundant machines per propeller can be utilised to reduce the failure impact of a single motor to a minor classification, which in return offers a route for feasible application of NRPDs. The use of NRPD for wingtip motors has a higher criticality and as a result are unlikely to be suitable for the application of NRPDs.

Similar to motor protection, the use of NRPDs for busbar protection is directly linked to the number of split busbars. This is because for an architecture with a limited number of busbars; the loss of a single busbar result in a failure impact higher than a minor failure, unless additional mitigation methods are applied. Whilst the use of large numbers of busbars can demonstrate no adverse effect on the propulsion, energy sources, and thrust. However, the larger the number of busbars the more independent energy sources and other components are required, which adds more weight to the

aircraft.

The use of NRPD for interconnecting feeder is dependent on the failure impact on the system, that is, if the loss of the interconnection between busbars when required is major or worse, Pyrofuses cannot be used. The risk of voltage imbalance between the two interconnected busses, transients due to switching and the sudden increase of load on one battery must be shown to be sufficiently low.

The development of mitigation measures to prevent common-failure modes and reduce the impact of a single failure to an acceptable level is critical to NRPD usage, especially in areas such as protection coordination, EMI, and lightning strike. As such, the following are the potential mitigation measures considered to enhance the reliability of power delivery to critical components (i.e. energy source, motors, busbars).

Since the Pyrofuse device is used for overcurrent protection. Overvoltage protection is necessary to protect against lightning strike and switching impulses. The proposed mitigation measure is to use surge arresters suitable to limit the voltage magnitude of lightning strikes to an acceptable level. From research, there are surge arresters available and being considered for aerospace applications [207]. Thus the proposed mitigation measure is to use surge arresters to limit the voltage magnitude of lightning strikes to an acceptable level. This can offer protection for sensitive electronics and mass tripping of protection devices. If the aircraft is not flying in lightning strike conditions, the Pyrofuse can be controlled to provide protection against overvoltage transients. The signal of the external triggering device can take voltage readings from battery or motor terminals depending on the location of the device. The controls can be thus adjusted to disconnect the Pyrofuse under an overvoltage event.

To prevent EMI-related spurious trip issues, the proposed mitigation measure is to provide a parallel-redundant Pyrofuse set-up. The set-up consists of an externally triggered Pyrofuse connected directly to the rest of the system as the primary and self-triggered Pyrofuse as a back-up. During normal operation, the self-triggered Pyrofuse is disconnected from the rest of the system and is connected after the primary fails (as shown in Figure 4.4). To connect the back-up to the rest of the system, an analogue circuit with a time-delay switch can be used to allow the fault to be cleared before

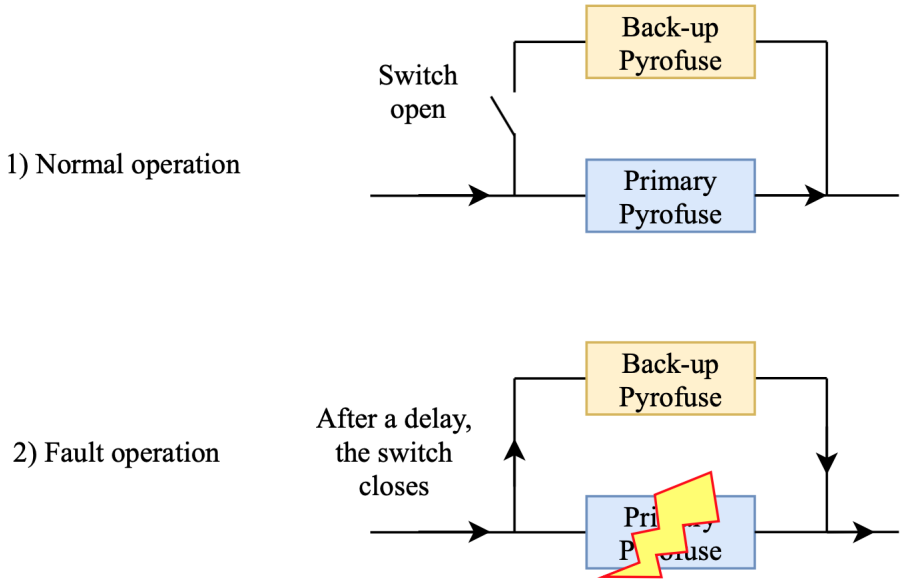

Figure 4.4: Parallel-redundant Pyrofuse set-up

connecting the back-up Pyrofuse. The time-delay chosen has to be selected rigorously to prevent the system from shutting down. While in the event of a short circuit using this set-up, the time-delay switch will connect the back-up Pyrofuse and trip as the overcurrent fault is still persistent. This proposal can provide immunity against EMI and overvoltage faults, but requires further study and analysis to validate the concept. The set-up can also help reduce the failure impact of NRPDs use for primary protection to a minor failure.

It is important to note that the inclusion of mitigation measures adds weight to the EPS beyond that which might be saved by using NRPDs. In addition to the possibility of worsening the failure rate due to the additional components in the system, which impact on adherence to failure rate certification requirements. However, if NRPDs are the only available technology then this may be unavoidable.

4.6 Summary

Through the review of relevant safety requirements, eVTOL configurations, and location-specific failure modes, this chapter has highlighted the challenges of the wide-spread

certification-compliant implementation of NRPDs in eVTOL applications. However, through this preliminary certification compliance assessment, opportunities for NRPD use have still been identified, particularly where the classification for the loss of a single protection device does not cause a major or worse failure. From the analysis, the precise classification of the loss of a single protection device is highly dependent on the aerodynamic configuration and the design of the EPS system. Thus understanding the different fault types and their impact on at the subsystem and aircraft level assist in understanding the safety requirement for the development of a resilient EPS architecture. From this, it has been shown that NRPDs can most easily be utilised in locations within the power system where there is likely to be considerable natural redundancy and oversizing (often due to other design size, weight and cost design drivers), for example at the propulsion motors and power sources. The findings of this chapter have provided assessment and guidance to design a certifiable power system architecture with non-resettable protection devices for primary protection, which answers the second research question presented in chapter 1.

A potential solution to prevent common-failure modes and reduce the impact of a single failure to an acceptable level has been identified in this chapter. From this, the work in this thesis has contributed to the second research question, where a process for designing a certifiable power system architecture that incorporates Pyrofuses which are non-resettable protection devices for primary protection has been identified.

Further work required to perform a true systems trade of adding redundancy/oversizing against weight saved in NRPDs, this will be valuable to provide clearer guidance to eVTOL community. Additionally, further tests is required to investigate the behaviour of the Pyrofuse under lightning strike transients and its impact on the coordination of the Pyrofuses in the system. The potential parallel-redundant solution and Pyrofuse behaviour can be further investigated using the Pyrofuse model in Chapter 3.

Chapter 5

Design Methodology for a Certification-Compliant Electrical Power System Architecture

The significant change from the current state of the art aircraft to eVTOL, is the use of electrically driven propulsion systems. This change necessitate disruptive EPS architectures and technologies to meet performance (e.g. weight), functionality, and certification requirements, combined with much greater levels of coupling with non-electrical systems, such as aerodynamics. The regulatory bodies [48–50] have established new stringent certification standards to address the novelty of eVTOL aircraft compared to the state of art aircraft.

However, the design of the EPS to meet regulatory safety requirements is oversimplified at an early stage in the design methodologies published in the literature, and the role of the EPS to meet safety requirements is overlooked until the later stages of the design process. Delaying the full consideration of the role of the EPS until after the initial design phase; first, risks an aircraft design that does not meet initial design and mission constraints, in terms of weight and range. Secondly, by considering the

EPS in tandem with the wider aircraft design will offer routes to open up new design spaces for optimisation of the overall system design.

To address this gap in the design process, this chapter proposes the first design methodology to capture a certification-compliant EPS architecture at the preliminary design phase of eVTOL design. The methodology provides a systematic process to integrate mission requirements, aircraft aerodynamics, projected future availability of EPS technologies, and safety requirements to identify a certification-compliant EPS architecture. Secondly, it enables the quantification of the impact of available EPS technologies into a certification-compliant EPS design and feasible mission profile. The chapter present a case study to quantify the risks and impact of a certification-driven EPS architecture on aicraft weight and mission profile when considered at a later stage of the design process.

5.1 System Design Methodologies and Certification Processes

5.1.1 Safety Guidelines and Methods for Certifiable Systems

The high level requirement from the certification documentation states that the aircraft must demonstrate the ability to maintain flight and land safely after experiencing a fault in the system. The inability to land safely, resulting in catastrophic failure, need to be designed to be extremely improbable [48, 50]. To demonstrate compliance to the certification regulations, aerospace recommended practice (ARP) and guidelines are used, e.g. ARP4754A and ARP4761 [195, 210]. In conventional aircraft design the development assurance processes in ARP4754A, provide guidance for aircraft and systems development that is compliant with certification regulations. This includes definitions of safety requirements, methods, and practices to satisfy the safety requirements from the regulatory bodies. Following from this, the Society of Automotive Engineers (SAE) standard aerospace recommended practice, ARP4761, provides analytical methods to derive the architecture-specific severity of faults and establish the safety requirements required by ARP4754A. This verifies the system is compliant with certification regu-

lations. The proposed methodology in this chapter incorporates the ARP guidelines with additional design steps to guide the development of the EPS architecture to be a certifiable design within the design constraints, e.g. weight and safety .

5.1.2 Existing EPS Design Methodologies

System level design methodologies for the design of EPS architecture in the literature are focused on fixed-wing aircraft such as hybrid-electric aircraft, and more electric aircraft [211]- [215]. However, compared to eVTOLs, these aircraft have different configuration design and flight mechanism: electrical power is provided by a combination of gas turbine driven generators and batteries in much larger aircraft at higher power levels (>1MW propulsive power for hybrid electric aircraft); split between electrical and non-electrical propulsion: eVTOL are all electric, whereas hybrid electric are a mix of gas turbine and electrical propulsion; flight mechanism: rolling take-off versus vertical take-off and landing and the required transition between hovering and cruise phases. Particularly, the flight mechanism aspect present additional considerations to address the disparity in the novel aerodynamic configuration for certification-compliant design.

Flynn et al. [214] presented a comprehensive EPS design framework focused on the application of fault management at an early stage of aircraft development. Additionally, Jones et al [215] present a customised modelling framework based on SAE AIR 6326 for efficient early stage of EPS architecture for next-generation aircraft. Both frameworks provide ways of systematically designing a viable EPS. However, these design methodologies do not address aerodynamic-electrical failure interdependencies. These inter-system relationships heavily influence the design approach to meet safety and weight requirements of the EPS of any aircraft with full or hybrid electric propulsion. In line with this, it is of paramount importance to understand and capture these interdependencies for eVTOL aircraft; where the DEP is closely coupled to the aerodynamic structure, and resulting in failure modes at an aircraft level influencing the EPS design. By doing this, the EPS can be designed to provide support where possible to mitigating these failure cases.

Therefore, there is a need for a more summarised EPS design methodology for eVTOL aircraft, which incorporates aerodynamic-electrical failure interdependencies while utilising industry-standard safety assessment guidelines to meet certification regulations.

5.1.3 Existing eVTOL-Specific System Design Methodologies

Conceptual design methodologies developed specifically for eVTOL are presented in the literature, with a limited scope on the EPS as the main focus is on the assessment of a certain aerodynamic design. As a result, the EPS architecture is often oversimplified. For example, Jain et al. [216] propose a methodology focused on the aerodynamic configuration of the aircraft with coaxial ducted tilt rotors and wings. However, only the sizing of the battery is considered for the EPS design. Akash et al. [217] present a conceptual design methodology of an eVTOL aircraft for intercity mission of up to 500 km. The conceptual methodology consider the sizing of the battery and electric motors in their eVTOL design methodology, which is focused on the aerodynamic design and the systems allocation in the aircraft to satisfy intercity mission range requirements. Cole et al. [218] present a conceptual design method for an electric helicopter with a single main rotor and lift-augmented compound. The methodology advances conventional methods in the literature for the design of a fuel-based helicopters to an electric helicopter by considering the weight of the EPS and energy storage, rather than conventional kerosene.

In both [217] and [218] the consideration of safety measures to address the impact of potential electrical common failure modes on the EPS is overlooked, risking the down selection of an aircraft topology which at later stages will require an EPS design to meet certification requirements which does not meet performance design criteria for the aircraft.

Maestre et al [219] and Palaia et al [220] both propose a conceptual design methodology for eVTOL aircraft, which includes aerodynamic design, mission performance, sizing and weight estimation of the EPS and propulsion system. In both cases an extra thrust factor is included to oversize the motors for a failure. The methodology in [219]

considered a contingency of 10% of the MTOW to factor in any additional changes to the aircraft design at later stages. Redundancy is provided by assigning two batteries per motor [219]. In [220] , a 5% extra thrust factor of the maximum take-off weight (MTOW) for the case of a single motor failure is applied. However, the analysis behind the motor failure and the design of the EPS architecture is oversimplified. The failure modes and their impact on the system was overlooked, which highly influences the required oversizing of the EPS and protection strategies to maintain safe flight after a failure. This simplified approach risks the outcome that the estimated extra thrust factor is insufficient to enable safe landing in the event of a single motor failure and hence the inability to meet certification requirements.

Bertram et al. [52] and Osita et al. [221] propose a methodology to estimate the total weight of eVTOL aircraft, and the influence of weight on aircraft performance. The methodologies consider the mass estimation of EPS components such as, the energy storage, motors, and power electronics. Yet, the presented design methodologies do not incorporate safety measures to the EPS architectures such as component oversizing, redundancy, and battery emergency reserve to the total weight of the aircraft.

J. Booker et al. [51] present a systematic method for assessing the reliability of eVTOL EPS architectures to meet the reliability targets of regulatory bodies. However this method requires a pre-defined EPS architecture with allocated safety measures to start architecture evaluation. NASA recent report [185] have presented a detailed EPS architecture for NASA eVTOL conceptual aircraft to evaluate their reliability and safety as per the certification requirements. The report provides descriptive FMECA and Fault Tree Analysis (FTA) using a pre-defined EPS. Additional guidance is required to translate the requirements from the FHA. This is to develop the EPS architectures within aircraft design constraints of weight and safety at the preliminary phase, to then be assessed using the presented FTA and FMECA analyses. This includes the consideration of the safety measures to reduce the severity of failures in accordance with the certification requirements and weight constraints.

It is evident that existing methodologies for eVTOL aircraft conceptual designs in the literature are very limited in capturing and considering the design interdependencies

between the EPS design, safety requirements, the wider aircraft concept design, eVTOL mission profiles for a certification-compliant EPS architecture. This reiterates the need to establish a systematic approach to develop a certification compliant EPS architecture for eVTOL aircraft.

5.2 Methodology for a Certification-Compliant Architecture

The proposed systematic methodology for the early stage capture of a certification-compliant eVTOL EPS, which incorporate the influence of the aerodynamic aspects of aircraft into the certification requirements and hence the EPS architecture. The EPS design methodology has been structured around industry standards, specifically ARP4761 [195], the system safety assessment, with the safety development process ARP4754A [210], to show compliance to certification requirements.

The methodology is divided into three main sections as presented in Figure 5.1: the aircraft design process (yellow bubble), safety assessment guidelines (orange bubble), and the development of the EPS architecture (red bubble). From the previous section, the presented parts were documented in the literature as separate processes which introduce limitations to the design. This thesis presents a methodology with novel integrated linkage between the different processes, as shown in yellow, orange, red bubbles, as seen in Figure 5.1.

The sequence of the initial design decisions to develop the EPS architecture is indicated by the black arrows. The design process is iterative, as indicated by the dashed, arrows. This is essential to ensure the EPS design meets the safety criteria, and is therefore certifiable, and to ensure the EPS is within the weight budget, which is set as a design requirement to start the aircraft design process.

5.2.1 Step 1: Aircraft Concept Design

The input to the aircraft concept design step is the flight mission profile (includes speed, range) and number of passengers. Step 1 is the conceptual design of the aircraft

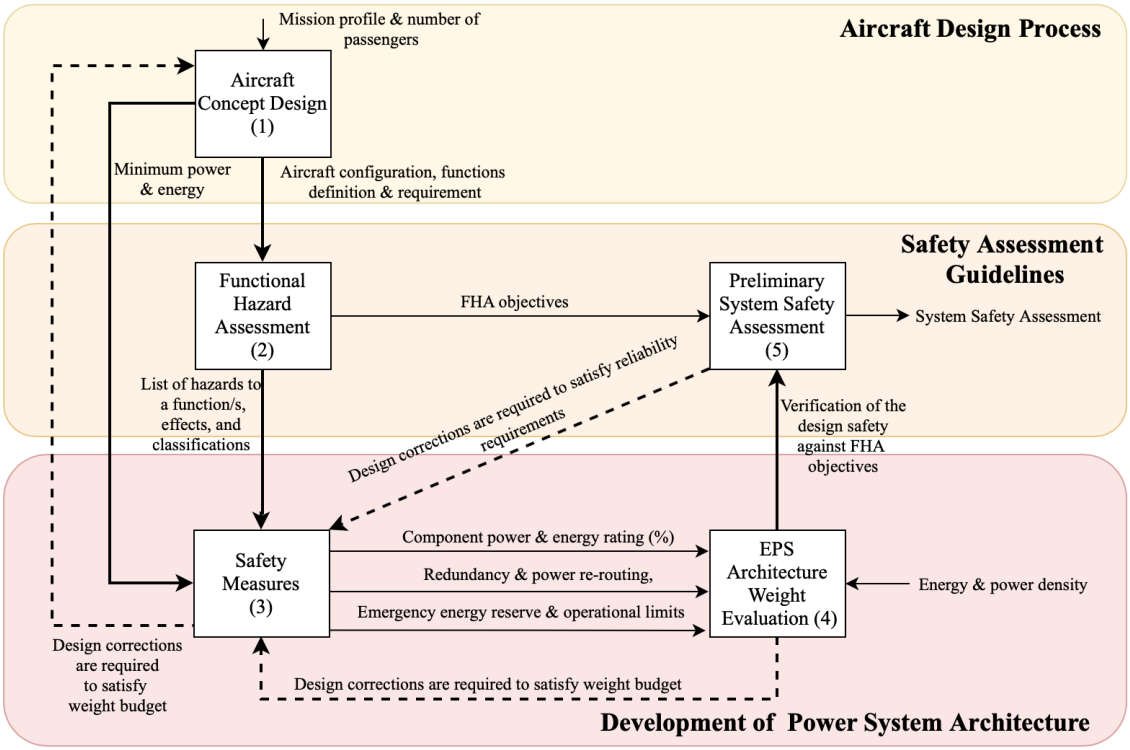

Figure 5.1: Systematic Methodology to Develop Airworthy Design of the Electrical Power System Architecture

which is completed by aerodynamic and flight physics engineers. The required output of Step 1 for the design process, is the lift-to-drag (L/D) ratio, disc loading, number, and arrangement of motors (e.g. stacked motors), and MTOW. The output is used to calculate the minimum power and energy requirements to perform the required mission; The hover power profile of the aircraft is computed using 5.1, and the cruise power of the aircraft is computed is using 5.2.

From Step 1, the aircraft configuration, functions, and requirements are output. These are passed to Step 2 where an FHA is performed. This is essential to identify potential hazards affecting the aircraft's ability to maintain flight in order to meet the safety requirement from the certification regulations.

The second output is the calculated power and energy for the required mission profile is also output from Step 1. This power and energy are considered as the "minimum" requirement, which is passed to Step 3, to include the safety to mitigate a failure in

the system, the resultant oversized power is used to size the EPS.

5.2.2 Step 2: Functional Hazard Assessment (FHA)

In Step 2, the FHA is performed using the data from Step 1 combined with the FHA procedure described in [195]. From this a list of aircraft functions and their associated failure conditions and effect on the aircraft's ability to maintain flight. The list highlight functionalities and components critical to flight safety (e.g. how many motors or batteries the design is tolerant to before requiring immediate landing). This list is passed to Step 3.

The second output from Step 2, which is the safety objectives identified in the FHA, are passed to Step 5. The safety objectives are used to validate if the safety measures of the proposed EPS architecture have addressed the potential failures and their impact on the aircraft and system functions, and are within acceptable limits as per EASA failure conditions [50]. It is important to note that the FHA must be updated throughout the development of the aircraft design to re-evaluate the safety implications of any changes to the aircraft's concept design. This is to capture any new functions or failure conditions that might be identified later in the development cycle.

5.2.3 Step 3: Safety Measures

During Step 3, the list of critical functionalities are used to assign safety measures in the EPS design, with the aim to maintain safe flight in the event of failure.

The safety measures include component redundancy, overrating components capacity for a failure of a component/functionality, electrical power re-routing, and emergency reserves. From this, number of viable architecture solutions are identified taking account of the critical functionalities and the safety measures. These are output to Step 4, where their weight will be evaluated.

The feedback loop from Step 3 to Step 1, as seen in Figure 5.1, allows the iteration of the high level aircraft design, if the weight of the EPS surpasses the weight budget. The decision for aircraft design corrections should be applied as a final act, only if after, all EPS design options were examined, and no viable solution which meets the weight

budget can be found. Aircraft design corrections includes reduction of the mission range or number of passengers to satisfy the weight budget.

5.2.4 Step 4: Electrical Power System Architecture Weight Evaluation

In Step 4, the weight of the EPS architecture is evaluated using the power and energy requirements from Step 3 to size the EPS components. Additionally, a down-selection process takes place, to select an EPS design which will meet the weight budget from the mission profile in Step 1. EPS architectures goes on down-selection process to select a design within the weight budget. The EPS architectures which fall within the acceptable weight are passed onto step 5 for the Preliminary System Safety Assessment (PSSA). If none of the proposed EPS architectures meets the weight requirements, then the process returns to step 3 (see Figure 5.1) to implement different safety measures and iterate the EPS system design to satisfy the design weight budget.

5.2.5 Step 5: Preliminary System Safety Assessment (PSSA)

The downselected architectures from Step 4 are passed to Step 5, along with the FHA safety objectives from Step 4. Within Step 5, a PSSA is carried out to determine if the proposed architecture can meet the safety objectives identified by the FHA. The process at Step 5 first verifies whether the system level EPS architecture design meets the reliability and safety objectives identified in the FHA. This is achieved by quantitative analysis using FTA, FMECA, and Common Cause Analysis (CCA). The final selection of EPS architecture is based on the trade-off between cost and weight while meeting the safety objectives. The next step from the PSSA is a more detailed design at the sub-system level and further reliability analysis that summarises the findings from the FHA, PSSA, FMECA, and CCA to present to certification bodies and demonstrate safety requirements compliance.

However, if the outcome of the PSSA shows that none of the proposed EPS architectures meet the safety objectives of Step 2, then the process returns to Step 3 as shown in Figure 5.1). This is to ensure the implemented safety measures can meet the

FHA safety objectives of Step 2, and the validation process in Step 5.

5.3 Derivation of Energy and Power Requirements for Mission Profile

This section presents a series of eVTOL aerodynamic equations from literature used to compute the minimum power and energy of step 1 of the proposed methodology in Figure 5.1. Figure 5.2 presents the general mission profile for eVTOL aircraft which consists of vertical take-off, climb, cruise, and vertical landing. In this study, the phases with key performance drivers of the power and energy model requirements to design the EPS architecture are considered; these are the hovering and cruise phase highlighted in red in Figure 5.2. Where the hovering power is the maximum power achievable during flight which is used to size the EPS technologies, and the cruise phase is the longest segment of the flight hence significantly influencing the energy consumption and battery sizing.

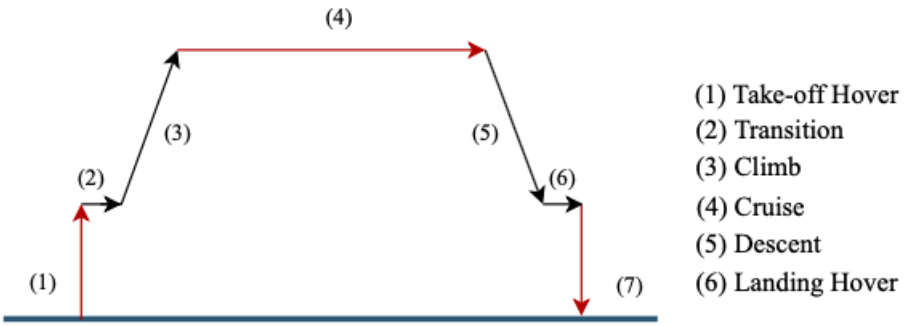

Figure 5.2: EVTOL Aircraft Mission Profile

5.3.1 Hovering Power

The hover power P_{hover} (in W) is calculated based on blade element momentum theory on the actuator disc using the open propeller (5.1) [15, 24]. Full derivation of (5.1) is given in [24].

$$P_{hover} = \frac{T_{hover}^{\frac{3}{2}}}{\sqrt{2 \cdot \rho \cdot A}} \tag{5.1}$$

Where T_{hover} (in N) is the thrust of the propulsion system during hover phase, ρ_{sea} is the air density at sea level (1.225 kgm^{-3}), and A is the total disc actuator area (in m^2). From the hovering time and power, the energy consumed can also be computed using (5.10).

The hovering power for a ducted propeller design [24] is shown in (5.2). The ducted design can offer reduced noise emission in comparison to open rotor design. However, this comes with the cost of increased disc loading (power or thrust against disc actuator area), which increases the power requirement for the hovering phase [24]. For coaxial rotor design (5.2) can also be used to calculate the hovering power; in addition to a multiplication of an interference factor which varies from 1 for zero interference to $\sqrt{2}$ for maximum interference [15].

$$P_{hover} = \frac{1}{2} \cdot \frac{T_{hover}^{\frac{3}{2}}}{\sqrt{\rho \cdot A}} \tag{5.2}$$

5.3.2 Cruise Phase

The cruise power in a steady level flight assumes all forces are applied at the centre of gravity, where the thrust (T) is equal to the aerodynamic drag (D) shown in (5.3), lift is equal to the aircraft weight (W) shown in 5.4.

$$T = D \tag{5.3}$$

$$L = W \tag{5.4}$$

The aircraft weight in 5.5 considers the ($MTOW$) in kg multiplied by the gravitational acceleration (g) of 9.81 ms^{-2}, as illustrated in (5.5).

$$W = MTOW \cdot g \tag{5.5}$$

Combining and re-arranging the terms in (5.3), (5.4) and 5.5, gives an expression

for the thrust as shown in (5.6)

$$T = \frac{D}{L} \cdot W = \frac{D}{L} \cdot (MTOW \cdot g) \tag{5.6}$$

The expression in (5.6) is further rearranged into (5.7).

$$T = \frac{MTOW \cdot g}{(\frac{L}{D})} \tag{5.7}$$

The averaged power requirement for the cruise phase can then be obtained using the thrust from (5.7) and the cruise speed (in V_c) in ms^{-1} in addition to the propulsion system efficiency (η_c) requirement during cruise, using (5.8) [222].

$$P_{cruise}(W) = T \cdot V_c \cdot \eta_c = \frac{MTOW \cdot g}{\frac{L}{D}} \tag{5.8}$$

From (5.8), it is evident that the key performance driver during the cruise phase is the Lift-to-Drag ratio (L/D), the cruise speed (V_c), and the propulsion system efficiency (η_c). The expression of the L/D ratio is given as (5.9) [223, 224].

$$\frac{L}{D} = \frac{C_L}{C_D} = \frac{C_L}{C_L + K \cdot C_L^2} \tag{5.9}$$

Where C_L is the coefficient of lift, C_D is the coefficient of drag, and K is the induced drag factor which is inversely proportional to the aspect ratio of the wing and Oswald efficiency factor [223, 224]. Accordingly, the L/D ratio is affected by both the amount of parasitic drag formed from the aircraft body and the induced drag corresponding to the amount of lifting force [224, 225]. The induced and parasitic drag are also affected by the cruise speed; the minimum point of the combined total drag provides the speed for maximum range [226, 227]. This step is usually completed in the detailed design phase where multifactor analysis in multiple iterations are required to match the desired performance and mission profile of the vehicle.

The energy consumption for each flight phase can be calculated using (5.10).

$$Energy = P \cdot t_{hr} \quad (wh) \tag{5.10}$$

Where (t_{hr}) is time in hour, and power (P) in W. Since the highest energy demand is during the cruise phase as the time spent during this phase is the longest, and the highest power demand phase is the hover phase but with a short time. In this study, the energy of both hover and cruise phase are considered. The expression for the sum of energy consumption for the hover phase and cruise phase is given in (5.11).

$$Energy_{sum} = E_{hover} \cdot E_{cruise} \quad (wh) \tag{5.11}$$

E_{hover} is the energy consumption during the hovering phase, and E_{cruise} is the energy consumption during cruise phase. From 5.11, the weight of the battery can be computed for a given battery energy density.

5.4 Case Study: Impact of Certification-Compliant EPS Architecture on Aircraft Mission

The case study focuses on the development of the EPS architecture section of the methodology (red bubble) in Figure 5.1. The objective is to demonstrate the risk impact of underestimating the safety requirements for the design of the EPS architecture on the aircraft weight and mission for a given aircraft concept, and thus highlight the importance of considering the EPS design at the early stage of aircraft design process.

5.4.1 Step 1: Aircraft Concept Design

A multirotor eVTOL configuration is considered for the case study to demonstrate the proposed methodology and associated weight impact. The eVTOL design concept used in this case study is the example of the multirotor design presented in Chapter 4 Figure 4.1. The initial design parameters and mission requirements for this concept are presented in Table 5.1. The data in Table 5.1 are used to compute the power and energy for the required mission using the equations from literature presented in the previous section. The assumed L/D ratio for the cruise phase is 5; this value is the average of the different types of L/D ratios for helicopters given in [242].

Table 5.1: Top-level Requirement of the Aircraft Design Concept Figure 4.1

Parameters	**Value**	**Reference**
MTOW	2200 kg	[229]
Cruise L/D	5	Assumed [242]
Speed	120 km/hr	[229]
Number of motors	8	[229]
Actuator disc area	24.6 m^2	Computed [231]
Range	30 km	[230]
Hover time	1 minute	[222]
Cruise time	15 minutes	[229]

Using the mission profile and the parameters of the aircraft configuration in Table 5.1, the computed power and energy for the required mission are shown in Figure 5.3.

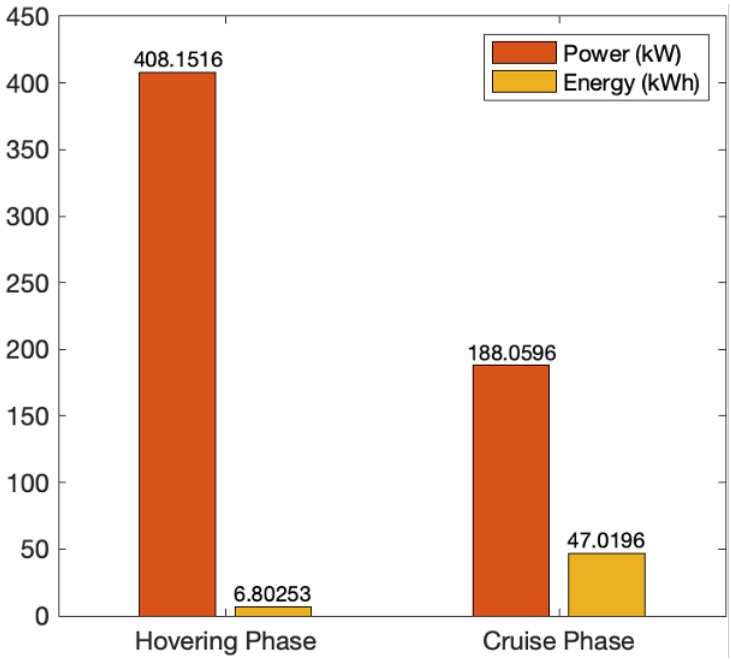

Figure 5.3: Mission Profile Power and Energy Requirements for the multirotor design concept in Figure 4.1

For this particular case study, the minimum hovering power is 408.15 kW. An additional 5% of power is needed for avionics and secondary, non-propulsive electrical systems [220], however it is not considered in this case study. The resultant energy

consumption for a range of 30 km is 47 kWh without consideration of additional safety margins.

5.4.2 Step 2: Functional Hazard Assessment

In Step 2, the potential hazards and associated mitigation actions are identified and assessed (see chapter 4). The failure conditions with highest impact on aircraft safety associated with aircraft functions are identified, this is used to address the level of safety in the EPS architecture design. The FHA is a thorough process, to demonstrate the risks associated with EPS architecture design, the function with the most impact is considered for this case study, and that is "provide thrust".

From the aircraft design in Step 1 Figure 5.1), considering the case of the loss of one motor, in order to maintain the balance of the aircraft after this failure, there must be a significant reduction or shutdown of thrust provided by the diagonally aligned motor [232, 233]. The loss of one motor leads to the effective loss of two motors out of eight. Any further loss of motors will prevent the aircraft's ability to land safely, and thus could lead to a catastrophic failure. Therefore, the EPS architecture must be designed to maintain safe flight after a single motor failure.

5.4.3 Step 3: Safety Measures

From the results in the FHA in step 2, the EPS architecture should demonstrate the aircraft ability to land safely in order to comply with the safety requirements from the certification regulations [48, 50]. First, a preliminary fault protection strategy is required to address potential failures of a multirotor design. Common mode failures should also be taken in consideration when designing the EPS to prevent the loss of aircraft, this includes short circuit faults, lightning strikes, and battery thermal runway.

Additionally, thorough reserve planning specific to the aircraft type, cruise speed, and mission range is expected to ensure there is enough time for re-routing and safe landing in emergency scenarios [50, 188, 244]. There is not a specific value for the amount of reserve from the regulatory bodies yet. As such for this case study, 30% of the total energy capacity for emergency reserve, and additional 20% limitation of

battery state of charge for lifecycle longevity.

To simplify the latter energy and power scaling calculations, minimum power and energy requirement of step 1 (seen in Figure 5.3) are normalized as percentages in the following architectures. For example, the minimum power required for hovering is represented at 100%, and at the latter stage, any excess of power or energy capacity from the architecture is then multiplied by the minimum requirement to calculate the weight of the EPS architecture..

The study starts with the "baseline architecture" used to illustrate the impact of oversimplifying the EPS architecture at the initial stage of development. The following EPS architectures refinements considers different safety measures with the aim of ensuring power continuity after a failure.

1) Baseline Architecture

The initial architecture considered in this study is a baseline architecture with eight electrically independent distribution channels supplying power from each of the eight batteries to the motors as illustrated in Figure 5.4.

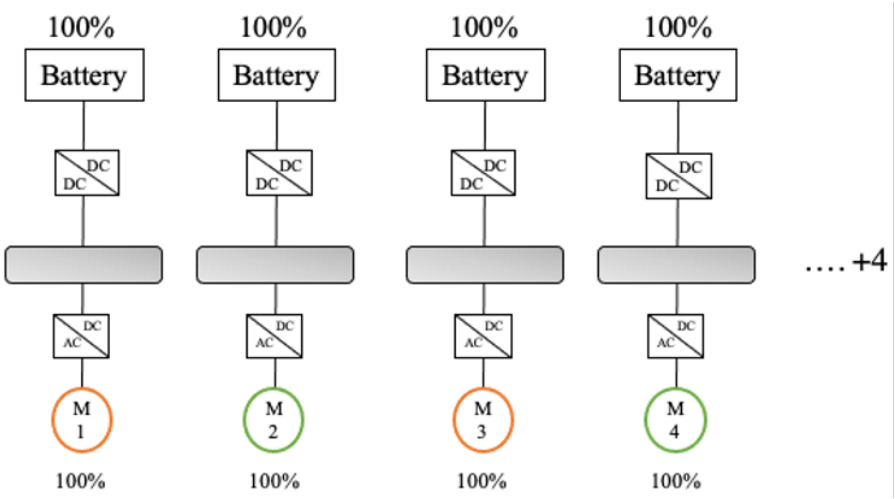

Figure 5.4: Baseline Architecture

Following the approach in the published literature [216, 217, 220] the sizing of the components is equal to the minimum power and energy requirements of step 1; which excludes any safety measures or battery reserves. This architect acts as a starting point

from which to determine certification-compliant EPS designs.

Isolation between channels in the baseline architecture reduces the risk of common mode and cascading failures. However, this isolation also reduces system redundancy, and the loss of one motor will significantly impact on the ability of the aircraft to land safely [232, 233]. This is because the baseline architecture does not include any additional power to distribute the thrust and balance of the aircraft forces.

Therefore, design corrections are required using the feedback loop to consider oversizing or an alternative architecture. Oversizing components for this architecture can satisfy the safety requirements with sufficient isolation, but comes with a cost of significant excess of weight. The following architectures addresses the limitations of this baseline architecture by incorporating system level safety measures to improve the safety of the system.

2) Architecture 1: Bus-tie Architecture

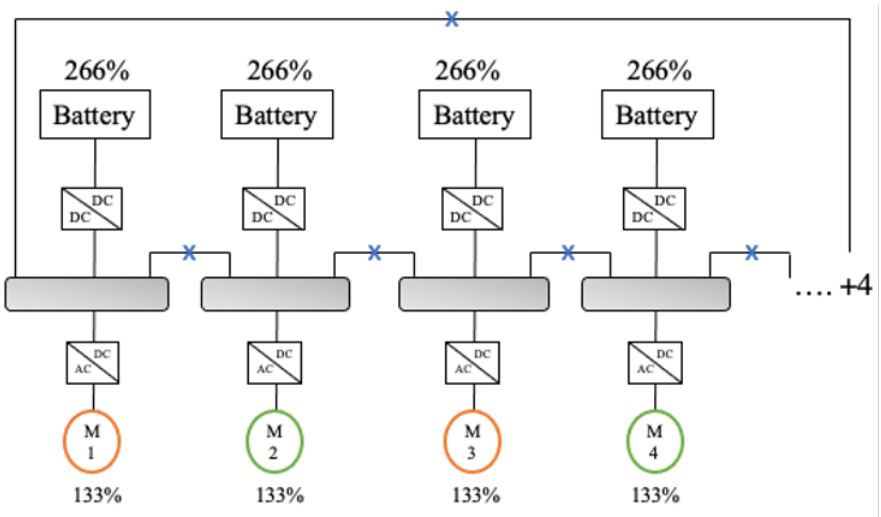

Figure 5.5: Redundant System with Bus Interconnectivity

Figure 5.5 presents an architecture to overcome the limitations of the baseline architecture with isolated channels. In this solution, interconnectivity between distribution channels enables different batteries to supply different motors. The interconnect switches are open during normal operations, isolating the eight distribution channels and the power supply from each battery to each motor. In case of a failure in any

channel or battery, and once the fault is isolated, the corresponding interconnection switches closes to re-route power to the healthy motors.

The EPS components must be oversized to accommodate the increased power flow in the case of a fault occurring. The sizing of the electric motors is based on the loss of two motors out of eight motors, where the thrust lost is distributed amongst the remaining motors. This is achieved by dividing the total power of the motors by the 6 remaining motors, which requires motors to be sized 133.3%, which is 33% higher than the baseline architecture. This percentage value is subject to increase to include the additional drag caused by the failed propellers [15]. Due to the interconnection in the bus-tie architecture, each battery is designed to supply two motors. Therefore, the energy capacity is sized to 266% of the minimum energy requirement passed down from Step 1.

This architecture offers a great degree of redundancy and component oversizing in the event of a battery or motor failure. Requiring additional space for cabling, power electronics and controls for the interconnection, and power distribution units, which adds weight to the EPS architecture. The interconnection switches and controls introduces complexity to the system. That is, the ability to detect that the fault has been cleared before connecting the nearby channel, and to balance the voltage between the two channels to prevent the loss of the two channels.

3) Architecture 2: Partial Redundant Batteries Architecture

The bus-tie architecture in Figure 5.5 can be modified further to reduce the oversizing of batteries and interfacing power electronics, to be able to supply power in the case of a battery failure. This is achieved by having two batteries per motor, as indicated in Figure 5.6. Partial redundancy has a similar functionality to the bus-tie technique, which is to continue supplying power to healthy motors in the event of a single battery failure.

The architecture shown in Figure 5.6 includes partial redundancy in the battery's capacity for each motor. As a result, the total energy required for each motor is split between two batteries, and the resulting combined energy of two batteries for

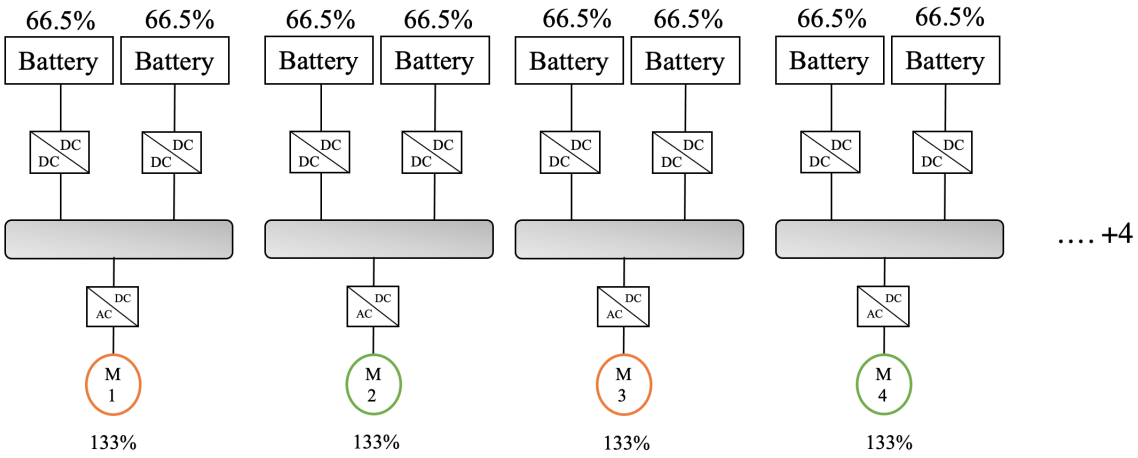

Figure 5.6: Partial Redundant Batteries Architecture

each motor is 133% of the minimum energy requirement given from Step 1 Figure 5.1. While for the electric motors, the sizing is similar to the bus-tie architecture, which is based on the loss of two motors out of eight motors.

In normal operation, the two batteries of the same bus is sharing the required power to the motor. In the event of a battery failure, the affected bus will only be able to supply 66.5% of the demand to the connected motor. There will be slight reduction of power if the fault occurred during hovering as the affected bus can only supply 66.5% of thrust to the motor, while 100% of thrust per motor is required during hovering phase. Whereas cruise and landing require around 50% of thrust per motor (as can be seen in Figure 5.3). In case of a motor failure, a single distribution channel is lost. All the operating batteries in the remaining busses is able to provide the additional power required per motor to balance the aircraft and maintain flight to the nearest landing site.

5.4.4 Step 4: Electrical Power System Weight Calculation

Table 2.2 presented in chapter 2 provides a list of the power and energy density of the state of art technologies and future technology progression. Due to the lack of technology roadmaps for protection technologies, for this case study, a SSPC module with a power density of 28.8 kW/kg was chosen scaled to the power requirements of

the application [173], and remains the same throughout in 2025 and 2030.

Table 5.2: Summary of the Key Design Measures from the Presented Architectures

Safety Measures	**Baseline**	**Arch. 1**	**Arch. 2**
Tie-bus	x	✓	x
Dual motors	x	x	x
Dual batteries	x	x	✓
Dual converters	x	x	✓
Dual inverter	x	x	x
Motor oversizing	x	✓	✓
Battery oversizing	x	✓	✓
Excess power per motor	-	1.33x	1.33x
Excess energy per battery	-	2.66x	1x
Power System Weight (kg)	519.7	2194.8	909

Table 5.2 presents a summary of the safety measures in each architecture presented in Step 3, these are the baseline architecture, architecture 1, and architecture 2. Safety measures that are not included in an architecture is marked with a red cross, and safety measures that are included in an architecture are marked with a green tick. Using the power and energy densities of key components, the weight estimation of the EPS architectures are thus presented in Table 5.2 .

From Table 5.2, the baseline architecture result in a system weight of 519.7 kg, but at the expense of having minimal safety measures, limited to redundant isolated channels. While the other architectures consider multiple safety measures and emergency reserve to manage different failure scenarios resulting in an increased weight of; 1675.1 kg for architecture 1 and 389.3 kg for architecture 2 compared to the baseline architecture.

Figure 5.7 shows the weight breakdown of the key technologies considered for the different architectures using state of the art EPS technologies in 2017. In all the architectures the battery is the most dominant component in weight, followed by the electric motors. The power conversion units (i.e. inverters and converters) show to have the minimum weight contribution to the power system mass for all 3 architectures considered. However, the weight of the cooling system for power electronics is not considered

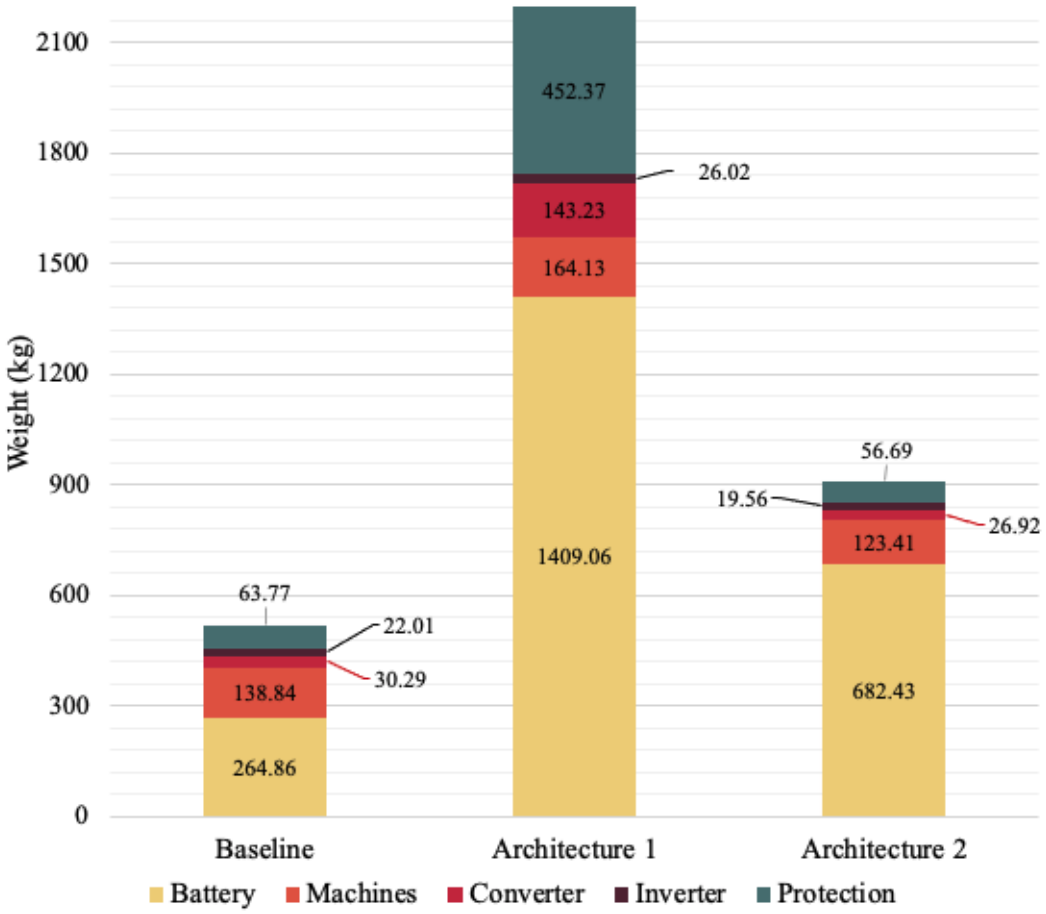

Figure 5.7: Weight Breakdown of Technologies used for the Proposed Architectures

which contribute to significant weight to the devices [171,172]. Architecture 1 have the highest weight for protection technologies compared to the other architectures; this is primarily due to the electronics required for the interconnection between channels.

Figure 5.8 compares weight of the proposed architectures using power and energy densities for technologies from 2017 projected up to the year 2030, using the technology roadmaps presented in Chapter 2. The yellow segment represents the weight of the battery, and the orange segment represents the weight of the EPS excluding the batteries.

From the mission specifications presented in Table 2, the aircraft MTOW is 2200 kg. A combined 45% assumption of the eVTOL MTOW capacity ($\approx$ 990 kg) is allocated for the airframe ($\approx$330 kg) [234], payload (500 kg), avionics, cabling, and other onboard

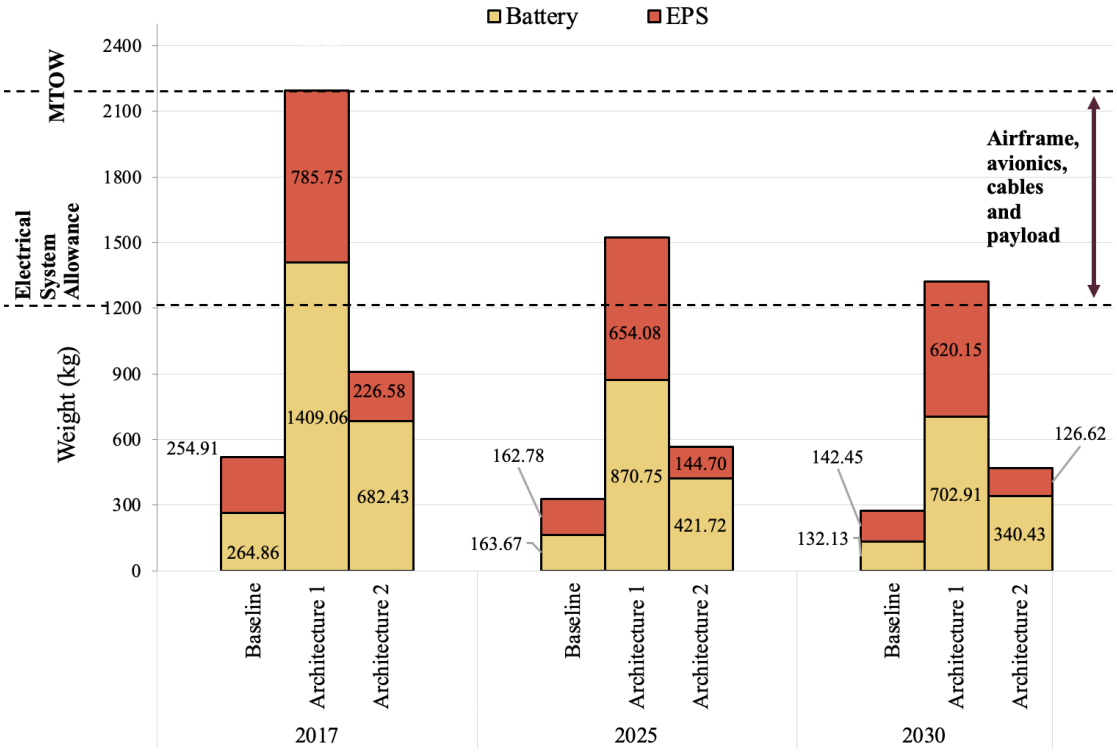

Figure 5.8: Impact of Technology Advancement on the Aircraft Overall Weight

systems (160 kg) [235], and is indicated in Figure 5.8. Hence the maximum allowable weight of the EPS (including batteries and cooling system) is $\approx$ 1210 kg equivalent to 55% of the MTOW.

Using technologies from 2017, the results shows that architecture 2 is under the maximum allowable weight for the EPS by 301 kg. However, architecture 2 only becomes viable using current technologies if the weight the cooling system, cabling, low voltage system, and the additional power required for onboard systems and avionics is equal or below 301 kg. Which is infeasible.

By inspection of Figure 5.8, architecture 2 become viable using technological projections by 2025, while the weight of architecture 1 still surpasses the MTOW constraints in 2030. Depending on the entry to service targets, only the architectures that are under the allocated weight budget of 45% the MTOW, are passed to the PSSA in Step 5 for safety validation and verification.

5.4.5 Step 5: PSSA

In Step 5, the developed architecture is assessed based on the system FHA functions and safety objectives, using quantitative analysis techniques, such as FTA and CCA. The PSSA step is critical to the selection of a certification-compliant EPS architecture. However, the process is not considered for each architecture in details for conciseness.

For example, the system FHA is dependent on the design of the EPS architecture, where the loss of a single component in the baseline architecture can result in a catastrophic failure ($1x10^{-9}$ per flight hour), and result in major failure for architecture 1 and 2 ($1x10^{-5}$ per flight hour), see 4.1 for classification definition. This function and probability of failure is used as an objective for the EPS design to meet.

In the FTA, the function is broken down to component-level to identify all the root causes [195]. The accumulative failure rate of each component in the system is then used to verify if the system meets the FHA safety objectives or not. That is, if the accumulate failure rate for the loss power distribution to one motor failure condition is below $1x10^{-9}$ per flight hour, the safety objective has not been met. Thus, alternative architecture should be considered.

5.4.6 Final Evaluation

Converting the available weight budget from Figure 5.8 to extended mission range, the results of the achievable range of each architecture is shown in Figure 5.9. As expected, the baseline architecture can perform a mission range of 30 km by 2017, showing a maximum achievable range of 120 km; this range is 114 km longer than architecture 1 and 75.5 km longer than architecture 2. However, to reiterate, in reality, an aircraft with an oversimplified safety measures will not meet certification regulations, hence the given range is not possible as the increased weight of the safety measures to the EPS decreases the range as illustrated in architecture 1 and 2. In spite of that, with added safety measures, the results show that the architecture 2 is capable of preforming a range of 44.5 km in 2017 as shown in Figure 5.8. However, architecture can be considered feasible only if the weight of the cooling system, cabling, low voltage system is under 301 kg. As the available weight budget increases in consistent with the progression of

technologies, a notable increase of distances can be seen for the architectures in Figure 5.9.

As for architecture 1, to achieve a range of 30 km, the weight of the EPS must be reduced by 984 kg, which is the excess weight beyond the maximum allowable weight for the EPS. At this stage, design corrections are required to reduce the weight of the applied safety measures, the design is then reiterated back to Step 3 in Figure 5.1. For example, design corrections to reduce the number of interconnections, which in turn reduces the oversizing of the battery of architecture 1. Reducing the number of interconnection also allows mechanical and electrical seperation between the busses. Another method is to allow all the batteries to share the load in case of a single motor failure, this offset the need to overly size the batteries.

If none of the added safety measures reduces the weight below the maximum allowable weight for the EPS, then design iteration is required at aircraft concept design stage (Step 1 in Figure 5.1), which necessitates reduction in the mission range or number of passengers for a viable aircraft design.

5.5 Discussion

The presented methodology adopts the conventional processes and demonstrate it for eVTOLs to highlight the importance of EPS architecture and protection strategies at an early stage in the aircraft design process. As shown in Figure 5.1. The case study has shown the approach to execute safety analysis of ARP4761 and ARP4754A processes to assess and certify novel technologies and EPS designs for eVTOL aircraft.

The execution of safety analysis for conventional aircraft differs from eVTOL aircraft, where the EPS are used in low voltage secondary systems and are light in weight, facilitating safety application. With the increase of power and voltage levels for eVTOL aircraft, new high voltage technologies for aerospace applications are required which are either in low maturity or heavy, requiring novel strategies to meet safety and weight constraints. As such, considering EPS at a later stage limits the number of options for certifiable solutions and the achievable range, as shown in Figure 5.9.

Nevertheless, the methodology presents the preliminary process, further work needs

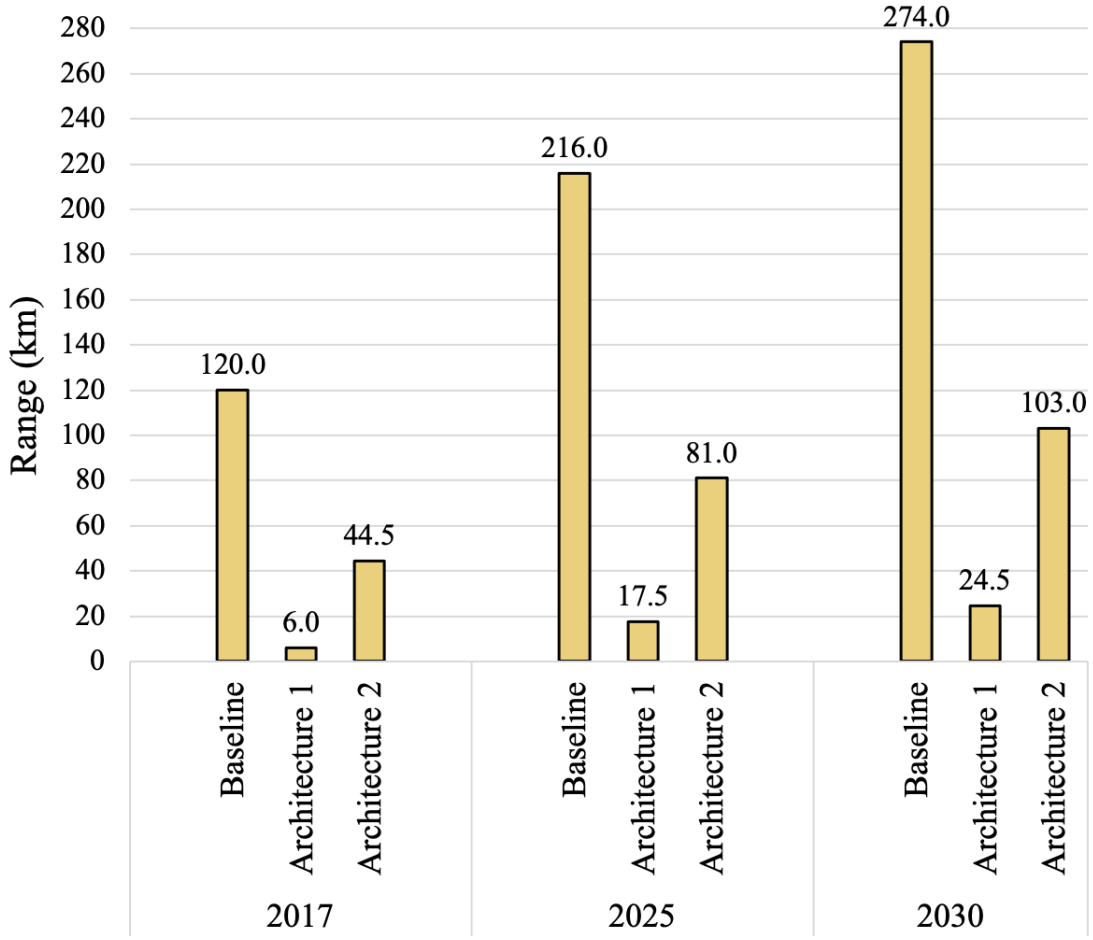

Figure 5.9: Impact of Technologies Advancement on the Mission Range

to be completed at a detailed design stage with rigorous testing to confirm that the quantitative and qualitive analysis performed at the preliminary stage has been met, showing confidence in the design to the regulatory bodies.

5.6 Summary

The work developed in this chapter describes a process to develop a certification compliant EPS architecture in a preliminary design phase of the eVTOL aircraft, where the development of the EPS architecture is carried out in parallel to the design of non-electrical systems, to ensure a certification compliant solution. The case study demonstrates that by considering ARP4761 and ARP4754A processes in an electrical

context to drive the EPS design, an EPS architecture which meets weight and functionality constraints, while ensuring that the aircraft is safe to fly, can be identified at an early stage of the aircraft design process. By incorporating technology roadmaps into this process, critical assessment of future options is possible to enable new design spaces and novel architecture options to be explored, for electrical and non-electrical power systems, with assurance that these aircraft will meet certification regulations. The presented methodology briefly demonstrated each step of the preliminary process of ARP4761 and ARP4754A. However, to complete the full process, further detailed work is required to demonstrate certification-compliance EPS architecture through detailed design and a thorough system-level safety analysis.

From this, the work presented in this chapter considers the essential factors when aiming to design an economically efficient and lightweight eVTOL aircraft that meets the aircraft design objective. These are certification requirements (i.e. safety considerations and recommend practices) to the design of the EPS in parallel with the aerodynamic design to plan and develop the most optimised solution at a preliminary stage of development. Thus, answering the first research question.

Chapter 6

Abstraction of Aerodynamic Electrical Relationships for Accelerated eVTOL Preliminary Design Process

The roadmaps of key power system technologies in Chapter 2 highlighted the technological challenges facing the emergence of UAM market has also presented the drive for technology progression that shapes viable designs for various mission profiles [61, 237]. One of the key technological challenges is application of available batteries for eVTOL designs that can transport an economic number of passengers for inter-city or intra-city missions, and potentially for multiple missions on a single charge [238]. To achieve this in the design, a need to translate the battery density to realise the mission range and maximum take-off weight of the aircraft (MTOW). While the current literature provides detailed aerodynamics design methodologies focused on the parameterisation of the wing and propellers to satisfy the required mission profile/range. However, these methodologies require detailed work at the drafting design phase and are limited to a certain aircraft configuration and flight mechanism. Therefore, this chapter presents a novel methodology that summarises the relationship between aircraft aerodynamics

and EPS requirements in a readily usable format. The methodology enables critical assessment of different aircraft aerodynamic configurations in parallel with EPS architectures to be performed and the ability to explore new design spaces and novel architecture options.

6.1 EVTOL Aircraft Design Methodologies

There are numerous preliminary design methodologies for eVTOL aircraft powered by batteries in literature. Most of these methodologies focus on propulsion and the aerodynamic design of the aircraft to calculate the power and energy consumption of the flight mission in order to estimate the mass of the battery [217, 219, 239]. This is mostly due the mass of the battery being the heaviest component amongst the EPS components. The authors in [219, 239] presented a methodology focused on the design of efficient propellers of a tandem wing eVTOL aircraft for a specific mission profile. This type of method requires detailed calculation of propeller dimensions, airfoil selection, blade geometry optimisation to maximise efficiency and achieve the flight speed specified in the mission profile. G. Palaia et al. [220] proposes a workflow to estimate the weight of a conceptual aircraft for a required mission and demonstrated the design of a box-wing eVTOL aircraft. A.Jain [216] presented a conceptual baseline guide demonstrated through the design of a coaxial ducted tilt rotors and wings aircraft configuration. In summary, existing preliminary design methodologies require detailed work at the drafting design phase and are their scope of work is limited to a certain aircraft configuration and flight mechanism. In order to realise the achievable mission range for different aircraft types using available technologies, EPS architecture assessment studies is required. From the results in Chapter 5 the EPS architecture and technologies can limit the viability of aircraft concept designs due to the inclusion of safety requirements hence increasing the weight aircraft beyond design constraints. Therefore, there is a need for a tool or a methodology to investigate the impact of key aerodynamics design factors on power requirements and the design of the EPS. This initiative combined n with the methodology developed in chapter 5, enables the complete assessment of EPS architectures for different eVTOL concept designs, and to

explore new design spaces and novel architecture options.

While the methodologies in the literature offer a top-down approach requiring detailed aerodynamic design of the propulsion system to compute the energy consumption to estimate the mass of the battery. This chapter presents abstracted design methodology reducing modelling efforts and enabling multidisciplinary design analysis at the initial stages of design. As such, the accelerated/abstract methodology provides the first step into assessing the feasibility of a mission or aerodynamic design of the aircraft using available technologies at a certain timeline, offering usability and applicability to assess and down select conceptual aircraft designs aligned with mission profile.

The methodology considers the hovering and cruise phase of the flight mission as both includes key performance drivers with significant impact on the power and energy requirement. From these, a generalised abstraction equations summarising the relationship between the aerodynamic blade element theory and the power requirement foe wide range of aircraft sizes are presented in this chapter.

Following from this preliminary analysis, more detailed analysis can then be carried out to calculate the corresponding propeller parameters, blade geometry, wing design and airfoil selection to achieve the required energy consumption. The case studies presented in the chapter demonstrate the usability of the proposed methodology can be used for a wide range of designs within the presented boundaries. The case study also validates the accuracy of the results from the methodology using eVTOL aircraft designs in literature.

6.2 Abstraction of eVTOL Design Equations

This section provides the abstraction design methodology to estimate the power and energy requirement of the hovering and cruise phase for use at the preliminary design stage. The methodology was developed by taking a range of key design parameters such as weight, speed, total propeller area, and mission range that are seen suitable for eVTOL aircraft to calculate the power requirement for hover and cruise phase. The calculation of power requirement is done using the theoretical equations presented in chapter 5. The results were then combined into a three-dimensional surface plot using

Surf function [236]. Then, polynomial curve fitting equation is used to best represents data points and hence the relationship between three variables. The resultant polynomial equation abstracts the aerodynamic parameterisation required for the hovering and cruise phase to allow the user to easily perform EPS assessment studies for various aircraft designs. The abstracted design equations are bounded to MTOW of 800 kg to 3175 kg, mission distance from 30 km to 250 km, disc actuator area between 2 m^2 and 39.2 m^2, and airspeed from 54 m/s to 90 m/s using typical speed of existing applications.

Figure 6.1 summarises the step-by-step application of the abstraction design methodology. The orange shaded area presents the values taken from the abstracted equations, and the yellow shaded area presents the additional multiplication factors to reflect different L/D and efficiency compared to the baseline.

6.2.1 Hovering Phase

Figure 6.2 presents a 3D surface plot of the computed minimum hovering power using (5.1) for different disc actuator areas from 2 m^2 to 39.2 m^2, and aircraft weights from 800 kg to 3175 kg. The "x-axis" presents the MTOW in kg, the "y-axis" presents the total propeller area (A_{tp}) in m^2, and the "z-axis" presents the computed hovering power for the different total propeller areas and MTOWs. As seen from Figure 6.2, a total propeller area of 40 m^2 and MTOW of 3000 kg results in a hovering power of approximately 500 kW. While a total propeller area of 12 m^2 and MTOW of 3000 kg results in a hovering power of approximately 1000 kW. This shows that for a fixed MTOW, increasing the total propeller area contributes to higher hover efficiency; this means increasing the rotor radius for a given weight reduces the power requirement in the hovering phase.

From the 3D surface in Figure 6.2, a polynomial equation is generated to abstract the hovering power requirement for wide range of total propeller area and the MTOWs, shown in (6.1). The degree of the polynomial equation that best fit the data is determined, where W is of second degree and A_{tp} is of fifth degree. The abstracted hovering power in (6.1) is for open propeller configurations. For a ducted configuration, the

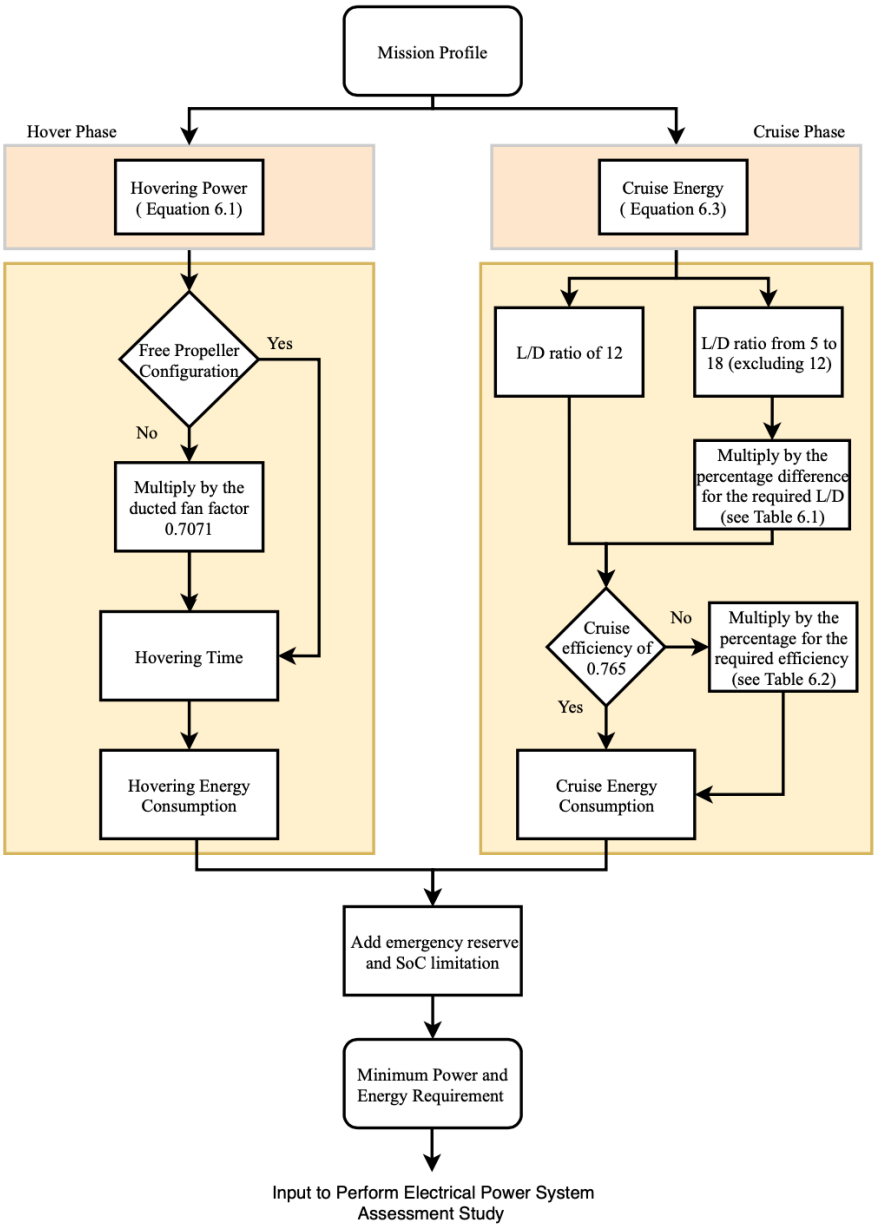

Figure 6.1: Summary of the Proposed Preliminary Design Methodology for Various Concept Designs.

result can be multiplied by a factor of 0.7071; which is the difference between (6.1) and (6.3). The abstracted hovering power (kW) in (6.1) covers total propeller areas from 2 m^2 to 39.2 m^2.

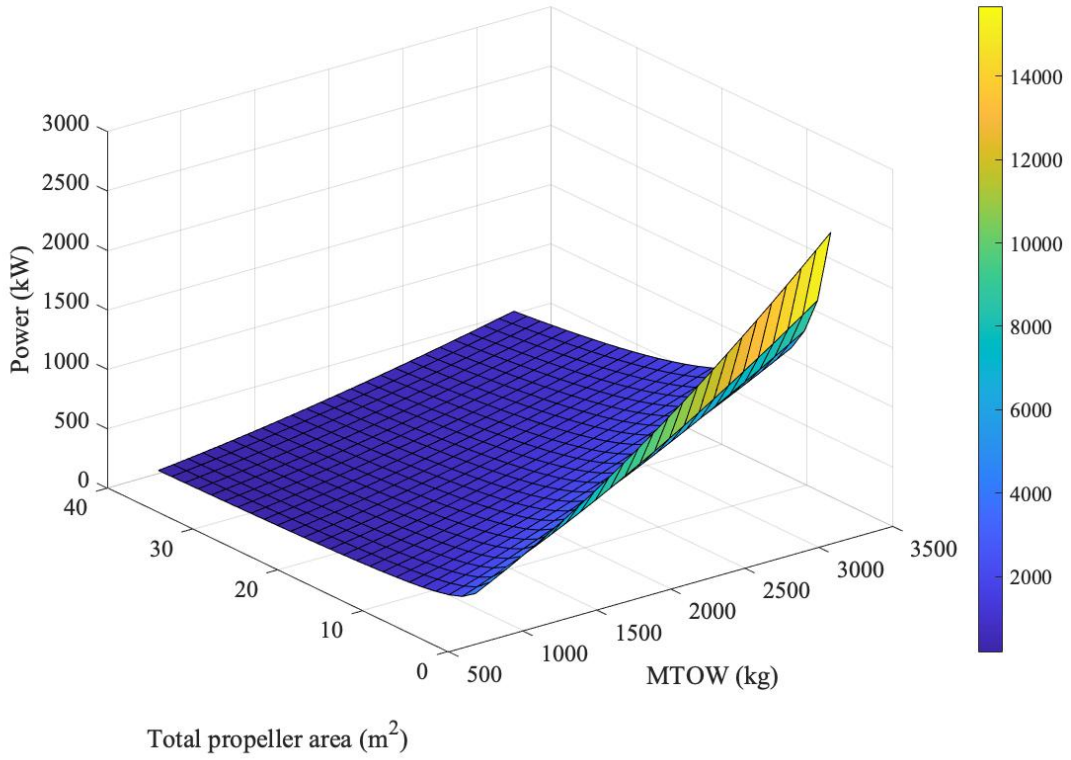

Figure 6.2: 3D Surface of the Minimum Hovering Power Requirement for a Variation of Total Propeller and Disc Loading.

$$\begin{aligned} HoverPower = {} & -48.06 + 0.603 \cdot W - 43.9 \cdot A_{tp} + 1.253e-04 \cdot W^2 - 9.153e-02 \cdot W \cdot A_{tp} \\ & + 9.442 \cdot A_{tp}^2 - 1.05e-05 \cdot W^2 \cdot A_{tp} + 6.83e-03 \cdot W \cdot A_{tp}^2 - 0.683 \cdot A_{tp}^3 \\ & + 4.002E-07 \cdot W^2 \cdot A_{tp}^2 - 2.165e-04 \cdot W \cdot A_{tp}^3 + 0.020 \cdot A_{tp}^4 + \\ & -5.078e-09 \cdot W^2 \cdot A_{tp}^4 + 2.397e-06 \cdot W \cdot A_{tp}^4 - 2.098e-04 \cdot A_{tp}^5 \end{aligned} \tag{6.1}$$

Where W is the maximum take-off weight of the aircraft (MTOW), and A_{tp} is the total propeller area.

The hovering energy can be computed by multiplying hovering power from the abstraction equation 6.1, and hovering time in hours. The equation for the total propeller area (m^2) is given in (6.2). This equation can be used to obtain the required number of motors this can be done by re-arranging the equation to provide an output for (n).

$$A_{tp} = \left(\frac{D}{2}\right)^2 \cdot \pi \cdot n \tag{6.2}$$

Where D is the diameter of the propeller blade in metres, and n is the number of motors.

6.2.2 Cruise Phase

Figure 6.3 shows the 3D plot of the minimum energy required for different aircraft MTOW and mission range. The "x-axis" presents the MTOW in kg, the "y-axis" presents the Range in (km), and the "z-axis" presents the computed energy consumption during cruise phase for the various MTOW and Range values. The presented results use a model with a L/D ratio of 12 and an efficiency of 0.765 [222] as an arbitrary baseline value in order to develop the methodology. The methodology provides different multiplication factors to represent variations as shown in Table 6.1 and 6.2. The cruise speed is illustrated in the colour bar starting from 54 km/hr in a step size of 1.5 up to 90 km/hr. The considered MTOW is from 800 kg which usually allow carrying one or two passengers, and for aircraft up to a MTOW of 3175 kg as stated by EASA [50,188], allows carrying up to five passengers. The mission range considered is from 30 for intra-city missions, to 250 km for intercity missions.

From the 3D surface in Figure 6.3, an polynomial equation is generated to abstract the cruise energy consumption in (kWh) for wide range of MTOWs and mission range values, shown in (6.3). The degree of the polynomial equation that best fit the data is determined, where W is of second degree and R is of first degree.

$$\begin{aligned} E_{cr} = & -4.742e-14 - 9.363e-18 \cdot W + 7.695e \\ & - 17 \cdot R \cdot 7.607e-21 \cdot W^2 + 2.965e-04 \cdot W \cdot R \end{aligned} \tag{6.3}$$

Where R is the range.

The value of the cruise speed (m/s) used in the cruise energy consumption equation 6.3 is presented in the colour bar of Figure 6.3. This value can be obtained by substituting the MTOW value and the result of the cruise energy from (6.3) into (6.4). The degree of the polynomial equation that best fit the data is determined, where E_{cr} is of first degree and W is of fifth degree.

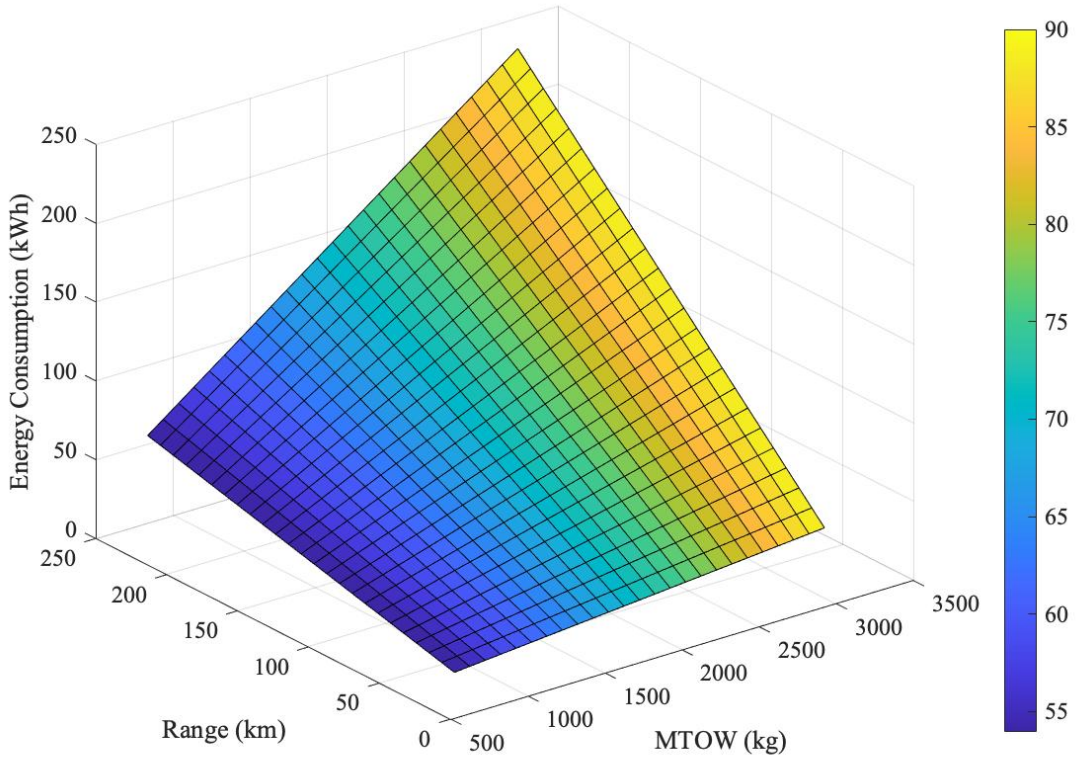

Figure 6.3: 3D Surface for Minimum Energy Requirement for different vehicles of L/D ratio of 12 given the Desired Range/Mission.

$$\begin{aligned} \textit{Flight Speed} = {} & 72 - 6.908e-02 \cdot W + 1.688 \cdot E_{cr} + 7.806e-05 \cdot W^2 - 1.908e \\ & - 03 \cdot W \cdot E_{cr} - 4.177e-08 \cdot W^3 + 1.021e-06 \cdot W^2 \cdot E_{cr} + 1.066e \\ & - 11 \cdot W^4 - 2.604e-10 \cdot W^3 \cdot E_{cr} - 1.044e-15 \cdot W^5 + 2.55e-14 \cdot W^4 \cdot E_{cr} \end{aligned} \tag{6.4}$$

With this simplification and identification of the required L/D ratio, Table 6.1 provides a list of L/D ratios and associated difference of the energy consumption in percentages from abstracted equation 6.3 when deviating from the baseline value of 12. The percentage difference illustrates the impact of the L/D ratio on the energy consumption for the same range and speed.

The chosen values of L/D ratio from 5 to 18 provide a range for existing eVTOL designs for estimating the energy consumption for a wide range of multirotor and winged eVTOL designs. From literature, the L/D ratio found for the multirotor eVTOL and helicopters is around 5 and less, and for winged eVTOL aircraft the L/D ratio ranges

from 10 to 20 depending on the aircraft design. In such instance, vectored thrust eVTOL carrying an economic payload (e.g., tilt propulsion, tilt wing configurations) can offer the highest L/D ratio (greater than a L/D of 13) when compared to lift-to-cruise and multirotor configurations [241–243].

Table 6.1: Impact of L/D ratio on the Required Energy Capacity on vehicles With the Same Speed

L/D ratio	**% Difference from Baseline L/D of 12**
5	-140%
6	-100%
7	-71.42%
8	-50%
9	-33.33%
10	-20%
11	-9.09%
12 (Baseline)	0
13	7.69%
14	14.29%
15	20%
16	25%
17	29.41%
18	33.33%

A similar process was applied to obtain results for a system with a different efficiency than the baseline 0.765 used in the cruise abstracted equation 6.3. Table 6.2 provides a list of different system efficiency and associated percentage difference from the baseline factor of 0.765. The list thus shows the impact of the efficiency difference on the cruise energy from the 0.765 used as a baseline value in the cruise abstraction equation to cover wide range of systems.

After estimating the energy for the hover and cruise phase, the next step is to add energy reserve as illustrated in Figure 6.1. For this study, emergency reserve of 20% of the total battery capacity is assumed sufficient to land the aircraft safely in emergency scenarios, and an additional 20% inaccessible top and bottom capacity to prolong the

Table 6.2: List of Difference factor for Different System Efficiencies in Comparison to the Baseline Efficiency of 0.765

Efficiency	**% Difference from Baseline System with Efficiency of 0.765**
0.9	82.35%
0.85	88.89%
0.8	95.42%
0.765 (Baseline)	0%
0.7	4.58%
0.65	11.11%
0.6	17.65%

battery lifecycle [222, 245]. This limitation result in allowing only 60% of the battery capacity to be used for the flight mission.

The output of the abstraction methodology provides the minimum power and energy requirement for the aircraft to perform the flight mission, as the output of step 1 shown in Figure 5.1 in chapter 5. Thus provides a start point to perform EPS assessment studies and identify suitable EPS architectures for a concept design.

6.3 Case Study: Validation of the Proposed Abstraction Methodology

The case study considers three different aircraft concepts used to validate the accuracy and usability of the proposed methodology and its applicability to wide range of designs.

6.3.1 Concept 1: Tilt Rotor eVTOL Configuration

Using the parameters in Table 6.3, theoretical equations (5.1) and (5.10) are used to estimate the theoretical power and energy requirements. The estimated hovering power required to hover the aircraft is 459.16 kW. Assuming the total hovering time is 1 minute, the energy consumption during the hovering phase is 7.65 kWh.

While using the abstracted (6.1), the hovering power is calculated as 472.72 kW,

Table 6.3: Parameter for Concept 1 eVTOL configuration

Parameters	**Value**	**Reference**
MTOW	2177 kg	[235]
Cruise L/D	18	[241]
Speed	89.4 m/s	[235]
Propeller area	18.8 m^2	Computed
Range	241 km	[235]
Hover time	1 min	Assumed
Energy Density	235 Wh/kg	[235]

and the hovering energy is calculated at 7.9 kWh. With regards to the cruise phase, the minimum energy required is 103.83 kWh for a L/D of 18 using (6.3). Table 6.4 shows the summary of the results comparison between the theoretical equations, abstracted design methodology, and the error between the values in percentages.

The following describes the L/D conversion from the baseline value of 12 to the required L/D of 18, using the abstracted equation 6.3 and the percentage difference in Table 6.1. The energy consumption for the cruise phase can be computed using the abstracted cruise energy in (6.3) provides 155.56 kWh for a L/D ratio of 12. Thus, to find the energy consumption for a L/D of 18, a factor of 33.33% (see Table 6.1) is applied to the energy results of (6.3), giving an energy requirement of 103.71 kWh. Using (6.4), the speed used for the resultant energy consumption is 89.3 m/s which is relatively close to the specified parameters in Table 6.3.

Table 6.4: Concept 1 Validation Results using 3D surface and Theoretical Equations

Parameter	**Theoretical Equations**	**Abstracted Design Equations**	**Difference (%)**
Hovering Power (kW)	459.16	472.7	-2.95%
Hovering Energy (kWh)	7.65	7.87	-2.95%
Cruise Energy (kWh)	103.83	103.71	0.1%
Total Energy (kWh)	185.79	185.98	-0.1%
Battery Weight (kg)	790.6	791.4	-0.1%

The total energy consumption for concept 1 is 185.98 kWh including the 40% battery capacity limits and reserve. Correspondingly, the weight of the battery with an energy density of 235 Wh/kg is 791.4 kg. The percentage difference from the theoretical equations and the presented abstract methodology shown in Table 6.4 is less than 0.5% and -3%.

6.3.2 Concept 2: Lift+Cruise eVTOL Configuration

Table 6.5: Parameter for Concept 2 eVTOL configuration

Parameters	**Value**	**Reference**
MTOW	1508 kg	[41]
Cruise L/D	12	[41]
Speed	66.9 m/s	[41]
Propeller area	12.56 m^2	Computed
Range	97 km	[41]
Hover time	1.67 min	[41]
Energy Density	200 Wh/kg	[41]

The parameters and performance data of concept 2 were acquired from [41], shown in Table 6.3, to verify the results of the abstracted equations presented in this chapter. The chosen computed propeller area is 12.56 m^2 for the 12-propeller aircraft matches the results of the hovering power and energy with the data provided in [41].

The hovering power and energy from reference [41] is 325 kW and 9 kWh, and the cruise energy is 37 kWh with cruise system efficiency of 0.9. Using theoretical equations (5.1) and (5.10), the hovering power is calculated at 323 kW and the hovering energy is 9.02 kWh assuming the hovering time is 1.67 minutes to match the hovering energy given in [41]. The computed cruise energy using the theoretical equations is 36.9 kWh with a system efficiency of 0.9.

The summary of the results from the abstracted design methodology, theoretical equations, and the error between the values in percentages are presented in Table 6.6. The results of the abstracted hovering power using (5.1) is very similar to the results

of the theoretical equations as seen in Table 6.6. While for the cruise phase, a factor of 82.35% is applied in addition to the abstracted cruise energy in (6.3) (see Table 6.2) to present the difference of the system efficiency from 0.765 (baseline) to the 0.9 efficiency of concept 2, giving an energy consumption of 35.71 kWh. The speed used in the resultant abstracted cruise energy consumption can be computed using (6.4). The speed result is 65.2 m/s which is relatively close to 66.9 m/s given in Table 6.3.

Table 6.6: Concept 2 Validation Results using 3D surface and Theoretical Equations

Parameter	**Theoretical Equations**	**Abstracted Design Equations**	**Difference (%)**
Hovering Power (kW)	324.12	325.45	-0.41%
Hovering Energy (kWh)	9.02	9.08	-0.41%
Cruise Energy (kWh)	36.9	35.7	3.22%
Total Energy (kWh)	76.5	74.6	2.5%
Battery Weight (kg)	382.7	373.12	2.5%

The total energy consumption is 74.6 kWh including the 40% battery capacity limits and reserve, which is very close to the value given in [41] of 75 kWh presenting a total error of 0.5%. From this, assuming the energy density of the battery is 200 Wh/kg, the weight of the battery is 373.12 kg. The percentage difference from the theoretical equations and the presented abstract methodology shown in Table 6.6 is less than 3.5% and -1%.

6.3.3 Concept 3: Tilt-jet eVTOL Configuration

To demonstrate the methodology using different eVTOL concepts, concept 3 is a thrust vectored eVTOL with ducted fans. Aircraft with a ducted fan configuration provides more thrust and power than a free propeller with the same disc loading [24]. The presented concept uses 36 fans with a diameter of 0.295 m giving a very small propeller area of 0.273 m^2 hence a large disc loading.

The hovering power presented in [24] is 2570 kW including onboard power and total system efficiency, hence a 1511 kW excluding any additions. The cruise power from the reference is 224 kW [24] using a system efficiency of 0.65. Using abstracted

Table 6.7: Parameter for Concept 3 eVTOL configuration

Parameters	**Value**	**Reference**
MTOW	3175 kg	[24]
Cruise L/D	18.26	[24]
Speed	300 km/hr	[24]
Propeller area	18.8 m^2	Computed
Range	200km	[246]
Hover time	1 min	Assumed
Energy Density	320 Wh/kg	[24]

equations, the hovering power for a free propeller configuration excluding additional power for onboard systems and efficiency using (5.1) gives 2146 kW and for a ducted fan configuration using (5.2) the hovering power is 1517 kW. The hovering time used in [24] is 1 minute, hence the result of the hovering energy is 25.28 kWh.

For the cruise phase, the calculated cruise power is 226.6 kW using theoretical equations for a L/D ratio of 18.26 which is very similar to the results in [24]. As the percentages provided in Table 6.1 only considers integer values hence the nearest value is chosen. Therefore, the cruise power and energy for a L/D of 18 using theoretical equations is 221.8 kW and 147.89 kWh respectively.

Using the abstracted hovering power in (6.1), a factor of 0.7071 is applied to represent the ducted fan configuration, giving a hovering power of 1541.6 kW and a hovering energy of 25.69 kWh for 1 minute. The abstracted cruise energy in (6.3) uses a system efficiency of 0.765 and a L/D ratio of 12, while concept 3 uses system efficiency of 0.65 and L/D of 18 (rounded). Thereby, factor of 17.69% and 33.33% are applied to the abstracted cruise energy in (6.3) to represent for a system efficiency of 0.65 and a L/D of 18, accordingly (see Table 6.1 and 6.2). Table 6.8 present the summary of the results from the abstracted design methodology, theoretical equations, and the error between the values in percentages.

The total energy consumption is 288.9 kWh including the 40% battery capacity limits and reserve. Hence the weight of the battery for the specified mission with an

Table 6.8: Concept 3 Validation Results using 3D surface and Theoretical Equations

Parameter	**Theoretical Equations**	**Abstracted Design Equations**	**Difference (%)**
Hovering Power (kW)	1517	1541.6	-1.59%
Hovering Energy (kWh)	25.28	25.69	-1.59%
Cruise Energy (kWh)	147.89	147.67	0.14%
Total Energy (kWh)	288.64	288.9	-0.1%
Battery Weight (kg)	902	902.9	-0.1%

energy density of 320 Wh/kg is 902.9 kg using the abstracted design methodology. The percentage difference from the theoretical equations and the presented abstract methodology shown in Table 6.8 is less than 1% and -2%.

6.4 Summary

The work conducted in this chapter offers a novel abstract design methodology summarising the relationship between aircraft aerodynamics and EPS requirements in a readily usable format for EPS assessment studies. The abstract design methodology enables to perform complete feasibility assessment of different aircraft configurations from the aircraft aerodynamics to the design of the EPS architecture at initial stage of design. In contrast to the design methodologies in the literature, the proposed methodology does not require a pre-defined aircraft structure or a detailed design of the aircraft aerodynamics and propeller geometry nor the expertise, which is required at the next stages latter of the preliminary phase. The methodology is validated using theoretical equations and conceptual designs from the literature showing a difference of less than 4%. Further work is to consider the relationship between the lift-to-drag ratio and the speed to investigate the impact of variation of speed values for a fixed lift-to-drag ratio on the EPS design.

The work in this chapter compliment design methodology for a certification-compliant EPS architecture presented in Chapter 5 to answer the research question (1). Combining the presented abstraction methodology with Chapter 5 enables a comprehensive

feasibility assessment of various aircraft configurations, encompassing aircraft aerodynamics and EPS architecture design, at the initial stage of aircraft design.

Chapter 7

Conclusions and Future Work

With the continuous growth of the population in urban areas, public transportation will face substantial pressure, and the proliferation of vehicles will exacerbate congestion problems in ground transportation. The eVTOL aircraft has been proposed as a solution to alleviate road congestion by facilitating greener and quieter aviation, offering a more time-efficient commuting option compared to helicopters.

However, electrically driven propulsion systems for novel eVTOL aircraft represent a significant step change from the use of electrical power for secondary on-board systems for state of the art more- electric aircraft, necessitating the use of new EPS architectures and technologies. This step change present its own challenges arise to achieve a low weight and low cost economic eVTOL design. This highlights the need for comprehensive understanding of the safe integration of EPS technologies and the aerodynamic-electrical failure dependencies to find a design solution for an economic eVTOL aircraft. The research work has resulted in methods that assess the aircraft configuration, sizing requirements, and safety requirements of the EPS for a certification-compliant design.

The summary of research results and outcomes are grouped according to the research questions and objectives identified in section 1.3, these are:

> ***"Research Question (1)***
> ***What are the essential factors to consider when designing an economically efficient and lightweight eVTOL aircraft"***

"Research Question (2)
What is the process for designing a certifiable power system architecture that incorporates non-resettable protection devices for primary protection"

Chapter 3 contributes to the second research question of this thesis. The chapter presents the first methodology to model a complete self-triggered Pyrofuse available in the public domain. The presented model enables the exploration of the design characteristics and operation of Pyrofuses within a DC system. The key outcome of this work has illustrated the tunability of the Pyrofuse device for use in a graded protection system. This is due to its hybrid configuration of pyroswitch and fuses to best fit the application. The results suggests that good protection coverage against a range of faults and failure modes can be realised with a purely Pyrofuse based protection system. However, Pyrofuses are non-resettable which presents challenges for use as a primary protection for the EPS. Where an externally triggered Pyrofuse is prone to EMI failures which can result in triggering the Pyrofuse in normal operations. And, self- triggered devices uses a fuse as the current sensor, where the fuse is a normal DC fuse which is dependent on the magnitude of current.

Chapter 4 presents one of the key contributions of this thesis, that is a methodology for a preliminary certification compliance assessment for the use of Pyrofuses in eVTOL concept designs. This was completed by looking through the review of relevant safety requirements, eVTOL configurations, and location-specific failure modes. This chapter contributes to both research question (1) and research question (2).

It is evident from the results that the precise classification of a fault is highly dependent on the aerodynamic configuration and the design of the protection system. To use non-resettable devices, it is critical to demonstrate minor failure impact on the aircraft after the loss of a single non-resettable device. From this, the work in this thesis have proposed a parallel-redundant Pyrofuse set-up. The set-up consists of an externally triggered Pyrofuse connected directly to the rest of the system as the primary

and self-triggered Pyrofuse as a back-up. This proposed solution address issues related to EMI-related spurious tripping of all Pyrofuses, and the thermal limit of the sensor fuse in a self-triggered Pyrofuse. This findings of this work contributes to research question (1). Following from this, the concluding remarks are:

- The Pyrofuse device can be implemented in for a multirotor, vectored thrust, and lift plus cruise configurations with 10 motors or more. yet challenges remain in demonstrating the mass tripping of Pyrofuses are extremely improbable. This requires extensive testing of the EPS against lightning strikes, short-circuit high impedance faults, and EMI.

- Configurations with less than 10 motors requires a set of safety measures to maintain a minor failure impact on the aircraft and prevent common mode failures, which significantly increases the weight of the EPS. This makes the use of Pyrofuses not competitively viable for primary protection of such configurations.

- Realistically, the use of the Pyrofuse is thus restricted to multirotor configurations, where a configuration of 10 motors or more is realisable. Having a vectored thrust or lift plus cruise configuration of 10 motors or more significantly increases the hovering power requirement, which reduces the cruise efficiency and the long range capability of the configuration. Additionally, with the eVTOL market going towards developing vectored thrust eVTOL aircraft design for both intercity and intracity flight missions, the use of Pyrofuses for primary protection becomes infeasible.

- This conclusion address the first research question (1), that is the safety considerations associated with using Pyrofuses in the EPS can offset the weight savings and result in a heavier EPS eVTOL aircraft.

Chapter 5 presents the first design methodology to capture a certification-compliant EPS architecture at the preliminary design phase of an eVTOL aircraft. The methodology introduces an integrated link between the aircraft concept design, including mission requirements and aircraft aerodynamics, availability of EPS technologies, and certification, to the design of the EPS architecture that enables safety requirements to be

met. The roadmaps of EPS technology presented in Chapter 2 is combined with the proposed methodology for a certification-compliant EPS to quantify the impact of the safety requirements and EPS technologies on the viability of aircraft design for a given year. The highlight of the results are as follows:

- A complete consideration of the EPS in the early stage design process is essential to consider the amount of redundancy and oversizing required to address potential failures for compliance with certification regulations. While considering safety measures at a later stage will have a snowball effect on the aircraft design to meet the certification requirements or to be within the design constraints. This present a risk of impeding the project delivery or the inability to achieve the required design objectives.

- The aircraft developers in the eVTOL industry are driven by the need to develop a novel design to allure investors and shareholders. This often includes the need to overstate the capability of the proposed aircraft configuration with the cost of simplifying the EPS. For instance, Chapter 5 shows a multirotor configuration with a certifiable EPS design is limited to intracity transportation of less than 30 km using the currently available technologies (including the weight of the thermal system), and potentially to around 90 km as the technology progresses beyond 2030. Unless novel in-house technologies were developed allowing lighter weight aircraft for longer distances; thus ambitious range target from aircraft developers above the aforementioned results and timeline is deemed infeasible. That explains the shift of the eVTOL developers from multirotor configurations to either vectored thrust and lift plus cruise.

- This conclusion address the first research question (1), that is the safety considerations associated with using Pyrofuses in the EPS can offset the weight savings and result in a heavier EPS eVTOL aircraft

Chapter 6 compliment the design methodology for a certification-compliant power system architecture from Chapter 5 to answer the research question (1). Chapter 6 presents a novel abstract design methodology summarising the relationship between

aircraft aerodynamics and EPS requirements in a readily usable format for EPS assessment studies. The design methodology provides the start point to generate a set of EPS architectures and evaluate the overall weight of the EPS to the aircraft weight budget. The key contribution is the integrated design tool that is widely accessible to people with no prior experience in aerodynamics and applicable to many eVTOL aircraft designs. By combining the input from the proposed abstraction design methodology with the aircraft concept design phase in the methodology for certification-compliant EPS architecture presented in Chapter 5; it becomes possible to perform a comprehensive feasibility assessment of various aircraft configurations, encompassing aircraft aerodynamics and EPS architecture design, at the initial stage of aircraft design.

In conclusion, the literature reveals that EPS technologies and architecture design have not been given the highest priority in industry or public domain research. While, the current state of EPS technologies, in terms of safe integration into aircraft, is a limiting factor that has not received significant attention. This necessitates the need for holistic system level designs and weight assessment studies. The work in this thesis thus provides the tools, methodologies, and guidance for new market entrants or researchers in this field to understand the failure dependencies of the EPS in a high voltage system architecture. This understanding is crucial for effectively and accurately planning, optimising, and designing a resilient EPS architecture, ultimately leading to the achievement of a certifiable and an economically viable aircraft. These are, the step-by-step methodology in Chapter 5 provides the guidelines for a certification-compliant EPS architecture. Chapter 6 and 2 compliments the work in Chapter 5; Chapter 6 by generating abstracted power requirements of different eVTOL configurations in a readily usable format facilitating EPS assessment studies, and Chapter 2 by providing technology roadmaps. Chapter 2 also identified a potential lightweight Pyrofuse protection device for eVTOL applications. The Pyrofuse was developed, modelled, and tested in Chapter 3. The airworthiness of the non-resettable Pyrofuse device was assessed in Chapter 4 through certification requirements and electrical failure modes. Where Chapter 5 and Chapter 4 are the main contribution of this thesis, where its content has addressed the two research questions of this thesis.

7.1 Limitations and Future Work

The research presented in this thesis has explored several aspects from the review of power and energy requirements for different eVTOL configurations to the process of system-level and component-level safety assessment. The methodologies proposed enable the exploration of the design space, facilitating the development of a feasible and certifiable power system design within a defined timeframe. This section highlight further work and developments to complement the research outcomes.

7.1.1 Future work

- There is a necessity to elaborate on the Pyrofuse modelling methodology presented in Chapter 3 to incorporate the effect of thermal cycling degradation following the peak of a current fault. This becomes particularly relevant when modelling the self-triggered Pyrofuse, as the sensor fuse may be influenced by the heat and cooling cycles it undergoes when experiencing multiple short-duration transient faults below the fuse rating. Additionally, further studies on the arc model of the fuse to be added to the methodology to better estimate the total clearing time of the fuse if not provided by the manufacturer. It is also valuable to include an assessment of the impact of ambient temperature and altitude on the fuse tripping time.This expansion would significantly improve the accuracy of the Pyrofuse model which can be used to provide verification evidence of the system behaviour to the certification bodies.

- Chapter 4 has presented the first step into addressing solutions for the challenges of non-resettable devices for protecting flight critical systems. The potential mitigation measures to prevent common failure modes and reduce the risks of NRPDs to an acceptable level, incorporate the use of overvoltage protection devices such as surge arrestors, and the parallel-redundant Pyrofuse set-up using; self-triggered and externally triggered Pyrofuses. This is to eliminate overvoltage transients and EMI-related risks from mass tripping Pyrofuses. Further work is required to validate the proposed solution. This includes modelling the set-up in

simulation software and test the coordinatino of Pyrofuses in the event of lightning transients. 2) Quantitative assessment of the parallel-redundant Pyrofuse set-up. This could be beneficial in determining the usability of Pyrofuses for aerospace applications.

- The abstraction methodology discussed in Chapter 6 primarily focuses on abstracting the detailed aerodynamics design of the aircraft to calculate power and energy requirements for a wide range of aircraft configurations. However, there is a need for further improvement and expansion of the methodology's simplification and usability to investigate the impact of design on key factors, such as noise generation. Firstly, there is a limitation in the presented methodology regarding the direct link between the angle of attack, speed, maximum take-off weight, and the lift-to-drag ratio. This limitation hinders the ability to thoroughly analyse the impact of changing a single aerodynamic design factor on other aerodynamic factors and, consequently, the EPS system. Secondly, noise emissions from eVTOL aircraft pose a significant challenge for operations in urban areas. Therefore, it is crucial to conduct a study on abstracting the integration of motor speed and thrust required to lift the aircraft in order to estimate noise emissions. This analysis is essential for assessing the feasibility of different aircraft designs in terms of noise levels. Enhancing these aspects of the current abstract design methodology would greatly benefit designers in selecting an optimal aerodynamic design that incorporates available EPS technologies and meets safety requirements (by using methodology in Chapter 5), resulting in a lightweight and economically viable eVTOL design.

Bibliography

[1] Department of Transport, "Transport and Environment Statistics 2021 Annual report", Department of Transport, 2021.

[2] "COP26 declaration on accelerating the transition to 100% zero emission cars and vans", GOV.UK, 2022.

[3] "Transport - UN Climate Change Conference (COP26) at the SEC – Glasgow 2021", *UN Climate Change Conference (COP26) at the SEC – Glasgow 2021*, 2022. [Online]. Available: https://ukcop26.org/transport/. [Accessed: 03- Aug- 2022].

[4] "68% of the world population projected to live in urban areas by 2050, says UN — UN DESA — United Nations Department of Economic and Social Affairs", *United Nations*, 2018. [Online]. Available: https://www.un.org/development/desa/en/news/population/2018-revision-of-world-urbanization-prospects.html. [Accessed: 03- Aug- 2022].

[5] J. Holden and N. Goel, "Uber elevate: Fast-forwarding to a future of on- demand urban air transportation," Uber Elevate, 2016.

[6] "How Loud is an eVTOL?", *Archer*, 2022. [Online]. Available: https://archer.com/news/how-loud-is-an-evtol. [Accessed: 03- Aug- 2022].

[7] "Joby Confirms Revolutionary Low Noise Footprint Following NASA Testing — Joby", *Joby Aviation*, 2022. [Online]. Available: https://www.jobyaviation.com/news/joby-revolutionary-low-noise-footprint-nasa-testing/. [Accessed: 03- Aug- 2022].

[8] J. Bevirt, "How Quiet is the Joby Aircraft during Hover?", *Youtube*, 2021. [Online]. Available: https://www.youtube.com/watch?v=GHmXR0wBOiI. [Accessed: 03- Aug- 2022].

[9] M. Duffy, S. Wakayama, R. Hupp, R. Lacy and M. Stauffer, "A Study in Reducing the Cost of Vertical Flight with Electric Propulsion", in *17th AIAA Aviation Technology, Integration, and Operations Conference*, Denver, Colorado, 2017.

[10] H. Kim, A. Perry, amd P. Ansel, "A Review of Distributed Electric Propulsion Concepts for Air Vehicle Technology", in *AIAA/IEEE Electric Aircraft Technologies Symposium (EATS)*, Cincinnati, OH, USA, 2018, doi: 10.2514/6.2018-4998.

[11] A. Head, *eVTOL Basics For Investors*. eVTOL.com, 2021.

[12] M. Tarabanovska, "UAM and Infrastructure: To build or not to build", *Flight crowd*, 2020. [Online]. Available: https://www.flight-crowd.com/post/uam-and-infrastructure-to-build-or-not-to-build. [Accessed: 03- Aug- 2022].

[13] P. Brinkmann, "Air Taxi companies begin dueling publicly over standards for charging stations," Aerospace America, 2024. [Online]. https://aerospaceamerica.aiaa.org/air-taxi-companies-begin-dueling-publicly-over-standards-for-charging-stations/ [Accessed 24- Jan- 2024].

[14] Federal Aviation Administration, "Advanced Air Mobility — Air Taxis", [online]. https://www.faa.gov/air-taxis [Accessed 24- Jan- 2024].

[15] A. Bacchini. and E. Cestino, "Electric VTOL Configurations Comparison", *Aerospace* vol. 6, no. 3, p. 26, 2019. Available: 10.3390/aerospace6030026..

[16] M. Duffy, A. Sevier, R. Hupp, E. Perdomo, S. Wakayama, "Propulsion Scaling Methods in the Era of Electric Flight", in *2018 AIAA/IEEE Electric Aircraft Technologies Symposium*, Cincinnati, Ohio, 2018, doi: 10.2514/6.2018-4978

[17] W. Remmerie, "eVTOL certification interview with EASA", Air Sharper. 2023.[online] https://airshaper.com/blog/evtol-certification-interview-with-easa [Accessed 24- Jan- 2024].

[18] S. Salzwedel, "eVTOL certification interview with EASA", Air Sharper. 2021. [online] https://blogs.sw.siemens.com/podcasts/talking-aerospace-today/innovation-podcast-series-ep-3-evtol-power-density-and-thermal-management/a [Accessed 4- Feb- 2024].

[19] Aerospace Technology Institute, "Insight - Electrical Power Systems", 2018.

[20] S. Melo, F. Cerdas, A. Barke, C. Thies, T. Spengler and C. Herrmann, "Life Cycle Engineering of future aircraft systems: the case of eVTOL vehicles", *Procedia CIRP*, vol. 90, pp. 297-302, 2020. Available: 10.1016/j.procir.2020.01.060.

[21] A. Schwab, A. Thomas, E. Robertson and S. Cary, "Electrification of Aircraft: Challenges, Barriers, and Potential Impacts", National Renewable Energy Laboratory, 2021.

[22] D. Thisdell, "The magic number that makes electric flight viable", *Flight Global*, 2020. [Online]. Available: https://www.flightglobal.com/business-aviation/the-magic-number-that-makes-electric-flight-viable/140050.article. [Accessed: 03 - Aug - 2022].

[23] Roland Berger, "Aircraft Electrical Propulsion - The Next Chapter of Aviation?", [online]. URL: https://www.rolandberger.com/en/Insights/Publications/New-developments-in-aircraft-electrical-propulsion.html [Accessed: 21- Jan- 2020].

[24] P. Nathen, A. Bardenhagen, A. Strohmayer, R. Miller, S. Grimshaw and J. Taylor, "Architectural performance assessment of an electric vertical take-off and landing (e-VTOL) aircraft based on a ducted vectored thrust concept", Lilium, 2021.

[25] *Volocopter*, 2022. [Online]. Available: https://www.volocopter.com/solutions/volocity/. [Accessed: 03- Aug- 2022].

[26] "Volocopter Certification Progress Keeps Paris 2024 Debut In Sight", *Aviation Week*, 2022. [Online]. Available: https://aviationweek.com/aerospace/advanced-air-mobility/volocopter-certification-progress-keeps-paris-2024-debut-sight [Accessed: 24- Jan - 2024].

[27] "Volocopter VoloConnect", *Electric VTOL news*. [Online]. Available: https://evtol.news/volocopter-voloconnect. [Accessed: 03- Aug- 2022].

[28] "EHang 216", *Electric VTOL news*. [Online]. Available: https://evtol.news/ehang-216/. [Accessed: 03- Aug- 2022].

[29] C. Alcock, "China issues the world's first Evtol aircraft type certificate to Ehang's EH216-S Autonomous Vehicle," Future Flight. [Online]. Available: https://www.futureflight.aero/news-article/2023-10-13/china-issues-worlds-first-evtol-aircraft-type-certificate-ehangs-eh216-s [Accessed: 4- Feb- 2024].

[30] "Airbus Urban Mobility CityAirbus NextGen", *Electric VTOL news*. [Online]. Available: https://evtol.news/airbus-cityairbus-nextgen. [Accessed: 03- Aug- 2022].

[31] E. DOMINGUEZ-PUERTA, "Airbus CityAirbus NextGen", *Future Flight*, 2022. [Online]. Available: https://www.futureflight.aero/aircraft-program/cityairbus-nextgen?model=cityairbus. [Accessed: 03- Aug- 2022].

[32] "CityAirbus demonstrator", Airbus. [Online]. Available: https://www.airbus.com/en/urbanairmobility/cityairbus-nextgen/cityairbus-demonstrator. [Accessed: 03- Aug- 2022].

[33] "Bell Nexus 4EX", *Electric VTOL news*. [Online]. Available: https://evtol.news/bell-nexus-4ex/. [Accessed: 03- Aug- 2022].

[34] B. Sampson, "In depth: Bell Nexus eVTOL moves towards certification", Aerospace Testing International, 2020. [Online]. Available: https://www.aerospacetestinginternational.com/news/drones-air-taxis/in-depth-bell-nexus-evtol-moves-towards-certification.html. [Accessed: 03- Aug- 2022].

[35] "Lilium Jet", *Electric VTOL News*. [Online]. Available: https://evtol.news/lilium/. [Accessed: 03- Aug- 2022].

[36] J. Nevans, "Lilium extends eVTOL type certification timeline to 2025", *evtol.com*, 2022. [Online]. Available: https://evtol.com/news/lilium-extends-evtol-type-certification-timeline-2025/. [Accessed: 03- Aug- 2022].

[37] "Joby Receives Part 135 Certification from the FAA — Joby", Joby Aviation, 2022. [Online]. Available: https://www.jobyaviation.com/news/joby-receives-part-135-air-carrier-certificate/. [Accessed: 03- Aug- 2022].

[38] "VX4 — Urban Air Mobility", *Vertical Aerospace*. [Online]. Available: https://vertical-aerospace.com/vx4/. [Accessed: 03- Aug- 2022].

[39] "Supernal Debuts eVTOL Product Concept at CES 2024," Hyundai Press Release. [Online]. Available: https://www.hyundai.news/uk/articles/press-releases/supernal-debuts-evtol-product-concept-at-ces-2024.html [Accessed: 4- Feb- 2024].

[40] "Hyundai Motor Group and Safran Signed a Memorandum of Understanding for Advanced Air Mobility Development Cooperation", *Hyundai*, 2022. [Online]. Available: https://www.hyundai.news/eu/articles/press-releases/hyundai-motor-group-and-safran-signed-a-mou.html. [Accessed: 03- Aug- 2022].

[41] "Archer's Maker Aircraft", Archer. [Online]. Available: https://www.archer.com/maker. [Accessed: 03- Aug- 2022].

[42] "Archer Details Motor and Battery Design for the Midnight EVTOL Air Taxi", *future flight*. [Online]. Available: https://www.futureflight.aero/news-article/2022-11-18/archer-details-motor-and-battery-design-midnight-evtol-air-taxi. [Accessed: 24- Jan- 2024].

https://www.futureflight.aero/news-article/2022-11-18/archer-details-motor-and-battery-design-midnight-evtol-air-taxi

[43] "Overair (Karem) Butterfly", *Electrical VTOL News*. [Online]. Available: https://evtol.news/overair-butterfly/. [Accessed: 03- Aug- 2022].

[44] "Airspace Experience Technologies Mobi-one," Future Flight, https://www.futureflight.aero/aircraft-program/mobi-one. [accessed 4 - Feb - 2024].

"Airspace Experience Technologies (ASX) MOBi-One V3", *Electrical VTOL News*. [Online]. Available: https://evtol.news/airspace-experience-technologies-asx-mobi-one-v3. [Accessed: 03- Aug- 2022].

[45] "Dufour Aerospace aEro 3", *Electrical VTOL News*. [Online]. Available: https://evtol.news/dufour-aerospace-aero-3. [Accessed: 03- Aug- 2022].

[46] "Dufour Aerospace and Blueberry Aviation enter a long-term commercial partnership", *AVIATOR*, 2022. [Online]. Available: https://newsroom.aviator.aero/dufour-aerospace-and-blueberry-aviation-enter-a-long-term-commercial-partnership/. [Accessed: 03- Aug- 2022].

[47] C. Courtin, J. Hansman, "Safety Considerations in Emerging Electric Aircraft Architectures", in *Aviation Technology, Integration, and Operations Conference*, Atlanta, Georgia. 2018.

[48] Federal Aviation Administration, "Part 23- Airworthiness Standards: Normal Category Airplanes", Electronic Code of Federal Regulations. [Online]. Available: https://www.ecfr.gov/cgi-bin/text-idx?SID=685dc1ae97ae3f5e5569e47880fab01emc=truenode=pt14.1.23 [Accessed: Feb. 27, 2021].

[49] M. Hirschberg, "Commentary: FAA Changes Course on eVTOL Certification", Electric VTOL News, 2022. [Online]. Available: https://evtol.news/news/commentary-faa-changes-course-on-evtol-certification. [Accessed: 09- Aug- 2022].

[50] European Union Aviation Safety Agency, "Special Condition Vertical Take-off and Landing (VTOL) Aircraft". [Online]. Available: https://www.easa.europa.eu/sites/default/files/dfu/SC-VTOL-01.pdf [Accessed: Aug. 10, 2019].

[51] J. Booker, C. Patel and P. Mellor, "Modelling Green VTOL Concept Designs for Reliability and Efficiency", *Designs*, vol. 5, no. 4, p. 68, 2021. doi:10.3390/designs5040068.

[52] O. Bertram, F. Jager, V. Voth and J. Rosenberg, "UAM Vehicle Design with Emphasis on Electric Powertrain Architectures", in *AIAA SCITECH 2022 Forum*, San Diego, CA Virtual, 2022.

[53] C. Jones, K. Millar, K. Fong, R. Alzola, P. Norman and G. Burt, "A Modelling Design Framework for Integrated Electrical Power and Non-Electrical Systems Design on Electrical Propulsion Aircraft," in *2022 IEEE Transportation Electrification Conference Expo (ITEC)*, 2022. doi:10.1109/ITEC53557.2022.9813810.

[54] B. Hinman, "Hang in There: Why Hovering Matters in eVTOL Design", *Medium*, 2019. [Online]. Available: https://brian-is-flyin.medium.com/hang-in-there-why-hovering-matters-in-evtol-design-bf60aa5b69db. [Accessed: 10- Aug- 2022].

[55] E. Head, "What we know about Lilium's eVTOL batteries so far", *The Vertical Flight Society*, 2021. [Online]. Available: https://evtol.com/features/lilium-evtol-batteries-what-we-know/. [Accessed: 10- Aug- 2022].

[56] OXIS Energy, "OXIS ENERGY Progresses its Lithium Sulfur (Li-S) cell technology to 450 Wh/kg.", 2018.

[57] "About Amprius Technologies", *Amprius*. [Online]. Available: https://www.amprius.com/about. [Accessed: 03- Aug- 2022].

[58] "Product Pipeline", *PolyPlus*. [Online]. Available: https://polyplus.com/product-pipeline/. [Accessed: 09- Aug- 2022].

[59] "Building the Future of Batteries", *Sion Power*. [Online]. Available: https://sionpower.com. [Accessed: 09- Aug- 2022].

[60] T. Spendlove, "New HIU lithium-metal battery boasts 560 Wh/kg specific energy", *Charged EVs*, 2021. [Online]. Available:

https://chargedevs.com/newswire/new-hiu-lithium-metal-battery-boasts-560-wh-kg-specific-energy/. [Accessed: 09- Aug- 2022].

[61] Roland Berger, "Aircraft Electrical Propulsion - Onwards and Upwards", [online]. URL: https://www.rolandberger.com/publications/publication_pdf/roland_berger_aircraft_electrical_propulsion_2.pdf [Accessed: 21- Jan- 2020].

[62] Misra, A., "Summary of 2017 NASA Workshop on Assessment of Advanced Battery Technologies for Aerospace Applications", AIAA SciTech Forum and Exposition. [online]. Available: https://ntrs.nasa.gov/archive/nasa/casi.ntrs.nasa.gov/20180001539.pdf.

[63] K. Field, "Tesla Model 3 Battery Pack & Battery Cell Teardown Highlights Performance Improvements", *Clean Technica*, 2019. [Online]. Available: https://cleantechnica.com/ 2019/01/28/tesla-model-3-battery-pack-cell-teardown-highlights-performance-improvements/. [Accessed: 09- Aug- 2022].

[64] *High Energy Rechargeable Metal Cells for Space (LMP063767)*. Solid Energy Systems, 2017.

[65] "Amprius' Silicon Nanowire Lithium Ion Batteries Power Airbus Zephyr S HAPS Solar Aircraft", Amprius, 2018. [Online]. Available: https://amprius.com/corporate-announcements/amprius-silicon-nanowire-lithium-ion- batteries-power- airbus-zephyr-s-haps-solar-aircraft. [Accessed: 09- Aug- 2022].

[66] OXIS Energy, "OXIS ENERGY Progresses its Lithium Sulfur (Li-S) cell technology to 450WH/kg.", 2018.

[67] 24M, "24M Technologies, Inc. Awarded $9 Million From ARPA-E for Transformational Energy Technology", 2022.

[68] P. Lima, "CATL achieves 304 Wh/kg in new battery cells", *Push Electric Vehicles Forward*, 2022. [Online]. Available: https://pushevs.com/2019/03/30/catl-achieves-304-wh-kg-in-new-battery-cells/. [Accessed: 09- Aug- 2022].

[69] B. Wang, "Tesla's Maxwell Dry Battery and a Five Year Lead on the World", *Next Big Future*, 2019. [Online]. Available: https://www.nextbigfuture.com/2019/03/teslas-maxwell-dry-battery-and-a-five-year-lead-on-the-world.html. [Accessed: 09- Aug- 2022].

[70] M. Kane, "Amprius Ships First 450 Wh/kg, 1150 Wh/l Battery Cells", *Inside EVs*, 2022. [Online]. Available: https://insideevs.com/news/566876/amprius-ships-450whkg-battery-cells/. [Accessed: 09- Aug- 2022].

[71] "Battery500 project has achieved 350 Wh/kg and more than 350 cycles", *Green Car Congress*, 2020. [Online]. Available: https://www.greencarcongress.com/2020/05/20200528-battery500.html. [Accessed: 09- Aug- 2022].

[72] M. Kane, "Farasis Batteries With Silicon-Carbon Anode Get 25% Energy Boost", *Inside EVs*, 2021. [Online]. Available: https://insideevs.com/news/539398/farasis-batteries-energy-density-boost/. [Accessed: 09- Aug- 2022].

[73] M. Kane, "OXIS To Offer 450 Wh/kg Quasi Solid-State Li-S Cells In Fall 2021", *Inside EVs*, 2021. [Online]. Available: https://insideevs.com/news/502505/oxis-450-whkg-solidstate-cells/. [Accessed: 09- Aug- 2022].

[74] "Sion Power Introduces a Full-Scale Rechargeable Battery Targeting the Electric Vehicle Industry, Over 400 Wh/kg and 810 Wh/L", *Business wire*, 2021. [Online]. Available: https://www.businesswire.com/news/home/20210824005064/en/Sion-Power-Introduces-a-Full-Scale-Rechargeable-Battery-Targeting-the-Electric-Vehicle-Industry-Over-400-Whkg-and-810-WhL. [Accessed: 09- Aug- 2022].

[75] "Technology - Innolith", Innolith. [Online]. Available: https://innolith.com/technology/. [Accessed: 09- Aug- 2022].

[76] C. Randall, "SVOLT is reaching up to 400 Wh/kg in solid-state batteries", *electrive*, 2022. [Online]. Available: https://www.electrive.com/2022/07/22/svolt-is-reaching-up-to-400-wh-kg-in-solid-state-batteries/. [Accessed: 09- Aug- 2022].

[77] M. Kane, "Solid Power Installs Pilot Production Line For Solid-State Battery Cells", *Inside EVs*, 2022. [Online]. Available: https://insideevs.com/news/590430/solid-power-pilot-production-batteries/. [Accessed: 09- Aug- 2022].

[78] P. Zhang, "Gotion to mass-produce semi-solid-state batteries this year", *Cn EV Post*, 2022. [Online]. Available: https://cnevpost.com/2022/05/27/gotion-high-tech-to-mass-produce-semi-solid-state-batteries-this-year/. [Accessed: 09- Aug- 2022].

[79] M. Kane, "NIO Announces 150 kWh Solid-State Batteries For 2022", *Inside EVs*, 2021. [Online]. Available: https://insideevs.com/news/465188/nio-150-kwh-solid-state-batteries-2022/. [Accessed: 09- Aug- 2022].

[80] F. Lambert, "Tesla receives 4680 battery cell samples from Panasonic ahead of mass production", Electrek, 2022. [Online]. Available: https://electrek.co/2022/06/01/tesla-4680-battery-cell-samples-panasonic/. [Accessed: 09- Aug- 2022].

[81] "INR21700-P45B", *Molicel*. [Online]. Available: https://www.molicel.com/inr21700-p45b/. [Accessed: 09- Aug- 2022].

[82] "series production of battery cells 'made in Germany'", *CUSTOMCELLS*. [Online]. Available: https://www.cct-batteries.com. [Accessed: 09- Aug- 2022].

[83] "Lithium Primary Battery Packs", Custom Power. [Online]. Available: https://www.custompower.com/custom-battery-packs/lithium-primary. [Accessed: 09- Aug- 2022].

[84] N. Manthey, "InoBat scores lithium-silicon battery deal with Group14 - electrive.com", *electrive*, 2021. [Online]. Available: https://www.electrive.com/2021/08/24/inobat-scores-lithium-silicon-battery-deal-with-group14/. [Accessed: 09- Aug- 2022].

[85] G. Ruffo, "InoBat Proposes To Abandon Standard Battery Formats With AI", *Inside EVs*, 2020. [Online]. Available: https://insideevs.com/news/448170/inobat-abandon-standard-battery-formats-ai/. [Accessed: 09- Aug- 2022].

[86] "Solid Power awarded up to $12.5M to develop nickel- and cobalt-free all-solid-state battery cells; 500 Wh/kg target", *Green Car Congress*, 2021. [Online]. Available: https://www.greencarcongress.com/2021/10/20211002-solid.html. [Accessed: 09- Aug- 2022].

[87] "Innolith Claims It's On Path To 1,000 Wh/kg Battery Energy Density", *Inside EVs*, 2022. [Online]. Available: https://insideevs.com/news/343771/innolith-claims-its-on-path-to-1000-wh-kg-battery-energy-density/. [Accessed: 09- Aug- 2022].

[88] "Lyten introduces next generation Lithium-Sulfur battery for EVs; 3X energy density of Li-ion", Green Car Congress, 2021. [Online]. Available: https://www.greencarcongress.com/2021/09/20210923-lyten.html. [Accessed: 09- Aug- 2022].

[89] G. Cowan,"LLyten opens automated battery pilot line to produce lithium-sulfur batteries", Vertical mag, 2023. [Online]. Available: https://verticalmag.com/news/lyten-opens-automated-battery-pilot-line-to-produce-lithium-sulfur-batteries/ [Accessed: 24- Jan- 2024].

[90] C. Alcock, "Electric aircraft developers now have battery options with epic family rollout," *Future Flight*, 16-Jun-2021. [Online]. Available: https://www.futureflight.aero/news-article/2021-06-09/electric-aircraft-developers-now-have-new-battery-options-epic-family. [Accessed: 24-Nov-2022].

[91] H. Lugo, S. Clarke, T. Miller, M. Redifer, T. Foster, "X-57 Maxwell Battery from cell level to system level design and testing" [Online]. URL: https://ntrs.nasa.gov/citations/20180005737 [Accessed: 24-Nov-2022].

[92] F. Gulloci, "Turning Volts to VTOL", *The Vertical Flight Society* [online]. Available: https://vtol.org/files/dmfile/eVTOL-motors-Colucci_VF-JF181.pdf [Accessed: 21- Jan - 2020].

[93] DENSO, "Weight Reduction, Cooling Performance, and Reliability: Key Requirements for Air Mobility Motors — Mechanism of motors for DENSO's flying cars", 2021.

[94] H. Lin, H. Guo and H. Qian, "Design of High-Performance Permanent Magnet Synchronous Motor for Electric Aircraft Propulsion", in *21st International Conference on Electrical Machines and Systems (ICEMS)*, Jeju, Korea (South), 2018.

[95] E. Agamloh, A. von Jouanne and A. Yokochi, "An Overview of Electric Machine Trends in Modern Electric Vehicles", *Machines*, vol. 8, no. 2, p. 20, 2020. Available: 10.3390/machines8020020.

[96] YASA. "YASA 750", [online]. Available: https://www.yasa.com/yasa-750/ [Accessed: 21-Jan-2020].

[97] MAGNAX, "Next Generation Axial Flux Machines". [online] Available: https://www.magnax.com/technology [Accessed: 21-Jan-2020].

[98] NASA, "Electrical Machines", [online], Available: https://www1.grc.nasa.gov/aeronautics/electrified-aircraft-propulsion-eap/eap-for-larger-aircraft/electric-machines/ [Accessed: 21-Jan-2020].

[99] Volocopter, "Pioneering the urban air taxi revolution", [online], URL: https://press.volocopter.com/images/pdf/Volocopter-WhitePaper-1-0.pdf [Accessed: 29 Jan. 2020]

[100] M. Moore, "Distributed Electric Propulsion (DEP) Aircraft", [online], Available: https://aero.larc.nasa.gov/files/2012/11/Distributed-Electric-Propulsion-Aircraft.pdf [Accessed: 29-Jan-2020]

[101] "Aerospace Motor — Axial Flux Electric Motor Technology", *Evolito LTD.* [Online]. Available: https://evolito.aero/technology/. [Accessed: 10- Aug- 2022].

[102] "H3X — Electric Aircraft Propulsion", *H3x.tech.* [Online]. Available: https://www.h3x.tech. [Accessed: 10- Aug- 2022].

[103] "Electric Powertrain Technology Systems", *Helix.* [Online]. Available: https://ehelix.com/electric-powertrains/. [Accessed: 10- Aug- 2022].

[104] "APM-200 - Equipmake", *Equipmake.* [Online]. Available: https://equipmake.co.uk/products/apm-200/. [Accessed: 10- Aug- 2022].

[105] "AMPERE-220", *Equipmake.* [Online]. Available: https://equipmake.co.uk/products/ampere-220/. [Accessed: 10- Aug- 2022].

[106] "Integrated Motor — Controller: MAGiDRIVE™ - MAGicALL", *MAGicALL.* [Online]. Available: https://www.magicall.biz/products/integrated-motor-controller-magidrive/. [Accessed: 10- Aug- 2022].

[107] T. Lombardo, "Siemens Electric Aircraft Propulsion Unit: Inside the Digital Twin Design Strategy", *Engineering.com*, 2018. [Online]. Available: https://www.engineering.com/story/siemens-electric-aircraft-propulsion-unit-inside-the-digital-twin-design-strategy. [Accessed: 10- Aug- 2022].

[108] "Industry-Leading Products", *magniX.* [Online]. Available: https://magnix.aero/services. [Accessed: 10- Aug- 2022].

[109] A. Dubois, M. Geest, J. Bevirt, R. Christie, N. Borer and S. Clarke, "Design of an Electric Propulsion System for SCEPTOR's Outboard Nacelle", in *16th AIAA Aviation Technology, Integration, and Operations Conference*, Washington, D.C, 2016.

[110] "ENGINeUS™ Smart Electric Motors", *Safran.* [Online]. Available: https://www.safran-group.com/products-services/engineustm. [Accessed: 10- Aug- 2022].

[111] *Technical Data and Manual for EMRAX Motors / Generators.* Emrax, 2018.

[112] N. Zart, "The Pipistrel Alpha Electro, An Awesome 2-Seat Electric Trainer", *CleanTechnica*, 2017. [Online]. Available: https://cleantechnica.com/2017/11/13/pipistrel-alpha-electro-awesome-2-seat-electric-trainer/. [Accessed: 10- Aug- 2022].

[113] D. Sigler, "MagniX, an Australian High-Power and Torque-Dense Motor", Sustainable Skies, 2018. [Online]. Available: http://sustainableskies.org/magnix-australian-high-power-torque-dense-motor/. [Accessed: 10- Aug- 2022].

[114] G. Oshin, "Magnomatics high performance motor for aircrafts", *Linkedin*, 2022. [Online]. Available: https://www.linkedin.com/feed/update/urn:li:activity:6956662025305387008?updateEntityUrn=urnAli%3Afs_feedUpdate%3A%28V2%2Curn%3Ali%3Aactivity%3A69 56662025305387008%29. [Accessed: 10- Aug- 2022].

[115] C. Muller, "Opportunities and challenges of electric aircraft propulsion", Brugg, 2017.

[116] F. Anton, "eAircraft: Hybrid-elektrische Antriebe für Luftfahrzeuge", Potsdam, 2019.

[117] F. Anton, O. Otto, J. Hetz and T. Olbrechts, "Siemens eAircraft – Disrupting the way you will fly!", 2018.

[118] "268 (200kW - 500Nm)", *EMRAX*. [Online]. Available: https://emrax.com/e-motors/emrax-268/. [Accessed: 10- Aug- 2022].

[119] "228 (109kW - 230Nm)", *EMRAX*. [Online]. Available: https://emrax.com/e-motors/emrax-228/. [Accessed: 10- Aug- 2022].

[120] M. Gosálvez et al., "Green Flying Final Report", Technical University Delft, 2018.

[121] M. Toll, "New axial flux electric motors pack more EV power in a smaller package", *Electrek*, 2018. [Online]. Available: https://electrek.co/2018/05/03/axial-flux-electric-motors-more-ev-power-smaller-package/. [Accessed: 10- Aug- 2022].

[122] McLaren, “McLaren - the power behind Formula E”, 2014.

[123] *P400 R Series E-Motors*. YASA, 2018.

[124] D. Sigler, “Siemens Makes a Big, Light Motor”, *CAFE Foundation Blog*, 2015. [Online]. Available: http://cafe.foundation/blog/siemens-makes-big-light-motor-2/. [Accessed: 11- Aug- 2022].

[125] DENSO, “DENSO, Honeywell Co-Develop E-Motor for Lilium’s All-Electric Jet”, 2022.

[126] J. González, “Quark: The Lightweight Electric Motor Capable of Generating Unprecedented Power”, *Green Racing News*, 2022. [Online]. Available: https://greenracingnews.com/quark-the-lightweight-electric-motor-capable-of-generating-unprecedented-power/. [Accessed: 10- Aug- 2022].

[127] “High performance motors: 17 kW/kg power density”, SciMo. [Online]. Available: https://sci-mo.de/en/motors/Applications. [Accessed: 10- Aug- 2022].

[128] A. Datta, “Commercial Intra-City On-Demand Electric-VTOL”, The Vertical Flight Society, 2022.

[129] Mitsubishi Electric, “Mitsubishi Electric Develops World’s Smallest SiC Inverter for HEVs”, 2017.

[130] “Products - McLaren Applied”, *Mclarenapplied*. [Online]. Available: https://www.mclarenapplied.com/products?categories=10. [Accessed: 10- Aug- 2022].

[131] M. Hayes et al., ”650V, 7mOhm SiC MOSFET Development for Dual-Side Sintered Power Modules in Electric Drive Vehicles”, in *PCIM Europe 2017; International Exhibition and Conference for Power Electronics, Intelligent Motion, Renewable Energy and Energy Management*, Nuremberg, Germany., 2017.

[132] US Department of Energy, “FY2017 Electrification Annual Progress Report”, 2017.

[133] S. Rogers, "Advanced Power Electronics and Electric Motors (APEEM) R&D Program Overview", Program AMR and Peer Evaluation Meeting, 2011.

[134] Advanced Propulsion Centre UK, "The Roadmap Report - Towards 2040: A Guide to Automotive Propulsion Technologies", Advanced Propulsion Centre UK.

[135] M. Guacci, D. Bortis and J. Kolar, "High-Efficiency Weight-Optimized Fault-Tolerant Modular Multi-Cell Three-Phase GaN Inverter for Next Generation Aerospace Applications", in *2018 IEEE Energy Conversion Congress and Exposition (ECCE)*, Portland, USA, 2019.

[136] J. Liu, W. Su, X. Tai, et.l. "Development of an inverter using hybrid SIC power module for EV/HEV applications", in *19th International Conference on Electrical Machines and Systems (ICEMS)*, Chiba, Japan, 2016.

[137] D. Zhang, J. He, D. Pan, M. Dame, M. Schutten, "Development of Megawatt-Scale Medium-Voltage High Efficiency High Power Density Power Converters for Aircraft Hybrid-Electric Propulsion Systems", in *AIAA/IEEE Electric Aircraft Technologies Symposium (EATS)*, Cincinnati, OH, 2018. ISBN: 978-1-62410-572-2.

[138] "Electrical Power", Geaviation. [Online]. Available: https://www.geaviation.com/commercial/systems/silicon-carbide. [Accessed: 10- Aug- 2022].

[139] R. Jansen, C. Bowman, A. Jankovsky, R. Dyson and J. Felder, "Overview of NASA Electrified Aircraft Propulsion (EAP) Research for Large Subsonic Transports", in *53rd AIAA/SAE/ASEE Joint Propulsion Conference*, Atlanta, GA, 2017.

[140] "HPI-450", *Equipmake*. [Online]. Available: https://equipmake.co.uk/products/hpi-450/. [Accessed: 10- Aug- 2022].

[141] D. Zhang, J. He and D. Pan, "A Megawatt-Scale Medium-Voltage High-Efficiency High Power Density "SiC+Si" Hybrid Three-Level ANPC Inverter for Aircraft

Hybrid-Electric Propulsion Systems", *IEEE Transactions on Industry Applications*, vol. 55, no. 6, pp. 5971-5980, 2019. Available: 10.1109/tia.2019.2933513.

[142] S. Rogerson, "SiC DC-DC converter passes EV test", *Vehicle Electronics*, 2014. [Online]. Available: https://vehicle-electronics.biz/content/sic-dc-dc-converter-passes-ev-test. [Accessed: 10- Aug- 2022].

[143] K. Yamaguchi, K. Katsura, T. Yamada and Y. Sato, "High Power Density SiC-Based Inverter with a Power Density of 70kW/liter or 50kW/kg", *IEEJ Journal of Industry Applications*, vol. 8, no. 4, pp. 694-703, 2019. Available: 10.1541/ieejjia.8.694.

[144] "Products", *Drivetrain Innovation*. [Online]. Available: https://drivetraininnovation.com/products/. [Accessed: 10- Aug- 2022].

[145] "Inverter and Power Electronics", *SciMo*. [Online]. Available: https://scimo.de/en/power-electronics/. [Accessed: 10- Aug- 2022].

[146] A. Pescod, "Future 50: Norfolk firm to transform electric vehicles with new inverter", *Eastern Daily Press*, 2022. [Online]. Available: https://www.edp24.co.uk/news/business/equipmake-to-transform-electric-vehicles-with-new-inverter-8743652. [Accessed: 10- Aug- 2022].

[147] W. Martinez, C. Cortes, L. Muñoz and M. Yamamoto, "Design of a 200kW electric powertrain for a high performance electric vehicle", *Ingeniería e Investigación*, vol. 36, no. 3, p. 66, 2016. Available: 10.15446/ing.investig.v36n3.53792.

[148] G. Calderon-Lopez., A. Forsyth, "High power density DC-DC converter with SiC MOSFETs for electric vehicles" in *7th IET International Conference on Power Electronics, Machines and Drives*, 2014. doi:10.1049/cp.2014.0463.

[149] "RedPrime DC-DC Converter 200kW, 1200V", Zekalabs. [Online]. Available: https://www.zekalabs.com/products/non-isolated-high-power-converters/dc-dc-converter-200kw-1200v. [Accessed: 10- Aug- 2022].

[150] R. Bosshard and J. Kolar, "All-SiC 9.5 kW/dm3On-Board Power Electronics for 50 kW/85 kHz Automotive IPT System", *IEEE Journal of Emerging and Selected Topics in Power Electronics*, vol. 5, no. 1, pp. 419-431, 2017. Available: 10.1109/jestpe.2016.2624285.

[151] G. Su, C. White, Z. Liang, "Design and Evaluation of a 6.6 kW GaN Converter for Onboard Charger Applications" in *the 18th IEEE Workshop on Control and Modeling for Power Electronics*, Stanford, CA. 2017. doi:10.1109/COMPEL.2017.8013335.

[152] "High-Power Bidirectional DC/DC Converter for Hybrid-Electric Vehicle Applications", *Advanced Power Electronics Corporation.* [Online]. Available: http://apecor.com/highpower.php. [Accessed: 10- Aug- 2022].

[153] R. Erickson, D. Maksimovic, K. Afridi, D. Jones, et.l. "A Disruptive Approach to Electric Vehicle Power Electronics Final Report", 2017.

[154] A. Wienhausen, A. Sewergin, and R. Doncker, "Highly Integrated Two-Phase SiC Boost Converter with 3D-Printed Fluid Coolers and 3D-Printed Inductor Bobbins", in *PCIM Europe 2018; International Exhibition and Conference for Power Electronics, Intelligent Motion, Renewable Energy and Energy Management*, Nuremberg, Germany, 2018.

[155] J. Schanen, A. Baraston, M. Delhommais, P. Zanchetta and D. Boroyevitch, "Sizing of power electronics EMC filters using design by optimization methodology", in *7th Power Electronics and Drive Systems Technologies Conference (PEDSTC)*, Tehran, Iran, 2016.

[156] M. Hartmann, "Ultra-Compact and Ultra-Efficient Three-Phase PWM Rectifier Systems for More Electric Aircraft," Ph.D. dissertation, ETH Zurich, 2011.

[157] "HMDL 1000VDC MCCB", *Eaton.* [Online]. Available: https://www.eaton.com/sg/en-us/catalog/electrical-circuit-protection/eaton-hmdl-1000vdc-mccb.html [Accessed 14-No-2019].

[158] ABB, “ABB launches molded case circuit breakers for higher voltage solar power plants”, 2018.

[159] T. Sakuraba, R. Ouaida, S. Chen, and T. Chailloux, “Evaluation of Novel Hybrid Protection Based on Pyroswitch and Fuse Technologies”, in *International Power Electronics Conference*, Niigata, Japan, 2018.

[160] Koprivšek, M., ”Advanced Solutions in Over-Current Protection of Hvdc Circuit of Battery-Powered Electric Vehicle”, in PCIM Europe 2018, Nuremberg, Germany, 2018. ISBN: 978-3-8007- 4646-0.

[161] Lell, P., Volm, D., ”Innovative Safety Concept to Shutdown Short Circuit Currents in Battery Systems up to 1000V Based on Ultrafast Pyrofuse Technology”, in IEEE Holm Conference on Electrical Contacts, Albuquerque, NM, 2018. doi: 10.1109/HOLM.2018.8611656

[162] Bosch, ”Explosions that save lives”, [online]. Available: https://www.bosch-presse.de/pressportal/de/en/explosions-that- save-lives-200641.html [retrieved 20 Mar. 2020]

[163] Kambham, T. R. C. R., ”Pyro-Fuse Circuit”, Taxas Instruments Incorporated, [online]. Available: http://www.freepatentsonline.com/y2019/0123542.html

[164] Mersen, “Current Limiting Device to Address DC Aeronautics Power Distribution Systems”, 2016.

[165] Safran, “Safran and Pyroalliance announce a partnership for emergency pyrotechnic electrical shutdown solutions for future aeronautics electrical networks”, 2021.

[166] Z. Shen, G. Sabui, Z. Miao and Z. Shuai, “Wide-Bandgap Solid-State Circuit Breakers for DC Power Systems: Device and Circuit Considerations”, *IEEE Transactions on Electron Devices*, vol. 62, no. 2, pp. 294-300, 2015. Available: 10.1109/ted.2014.2384204.

[167] “ARPA-E awards $30M to 21 projects advance new class of high-performance power converters”, *Green Car Congress*, [online]. Available::

https://www.greencarcongress.com/2017/08/arpa-e-awards-30m-to-21-projects-advance-new-class-of-high-performance-power-converters.html [Accessed 14-No-2019].

[168] M. Terorde, F. Grumm, D. Schulz, H. Wattar, J. Lemke, "Implementation of a Solid-State Power Controller for High-Voltage DC Grids in Aircraft", in *PESS Power and Energy Student Summit*, 2015.

[169] D., Molligoda, P. Chatterjee, C. Gajanayake, A. Gupta, and K. Tseng, "Review of design and challenges of DC SSPC in More Electric Aircraft", in *2016 IEEE 2nd Annual Southern Power Electronics Conference (SPEC)*, Auckland, New Zealand, 2016. doi: 10.1109/SPEC.2016.7846117.

[170] KWx, "Solid-state 1kV DC breaker switch", 2020.

[171] J. Adhikari, T. Yang, J. Zhang, M. Rashed, et al., "Thermal Analysis of High Power High Voltage DC Solid State Power Controller (SSPC) for Next Generation Civil Tilt Rotor-craft", in *2018 IEEE International Conference on Electrical Systems for Aircraft, Railway, Ship Propulsion and Road Vehicles & International Transportation Electrification Conference (ESARS-ITEC)*, Nottingham, UK, 2019. doi: 10.1109/ESARS-ITEC.2018.8607314

[172] W. Kong, "Review of DC Circuit Breakers for Submarine Applications", Australian Government Department of Defense, Victoria, Australia, 2012.

[173] "SPDP50D375 datasheet", *Datasheetspdf*. [Online]. Available: https://datasheetspdf.com/pdf-file/1385810/Sensitron/SPDP50D375/1. [Accessed: 11- Aug- 2022].

[174] "SSP-21116 Datasheet Preview", *Datasheetarchive*. [Online]. Available: https://www.datasheetarchive.com/pdf/download.php?id=1e69c1b50e6211003ec60b727efa0e619fa839type=Mterm=SSP21116. [Accessed: 11- Aug- 2022].

[175] "SPDP50D28-1 Datasheet", *Datasheetspdf*. [Online]. Available: https://datasheetspdf.com/datasheet/SPDP50D28-1.html. [Accessed: 11- Aug- 2022].

[176] "MDSPC270M-50xL", *Hyjas*. [Online]. Available: http://www.hyjas.com/page12?product_id=326product_category=27. [Accessed: 11- Aug- 2022].

[177] *Short Form Catalogue Components & Solutions*. Esterline Power Systems.

[178] M. Flynn et al., "Protection and Fault Management Strategy Maps for Future Electrical Propulsion Aircraft", *IEEE Transactions on Transportation Electrification*, 2019. Available: 10.1109/tte.2019.2940882.

[179] National Academies of Sciences, Engineering, and Medicine, *Commercial Aircraft Propulsion and Energy Systems Research: Reducing Global Carbon Emissions*. Washington, DC: The National Academies Press, 2016. doi:10.17226/23490

[180] D. Li, L. Qi, "Energy based fuse modeling and simulation", in *IEEE Electric Ship Technologies Symposium (ESTS)*, Arlington, VA, 2013. doi:10.1109/ESTS.2013.6523781.

[181] W. Tian, C. Lei, Y. Zhang, et al, "Data analysis and optimal specification of fuse model for fault study in power systems", in *IEEE Power and Energy Society General Meeting (PESGM)*, Boston, MA. 2016. doi: 10.1109/PESGM.2016.7741864

[182] IEEE Industry Applications Society. 2018. "IEEE Guide For Performing Arc-Flash Hazard Calculations", IEEE Std 1584- 2002, Rev. 2018.

[183] Cooper Bussmann, "High Speed Fuses", [online]. Available: http://www.cooperindustries.com/content/dam/public/bussmann/ Electrical/Resources/Catalogs/North_American_High_Speed_F uses.pdf [retrieved 20 Mar. 2020]

[184] "Log-log scale plot", MathWorks. [online]. Available: https://uk.mathworks.com/help/matlab/ref/loglog [Accessed: 4- Feb- 2024].

[185] P. Darmstadt et al., "Hazards Analysis and Failure Modes and Effects Criticality Analysis (FMECA) of Four Concept Vehicle Propulsion Systems", National Aeronautics and Space Administration, 2022.

[186] Federal Aviation Administration, "Part 23 Accepted Means of Compliance Based on ASTM Consensus Standards", 2020. [Online]. Available: https://www.faa.gov/aircraft/air_cert/design_approvals/small_airplanes/small_airplanes_regs/media/part_23_moc.pdf, [Accessed: 27 -Feb - 2021].

[187] Advisory Circular, "FAA Accepted Means of Compliance Process for 14 CFR Part 23", U.S. Department of Transportation Federal Aviation Administration. 2017. [Online]. Available: https://www.faa.gov/documentLibrary/media/Advisory_Circular/AC_23_2010-1.pdf, [Accessed: 2- Dec - 2020].

[188] European Union Aviation Safety Agency, "Proposed Means of Compliance with the Special Condition VTOL". [Online]. Available: https://www.easa.europa.eu/sites/default/files/dfu/proposed_moc_sc_vtol_issue_1.pdf [Accessed: Jun. 1, 2020].

[189] "UK determines certification standards for new electric vertical take-off and landing aircraft ", UK Civil Aviation Authority, 2022. [Online]. Available: https://www.caa.co.uk/news/uk-determines-certification-standards-for-new-electric-vertical-take-off-and-landing-aircraft/. [Accessed: 09- Aug- 2022].

[190] "14 CFR § 21.17 - Designation of applicable regulations.", Legal Information Institute. [Online]. Available: https://www.law.cornell.edu/cfr/text/14/21.17. [Accessed: 09- Aug- 2022]..

[191] ASTM International, "eVTOL International Standards Workshop", Brussels, Belgium. 2019. [Online] https://www.astm.org/COMMIT/F44%20ASTM%20eVTOL%20Workshop%20Presentations_April2019.pdf, Accessed on: Dec. 2, 2020.

[192] Advisory Circular, "Systems and Equipment Guide for Certification of Part 23 Airplanes and Airships" U.S. Department of Transportation Federal Aviation Administration. 2011. [Online]. Available: https://www.faa.gov/documentLibrary/media/Advisory_Circular/AC_23-17C.pdf ,Accessed on Dec. 2, 2020.

[193] European Aviation Safety Agency, "Easy Access Rules for Normal, Utility, Aerobatic and Commuter Category Aeroplanes (CS-23) (Amendment 1)", EASA eRules, 2018.

[194] Advisory Circular "AC 25.1357-1A-Circuit Protective Devices Document Information" U.S Department of Transportation Federal Aviation Administration. 2017. [Online]. Available: https://www.faa.gov/documentLibrary/media/Advisory_Circular/AC_25_1357-1A.pdf Accessed on Feb. 8, 2021.

[195] SAE International, "ARP 4761: Guidelines and Methods for Conducting the Safety Assessment Process on Civil Airborne Systems and Equipment," 1996.

[196] Wang, P., "System Functional Hazard Assessment", in Civil Aircraft Electrical Power System Safety Assessment, ch. 4, pp. 69-99. 2017.

[197] Advisory Circular, "System Safety Analysis and Assessment for Part 23 Airplanes", U.S. Department of Transportation Federal Aviation Administration. 2011. [Online]. Available: https://www.faa.gov/documentLibrary/media/Advisory_Circular/AC_23_1309-1E.pdf, Accessed on Dec. 2, 2020.

[198] Chauhan, S., Martins, J., "Tilt-Wing eVTOL Takeoff Trajectory Optimization", Journal of Aircraft, vol. 57, no. 1, pp. 93-112, 2019. doi:10.2514/1.C035476

[199] Finger, D., Braun, C., Bil, C., "A Review of Configuration Design for Distributed Transitioning VTOL Aircraft", Asia-Pacific International Symposium on Aerospace Technology, Seoul, Korea .2017.

[200] Silva, C., Johnson, W., Antcliff, K., Patterson, M., "VTOL Urban Air Mobility Concept Vehicles for Technology Development" Aviation Technology, Integration, and Operations Conference. Atlanta, Georgia. 2018. doi:10.2514/6.2018-3847

[201] Fletcher, S., et al, "Determination of Protection System Requirements for DC UAV Electrical Power Networks for Enhanced Capability and Survivability", IET Electrical Systems in Transportation, vol.1, no. 4, pp. 137-147, 2011. doi:10.1049/iet.est.2010.0070

[202] Kumar, V., et al., "Factors affecting direct lightning strike damage to fiber reinforced composites: A review" Composites Part B: Engineering, vol. 183. 2020. doi: 10.1016/j.compositesb.2019.107688.

[203] Budinski, M., "Failure analysis of a bearing in a helicopter turbine engine due to electrical discharge damage", Case Studies in Engineering Failure Analysis 2. 2014

[204] Fisher, F., Plumer, J., Perala, R., "lightning direct effects handbook", 2002. [Online]. Available: https://apps.dtic.mil/sti/citations/ADA222716. [Accessed: 01- Dec- 2020].

[205] Advisory Circular, "Aircraft Electrical and Electronic System Lightning Protection", U.S. Department of Transportation Federal Aviation Administration. 2011. [Online]. Available: https://www.faa.gov/documentLibrary/media/Advisory_Circular/AC_20-136B.pdf

[206] Manadan, A., Johnston, R., Gupta, R., "*Systems and Methods for Redundant Control of Active Fuses for Battery Pack Safety*" US 11,710,957 B1, Jul 25, 2023. [Online]. Available: https://image-ppubs.uspto.gov/dirsearch-public/print/downloadPdf/11710957

[207] "Lightning Protection Products", Amphenol Aerospace.[Online]. Available: https://www.amphenol-aerospace.com/products/lightning-protection-productssection=techtechinfo=570.

[208] Department of Defence, "Requirements for the Control of Electromagnetic Interference Characteristics of Subsystems and Equipment", 2007.

[209] Turczyn, R., Krukiewicz, K., Katunin, A., Sroka, J., and Sul, P., "Fabrication and application of electrically conducting composites for electromagnetic interference shielding of remotely piloted aircraft systems", Composite Structures, vol. 232, p. 111498, 2020. Available: 10.1016/j.compstruct.2019.111498.

[210] SAE International, "ARP4754A: Guidelines for Development of Civil Aircraft and Systems", 2010.

[211] G. Thomas, J. Chapman, J. Alencar, H. Hasseeb, D. Sadey and J. Csank, "Multidisciplinary Systems Analysis of a Six Passenger Quadrotor Urban Air Mobility Vehicle Powertrain", in *AIAA Propulsion and Energy 2020 Forum*, Virtual Event, 2020.

[212] J. Chen, C. Wang, and J. Chen, "Investigation on the selection of Electric Power System Architecture for future more electric aircraft," *IEEE Transactions on Transportation Electrification*, vol. 4, no. 2, pp. 563–576, 2018.

[213] T. C. Cano, I. Castro, A. Rodriguez, D. G. Lamar, Y. F. Khalil, L. Albiol-Tendillo, and P. Kshirsagar, "Future of Electrical Aircraft Energy Power Systems: An architecture review," *IEEE Transactions on Transportation Electrification*, vol. 7, no. 3, pp. 1915–1929, 2021.

[214] M.-C. Flynn, C. E. Jones, P. J. Norman, and G. M. Burt, "A fault management-oriented early-design framework for Electrical Propulsion Aircraft," *IEEE Transactions on Transportation Electrification*, vol. 5, no. 2, pp. 465–478, 2019.

[215] C. Jones, P. Norman, and G. Burt, "A Modelling Framework for Efficient Design of Electrical Power Systems for Electrical Propulsion Aircraft" in *AIAA Propulsion and Energy 2021 Forum*, Virtual Event, 2021.

[216] A. Jain, K. Bavikar, A. Sanjay, M. Gupta, B. Ramesh Gupta and H. Dineshkumar, "Baseline procedure for conceptual designing of an eVTOL for Urban Air

Mobility", in *4th International Conference on Electronics, Communication and Aerospace Technology (ICECA)*, Coimbatore, India, 2020.

[217] A. Akash, V. Raj, R. Sushmitha, B. Prateek, S. Aditya and V. Sreehari, "Design and Analysis of VTOL Operated Intercity Electrical Vehicle for Urban Air Mobility", *Electronics*, vol. 11, no. 1, p. 20, 2021. Available: 10.3390/electronics11010020.

[218] J. A. Cole, L. Rajauski, A. Loughran, A. Karpowicz, and S. Salinger, "Configuration study of electric helicopters for Urban Air Mobility," *Aerospace*, vol. 8, no. 2, p. 54, 2021.

[219] J. Alba-Maestre, K. Prud'homme van Reine, T. Sinnige and S. Castro, "Preliminary Propulsion and Power System Design of a Tandem-Wing Long-Range eVTOL Aircraft", *Applied Sciences*, vol. 11, no. 23, p. 11083, 2021. Available: 10.3390/app112311083.

[220] G. Palaia, K. Abu Salem, V. Cipolla, V. Binante and D. Zanetti, "A Conceptual Design Methodology for e-VTOL Aircraft for Urban Air Mobility", *Applied Sciences*, vol. 11, no. 22, p. 10815, 2021. Available: 10.3390/app112210815.

[221] O. Ugwueze, T. Statheros, N. Horri, M. Innocente, and M. Bromfield, "Investigation of a mission-based sizing method for electric VTOL aircraft preliminary design," in *AIAA SCITECH 2022 Forum*, San Diego, CA & Virtual, 2022.

[222] A. Kasliwal et al., "Role of flying cars in sustainable mobility", *Nature Communications*, vol. 10, no. 1, 2019. Available: 10.1038/s41467-019-09426-0.

[223] A. Marco, "Aircraft Drag Polar", Flight Mechanics for Pilots, 2020. [Online]. Available: https://agodemar.github.io/FlightMechanics4Pilots/mypages/drag-polar/. [Accessed: 11- Aug- 2022].

[224] "The Lift Coefficient", Glen Research Center. [Online]. Available: https://www.grc.nasa.gov/www/k-12/airplane/liftco.html. [Accessed: 11- Aug- 2022].

[225] "The Drag Coefficient", Glen Research Center. [Online]. Available: https://www.grc.nasa.gov/www/k-12/airplane/dragco.html. [Accessed: 11- Aug- 2022].

[226] "Lift/Drag Ratio, Forces Interaction and Use", *SKYbrary Aviation Safety*. [Online]. Available: https://skybrary.aero/tutorials/liftdrag-ratio-forces-interaction-and-use. [Accessed: 11- Aug- 2022].

[227] P. Chung, D. Ma and J. Shiau, "Design, Manufacturing, and Flight Testing of an Experimental Flying Wing UAV", *Applied Sciences*, vol. 9, no. 15, p. 3043, 2019. Available: 10.3390/app9153043.

[228] S. Taarabt, et al. "Graduate Team Aircraft Design Competition: Electric vertical takeoff and landing (E-VTOL) aircraft mistral air taxi team name: The Huggy's Birds", 2019. [Online]. Available: 10.3390/app9153043.

[229] "Airbus Helicopters CityAirbus," *helis*, 2019. [Online]. Available: https://www.helis.com/database/model/CityAirbus/. [Accessed: 10-Nov-2022].

[230] G. Lecompte-Boinet, "CityAirbus demonstrator approaches First Flight," *Aviation International News*, 2019. [Online]. Available: https://www.ainonline.com/aviation-news/business-aviation/2019-03-02/cityairbus-demonstrator-approaches-first-flight. [Accessed: 10-Nov-2022].

[231] "CityAirbus performs first untethered flight," *Vertical Mag*, 2020. [Online]. Available: https://verticalmag.com/news/cityairbus-evtol-untethered-flight-test/. [Accessed: 10-Nov-2022].

[232] C. Courtin, A. Mahseredjian, A. J. Dewald, M. Drela and J. Hansman, "A Performance Comparison of eSTOL and eVTOL Aircraft", in *AIAA Aviation 2021 Forum*, Virtual Event, 2021.

[233] F. Wen, F. Hsiao, and J. Shiau, "Analysis and management of motor failures of hexacopter in hover," *Actuators*, vol. 10, no. 3, p. 48, 2021.

[234] O. Johnson, "CityAirbus Evtol Urban Air Mobility Program Presses Ahead," Vertical Mag, 2018. [Online]. Available: https://verticalmag.com/news/cityairbus-evtol-urban-air-mobility-programpresses-ahead/. [Accessed: 11- Aug- 2022].

[235] J. Bogaisky, "Has Joby Cracked The Power Problem To Make Electric Air Taxis Work?", *Forbes*, 2020. [Online]. Available: https://www.forbes.com/sites/jeremybogaisky/2020/11/23/joby-batteries-electric-aviation/?sh=3cfc2f9c76a7. [Accessed: 11- Aug- 2022].

[236] "surf", *MathWorks*. [Online]. Available: https://uk.mathworks.com/help/matlab/ref/ surf [Accessed: 2- Feb- 2024].

https://uk.mathworks.com/help/matlab/ref/surf

[237] A. Hussain, V. Rutgers and T. Hanley, "Technological barriers to the elevated future of mobility", *Deloitte Insights*, 2019. [Online]. Available: https://www2.deloitte.com/us/en/insights/focus/future-of-mobility/future-transportation-with-vtol.html. [Accessed: 11- Aug- 2022].

[238] X. Yang, T. Liu, S. Ge, E. Rountree and C. Wang, "Challenges and key requirements of batteries for electric vertical takeoff and landing aircraft", *Joule*, vol. 5, no. 7, pp. 1644-1659, 2021. Available: 10.1016/j.joule.2021.05.001.

[239] E. Beyne et al., "Final Report - Multi-Disciplinary Design and Optimisation of a Long-Range eVTOL Aircraft", Delft University of Technology, 2021.

[240] S. Melo, F. Cerdas, A. Barke, C. Thies, T. Spengler and C. Herrmann, "Life Cycle Engineering of future aircraft systems: the case of eVTOL vehicles", *Procedia CIRP*, vol. 90, pp. 297-302, 2020. Available: 10.1016/j.procir.2020.01.060.

[241] S. Sripad and V. Viswanathan, "The promise of energy-efficient battery-powered urban aircraft", *Proceedings of the National Academy of Sciences*, vol. 118, no. 45, 2021. Available: 10.1073/pnas.2111164118.

[242] A. Brown and W. Harris, "Vehicle Design and Optimization Model for Urban Air Mobility", *Journal of Aircraft*, vol. 57, no. 6, pp. 1003-1013, 2020. Available: 10.2514/1.c035756.

[243] A. Bacchini, E. Cestino, B. Van Magill and D. Verstraete, "Impact of lift propeller drag on the performance of eVTOL lift+cruise aircraft", *Aerospace Science and Technology*, vol. 109, p. 106429, 2021. Available: 10.1016/j.ast.2020.106429.

[244] M. Asselin, "Energy Reserves for Electrically Powered Aircraft", *Vertical Flight Society*, 2020. [Online]. Available: https://www.youtube.com/watch?v=HrM83Ui8pQs. [Accessed: 10-Nov-2022].

[245] N. Zazulia, "How Batteries Will Power the Next Evolution of Aviation", *Aviation Today*, 2019. [Online]. Available: https://www.aviationtoday.com/2019/06/12/uber-evtol-battery-testing/. [Accessed: 11- Aug- 2022].

[246] A. McIntosh, "Lilium's Chief Technology Officer, Alastair McIntosh, providing information on the architecture and technology of the Lilium Jet.", *Lilium Technology Blog*, 2021.

Bibliography